

Theory of Topological Superconductivity in Doped IV-VI Semiconductors

Zhe Li,^{1,2} Shengshan Qin,^{3,*} and Chen Fang^{1,4,3,†}

¹*Beijing National Laboratory for Condensed Matter Physics and Institute of Physics,
Chinese Academy of Sciences, Beijing 100190, China*

²*University of Chinese Academy of Sciences, Beijing 100049, China*

³*Kavli Institute for Theoretical Sciences, Chinese Academy of Sciences, Beijing 100190, China*

⁴*Songshan Lake Materials Laboratory, Dongguan, Guangdong 523808, China*

(Dated: June 29, 2022)

We theoretically study potential unconventional superconductivity in doped AB-type IV-VI semiconductors, based on a minimal effective model with interaction up to the next-nearest neighbors. According to the experimental implications, we focus on the spin-triplet channels and obtain the superconducting phase diagram with respect to the anisotropy of the Fermi surfaces and the interaction strength. All the states in the phase diagram are time reversal invariant and are topologically nontrivial. Specifically, in the phase diagram there appear a mirror symmetry protected topological Dirac superconductor phase, a mirror symmetry protected second-order topological superconductor phase, and a full-gap topological superconductor phase with winding number 4. The point group symmetry breaking of each superconducting ground state is also discussed.

PACS numbers: 74.70.-b, 74.25.Ha, 74.20.Pq

I. INTRODUCTION

Since the discovery of topological insulators^{1–3}, the study of topological phases in condensed matter systems has been rapidly developing. After efforts of a decade, numerous novel topological phases have been proposed^{4–7} and a large number of topological materials identified experimentally^{8–21}. In recent years, topological superconductors (TSCs), which are the superconducting analogy of the topological insulators, have become the research frontier^{22–37}. The TSCs are expected to host the Majorana modes which are believed to play an essential role in fault-tolerant topological quantum computing^{38–40}. In the pursuit of topological superconductivity, one proposal is to introduce superconductivity into the surface Dirac cone of a topological insulator, such that each superconducting vortex is expected to bind a single Majorana zero mode⁴¹. Evidences for the vortex bound Majorana zero modes have been observed in the Bi₂Te₃/NbSe₂ heterostructure^{29,42}, β -Bi₂Pd⁴³, the transition metal dichalcogenide 2M WS₂^{44,45}, and some iron-based superconductors^{31,46–54}.

In the above proposal the topological defect, *i.e.* the vortex, plays an essential role in realizing the Majorana modes, considering that the Majorana modes can not appear in the absence of the vortex. Different from the vortex proposal, the Majorana modes exit on the natural physical boundary in the intrinsic TSCs. In the intrinsic TSCs, exotic pairing structures, such as the p -wave and $(p+ip)$ -wave pairing on the Fermi surfaces, are vital. For instance, the Majorana modes were predicted to emerge at the ends of 1D p -wave SCs⁵⁵; the chiral superconductivity and chiral Majorana modes have been discussed a lot in the heavy-fermion SCs^{56–59} and the superconducting quantum Hall systems⁶⁰; the Rashba semiconductors in proximity to conventional superconductors ap-

plied with an external magnetic field, have also been predicted to host Majorana modes^{61–64}. The recently discovered doped superconducting topological materials^{65,66} provide another chance. Among them the most famous may be Bi₂Se₃^{67–70}, which has been confirmed to be superconducting^{71–75} when doped with Tm =Cu, Sr, Nb, Tl. Moreover, experimental measurements, such as thermodynamic⁷⁶, Nuclear magnetic resonance⁷⁷, scanning tunneling microscopy⁷⁸ (STM), etc.^{79–81}, reveal that the superconductivity is nematic, suggesting Tm_x Bi₂Se₃ (Tm =Cu, Sr, Nb) an odd-parity SC^{82,83}. While further experimental evidences are still needed, the progresses in Tm_x Bi₂Se₃ stimulate more enthusiasms in the doped superconducting topological materials.

Here, we turn our attention to the AB-type IV-VI semiconductors, typified by SnTe which is well known as the first topological crystalline insulator^{11,84}. Different from the topological insulators, even number of Dirac cones exist on the (001) surface in SnTe⁸⁴, which are protected by the mirror symmetry. With carrier doping, superconductivity has been confirmed in the series of materials experimentally^{85,86}. Recent soft point-contact spectroscopy measurements reveal a sharp zero-bias peak in superconducting Sn_{1-x}In_xTe⁸⁷. High-resolution scanning tunneling microscopy provide more evidences for the gapless excitations on the surface of superconducting Pb_{1-x}Sn_xTe⁸⁸. These experiments indicate possible unconventional superconductivity in the doped IV-VI semiconductors.

In this paper, motivated by the experimental progresses we perform a theoretical study on the superconductivity in under-doped AB-type IV-VI semiconductors. Our analyses are carried out based on an effective model capturing the Fermi surfaces in the strong spin-orbit coupling condition, and we consider the density-density interaction restricted up to the next-nearest neighbors.

We first classify the superconducting orders according to the irreducible representations (irreps) of the symmetry group, *i.e.* the point group O_h . It turns out that the leading order spin-singlet pairings are always topologically trivial without excitations in superconducting gaps. Therefore, we focus on the spin-triplet channels according to the experimental implications^{87,88}. We obtain the superconducting phase diagram by calculating the free energy on the mean-field level, with respect to the anisotropy of the Fermi surfaces and different interaction strength. We find that the superconductivity belonging to the A_{1u} , A_{2u} , E_u and T_{2u} irreps can appear in different regions in the phase diagram. Among these states, the A_{1u} and A_{2u} channels keep the symmetry group O_h , while the phase transition to the E_u and T_{2u} channels accompanies the symmetry breaking from the cubic O_h group to the tetragonal D_{4h} group. All these states are topologically nontrivial. Specifically, the system is in a first-order topological superconductor with winding number four in the A_{1u} and E_u states; while it is in a topological Dirac SC state with symmetry-protected nodal gap structures in the A_{2u} state, and there exist Majorana arcs on the surfaces correspondingly. For the T_{2u} channel, the system is a second-order TSC with helical Majorana hinge modes. The gapless surface/hinge modes and the point group symmetry breaking can be detected in experiments, serving as signatures for the topological superconductivity in the series of materials.

II. MODEL AND METHOD

We start with a brief review of the crystal and electronic structures of the AB-type IV-VI materials. This series of materials crystallize in the rocksalt structure which respects the O_h point group together with translational symmetry of face-centered cubic lattice as shown in Fig.1(a)(space group #225). The corresponding first Brillouin zone (BZ) is a truncated octahedron, as shown in Fig.1(b). In the BZ, there are four L points related by the C_4 rotational symmetry. At each L_n ($n = 1, 2, 3, 4$), the residual little group is D_{3d} which can be generated by the inversion symmetry, the C_3 rotation along the Γ -L direction and the mirror reflection parallel to the Γ ZL $_n$ plane. First principle calculations show that the AB-type IV-VI materials are semiconductors with a narrow direct gap near the four L points. Around the gap, the conduction bands and the valence bands are contributed by the p orbitals of the A-type elements and B-type elements, and the ordering of the bands determines the topological property⁸⁴. If the conduction band bottom (valence band top) is contributed by the B-type (A-type) element, the semiconductor is a topological crystalline insulator with even mirror Chern number; if the band ordering reverses, the semiconductor is topologically trivial. Upon carrier doping, four small Fermi pockets appear around the four L points, as sketched in Fig.1(b), and superconductivity shows up below the transition temperature in the IV-VI

semiconductors.

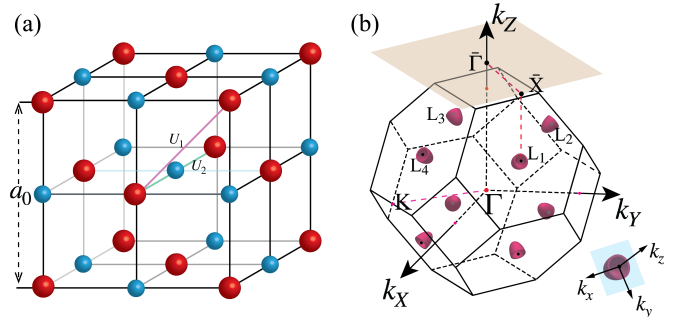


FIG. 1. (a) The lattice structure of the IV-VI semiconductors. The red and blue balls represent the A, B sublattices. U_1 and U_2 are the strength of the p -orbital density-density interaction between the nearest neighbors and next-nearest neighbors respectively. a_0 is the lattice constant of the conventional unit cell. (b) The first BZ of the IV-VI semiconductors. Upon carrier doping, small Fermi surfaces (the claret shells) appear near the four L points which are related by C_4 rotation. The transparent brown plane represents the surface BZ on the (001) surface. Notice that \bar{X} in the surface BZ is the projecting point of the L_1 and L_3 points in the bulk BZ. To describe the Fermi surfaces conveniently, besides the global reference frame described by k_x, k_y, k_z we introduce a set of local reference frames at the four L points. We use k_x, k_y and k_z to denote the coordinates in the local reference frame at L_1 , shown at the right bottom of the figure. The k_z axis goes along Γ - L_1 direction and k_x goes along Γ -K direction in the figure. The other three local reference frames can be obtained by taking C_4 rotation along k_z axis on the local reference frame at L_1 .

A. Normal-state Hamiltonian

We give a general discussion on the normal bands of the IV-VI semiconductors. Since the four small Fermi surfaces are related by the C_4 rotation, for simplicity we can focus on the one located at L_1 . Considering the symmetry constraints of the D_{3d} point group, the Fermi surface can be captured by a simple single-band model

$$H_0 = \sum_{\mathbf{k}, \sigma} \left(\frac{k_x^2 + k_y^2}{2m} + \frac{\xi k_z^2}{2m} - \mu \right) \hat{c}_{\mathbf{k}, s}^\dagger \hat{c}_{\mathbf{k}, s}, \quad (1)$$

where m is the effective mass and μ is the chemical potential, with $m, \mu > 0$ for the conduction bands and $m, \mu < 0$ for the valence bands. In the following analysis, it makes no difference for the conduction and valence bands, and we take $m, \mu > 0$ for simplicity. The other symbols in Eq.(1) are explained as below. (i) k_x, k_y and k_z are the momenta defined in the local reference frame at L_1 , as shown in Fig.1(b). (ii) Since the Fermi surface respects D_{3d} point group symmetry, a parameter ξ has been introduced to characterize the anisotropy in different directions. (iii) The subscript $s = \uparrow, \downarrow$ labels angular momentum $j_z = \pm \frac{1}{2}$ defined according to the C_3 rotation

along the Γ - L_1 direction rather than the real spin, since the spin-orbit coupling in the IV-VI semiconductors can not be neglected. (iv) Though the single-band Hamiltonian cannot describe the nontrivial topology in the IV-VI semiconductors, it is a good approximation in the low-doping condition, considering that the orbital character on the Fermi surfaces is dominated by either the p orbitals of the A-type elements or the B-type elements.

B. Interaction

To generate superconductivity, we consider the density-density interaction between the p orbitals. In general, interaction between different types of atoms needs to be taken into account. However, as mentioned above, in our consideration the orbital character on the Fermi surfaces are dominated by the p orbitals either from the A-type element or the B-type element, depending on whether the dopants are electrons or holes. Therefore, we can merely consider the interaction between the p orbitals in one sublattice, and we restrict the interaction to the next nearest neighbors

$$H_{\text{int}} = U_0 \sum_i \hat{n}_i \hat{n}_i + \frac{U_1}{2} \sum_{\langle i,j \rangle} \hat{n}_i \hat{n}_j + \frac{U_2}{2} \sum_{\langle\langle i,j \rangle\rangle} \hat{n}_i \hat{n}_j \quad (2)$$

where U_0 , U_1 and U_2 are on-site, the nearest neighbor and the next nearest neighbor interaction, as indicated in Fig.1(a). In the above equation, \hat{n}_i is the density operator on the i -th site defined as $\hat{n}_i = \sum_l \hat{n}_{i,l}$ with l denoting the freedom of spin and atomic orbitals, and $\langle ij \rangle$ and $\langle\langle ij \rangle\rangle$ denote the nearest neighbors and the next nearest neighbors, respectively.

By a Fourier transformation, we can get the interacting Hamiltonian in the reciprocal space

$$H_{\text{int}} = \sum_{\mathbf{q}} H_{\text{int}}(\mathbf{q}) = \frac{1}{N} \sum_{\mathbf{q}} (U_0 + U_1 f_1(\mathbf{q}) + U_2 f_2(\mathbf{q})) \hat{n}_{\mathbf{q}} \hat{n}_{-\mathbf{q}}, \quad (3)$$

where N is the number of the sites in the system and $\hat{n}_{\mathbf{q}} = \sum_{\mathbf{K},l} \hat{\psi}_l^\dagger(\mathbf{K} + \mathbf{q}) \hat{\psi}_l(\mathbf{K})$ and $f_\alpha(\mathbf{q}) = \sum_{\delta_\alpha} e^{i\mathbf{q} \cdot \delta_\alpha}$ with δ_α the bonds between the nearest (next-nearest) neighbors for $\alpha = 1$ ($\alpha = 2$). In the weak coupling limit, only the interaction between electronic states on the Fermi surfaces is essential. So we restrict the momentum \mathbf{K} and $\mathbf{K} + \mathbf{q}$ in the density operator within an area near the Fermi surfaces and have $\mathbf{K} = \mathbf{L}_n + \mathbf{k}$, $\mathbf{K} + \mathbf{q} = \mathbf{L}_m + \mathbf{k}'$, $|E_{\mathbf{k}} - \mu| < \delta\mu$, $|E_{\mathbf{k}'} - \mu| < \delta\mu$, where \mathbf{L}_m is the vector from the Γ point to L_m point; $E_{\mathbf{k}}$ is the kinetic energy of the states with momentum $\mathbf{L}_{1,2,3,4} + \mathbf{k}$; μ is the chemical potential and $\delta\mu$ is the cutoff energy in the summation, $\delta\mu \ll \mu$. We can derive $|\mathbf{k}|, |\mathbf{k}'| \sim k_F \ll |\mathbf{L}_{1,2,3,4}|$, $\mathbf{q} = \mathbf{L}_m - \mathbf{L}_n + \mathbf{k}' - \mathbf{k} = \mathbf{L}_{mn} + \tilde{\mathbf{q}}$ with $\mathbf{L}_{mn} = \mathbf{L}_m - \mathbf{L}_n$ and $\tilde{\mathbf{q}} \equiv \mathbf{k}' - \mathbf{k}$, $|\tilde{\mathbf{q}}| \ll |\mathbf{L}_{mn}|$. We substitute the relation $\hat{\psi}_l^\dagger(\mathbf{K} + \mathbf{q}) \hat{\psi}_l(\mathbf{K}) = \hat{\psi}_l^\dagger(\mathbf{k} + \tilde{\mathbf{q}} + \mathbf{L}_m) \hat{\psi}_l(\mathbf{k} + \mathbf{L}_n)$ into the interaction in Eq.3 obtaining,

$$H_{\text{int}} = \frac{1}{N} \sum_{\tilde{\mathbf{q}}, m, n} (U_0 + U_1 f_1(\mathbf{L}_{mn} + \tilde{\mathbf{q}}) + U_2 f_2(\mathbf{L}_{mn} + \tilde{\mathbf{q}})) \hat{\rho}_{\tilde{\mathbf{q}}, mn} \hat{\rho}_{-\tilde{\mathbf{q}}, mn}. \quad (4)$$

In the equation above, $\hat{\rho}_{\tilde{\mathbf{q}}, mn}$ is the newly defined density operator, $\hat{\rho}_{\tilde{\mathbf{q}}, mn} = \sum_{\mathbf{k}, l} \hat{\psi}_l^\dagger(\mathbf{k} + \tilde{\mathbf{q}} + \mathbf{L}_m) \hat{\psi}_l(\mathbf{k} + \mathbf{L}_n)$, where we use $\sum_{\mathbf{k}}$ to denote a cutoff on both the kinetic energy $E_{\mathbf{k}}$ and $E_{\mathbf{k} + \tilde{\mathbf{q}}}$ in the summation. When m equals to n , $m = n$, the interaction is contributed by the electrons within the same pocket, otherwise by the electrons from different pockets. The coefficients $f_i(\mathbf{L}_{mn} + \tilde{\mathbf{q}})$ obtained from the Fourier transformation are calculated to the second order of $\tilde{\mathbf{q}}$ in Appendix.A and listed in Table.I.

The interaction in Eq.4 includes all the states in p -orbitals from the atom A or B, however, superconductivities are contributed by the bands on the Fermi level. To capture the physical picture of the system, we project the states generated by the creation operator, $\hat{\psi}_l^\dagger(\mathbf{k} + \mathbf{L}_m)$, in the orbital basis to the band basis. We take the following three steps to accomplish such goal.

(i) In the low doping approximation, we treat the

bands of L points as the bands on Fermi surfaces, which are labelled by the angular momentum along ΓL , while we define the orbital l of $\hat{\psi}_l(\mathbf{k} + \mathbf{L}_m)$ in a global reference frame where the Z axis is taken along $[001]$ direction. For convenience we adopt a set of local reference frames on four pockets with $L_{1,2,3,4}$ point as the origin of each, respectively. The local reference frame of the first pocket is shown at the right bottom in Fig.1(b). We take k_z axis along ΓL_1 and k_x axis along ΓX . The other three reference frames can be obtained by taking the C_4 rotation on the first along k_Z . We use $\hat{\phi}_{m,w}^\dagger(\mathbf{k}) (\hat{\phi}_{m,w}(\mathbf{k}))$ to denote the creation (annihilation) operator in the m -th local reference frame and the orbital w is defined in the local frame coordinates k_x, k_y, k_z . The transformation from the global frame to the m -th local frame can be accomplished by \hat{U}_m , $\hat{\psi}_l^\dagger(\mathbf{k} + \mathbf{L}_m) = \hat{U}_m \hat{\phi}_{m,l}^\dagger(\mathbf{k}) \hat{U}_m^\dagger = \sum_w \mathcal{U}_{wl}^m \hat{\phi}_{m,w}^\dagger(\mathbf{k})$ and $\hat{\psi}_l(\mathbf{k} + \mathbf{L}_m) = \hat{U}_m \hat{\phi}_{m,l}(\mathbf{k}) \hat{U}_m^\dagger = \sum_w \mathcal{U}_{wl}^{m*} \hat{\phi}_{m,w}(\mathbf{k})$, where \mathcal{U}^m is the transformation matrix. We derive the density

TABLE I. The expansion of $f_i(\mathbf{q})$ in Eq.3 at $\mathbf{q} = 0$ and $\mathbf{q} = \mathbf{L}_{ij}$. $\tilde{\mathbf{q}}$ has the same magnitude as the Fermi momentum and very small compared with \mathbf{L}_{ij} , the vector from point \mathbf{L}_i to \mathbf{L}_j . We use \tilde{q}_{\parallel} to denote the component of $\tilde{\mathbf{q}}$ parallel to \mathbf{L}_{ij} .

Coefficient function	Expansion
$f_1(\tilde{\mathbf{q}})$	$6 - \frac{1}{2}a_0^2\tilde{q}^2$
$f_2(\tilde{\mathbf{q}})$	$3 - \frac{1}{2}a_0^2\tilde{q}^2$
$f_1(\mathbf{L}_{mn} + \tilde{\mathbf{q}}), m \neq n$	$-2 + \frac{1}{2}a_0^2\tilde{q}_{\parallel}^2$
$f_2(\mathbf{L}_{mn} + \tilde{\mathbf{q}}), m \neq n$	$3 - \frac{1}{2}a_0^2\tilde{q}^2$

operator under the new basis as,

$$\begin{aligned}
\hat{\rho}_{\tilde{\mathbf{q}},mn} &= \sum_{\mathbf{k},l} \hat{\psi}_l^\dagger(\mathbf{k} + \tilde{\mathbf{q}} + \mathbf{L}_m) \hat{\psi}_l(\mathbf{k} + \mathbf{L}_n) \\
&= \sum_{\mathbf{k},l} \hat{U}_m \hat{\phi}_{m,l}^\dagger(\mathbf{k} + \tilde{\mathbf{q}}) \hat{U}_m^\dagger \hat{U}_n \hat{\phi}_{n,l}(\mathbf{k}) \hat{U}_n^\dagger \\
&= \sum_{\mathbf{k},l,w,v} \mathcal{U}_{wl}^m \mathcal{U}_{vl}^{n*} \hat{\phi}_{m,w}^\dagger(\mathbf{k} + \tilde{\mathbf{q}}) \hat{\phi}_{n,v}(\mathbf{k}) \\
&= \sum_{\mathbf{k},w,v} \mathcal{D}_{wv}^{mn} \hat{\phi}_{m,w}^\dagger(\mathbf{k} + \tilde{\mathbf{q}}) \hat{\phi}_{n,v}(\mathbf{k})
\end{aligned} \tag{5}$$

where $\mathcal{D}^{mn} = \mathcal{U}^m \mathcal{U}^{n\dagger}$ is an identity matrix for intra-pocket interaction, $m = n$. We also calculate the matrix \mathcal{D}^{mn} , $m \neq n$, in the inter-pocket interaction in Appendix.B.

(ii) The first principle calculation shows that the bands on the Fermi level contributed by the states with the total angular momentum along $\Gamma\mathbf{L}$ equal to $\pm\frac{1}{2}$, $j_z = \pm\frac{1}{2}$. We change the orbital basis $|p_{x,y,z}, \uparrow(\downarrow)\rangle$ in local reference frames to $|J, j_z\rangle$, with $J = \frac{1}{2}, \frac{3}{2}$ and $j_z = \pm\frac{1}{2}$. The composition from orbital basis to angular momentum basis is shown in Table.II.

TABLE II. Relations between the basis in spin and atomic orbitals and the basis labelled by angular momentum J and j_z . All the states are defined in the local reference frame.

Angular Momentum	Atomic orbitals and spin
$ J = \frac{1}{2}, j_z = \frac{1}{2}\rangle$	$-\frac{1}{\sqrt{3}} p_z, \uparrow\rangle - \frac{1}{\sqrt{3}} p_x, \downarrow\rangle - \frac{i}{\sqrt{3}} p_y, \downarrow\rangle$
$ J = \frac{3}{2}, j_z = \frac{1}{2}\rangle$	$\sqrt{\frac{2}{3}} p_z, \uparrow\rangle - \frac{1}{\sqrt{6}} p_x, \downarrow\rangle - \frac{i}{\sqrt{6}} p_y, \downarrow\rangle$
$ J = \frac{1}{2}, j_z = -\frac{1}{2}\rangle$	$\frac{1}{\sqrt{3}} p_z, \downarrow\rangle - \frac{1}{\sqrt{3}} p_x, \uparrow\rangle + \frac{i}{\sqrt{3}} p_y, \uparrow\rangle$
$ J = \frac{3}{2}, j_z = -\frac{1}{2}\rangle$	$\sqrt{\frac{2}{3}} p_z, \downarrow\rangle + \frac{1}{\sqrt{6}} p_x, \uparrow\rangle - \frac{i}{\sqrt{6}} p_y, \uparrow\rangle$

(iii) Since $SO(3)$ symmetry is not respected in the lattice model, J is not a good quantum number. The states on Fermi level are mixed from $|J = \frac{1}{2}, j_z = \pm\frac{1}{2}\rangle$ and $|J = \frac{3}{2}, j_z = \pm\frac{1}{2}\rangle$. And we write the effective Hamiltonian as follows,

$$H_{\text{mix}} = h_0 \cos \theta \sigma_0 \tau_3 + h_0 \sin \theta \sigma_3 \tau_1. \tag{6}$$

In the Hamiltonian, Pauli matrices σ and τ act on the basis of j_z , $\{j_z = \frac{1}{2}, j_z = -\frac{1}{2}\}$ and J , $\{J = \frac{1}{2}, J = \frac{3}{2}\}$,

respectively. $\tan \theta$ describes the extent of the mixing, $h_0 \cos \theta$ as the energy splitting between the states with $J = \frac{1}{2}$, $J = \frac{3}{2}$ and $h_0 \sin \theta$ as the hybridization due to the crystal field. We obtain four eigenstates by diagonalizing H_{mix} and list in the following,

$$\begin{aligned}
|j_z = \frac{1}{2}\rangle_1 &= \left(-\sin \frac{\theta}{2}, \cos \frac{\theta}{2}, 0, 0\right)^\top \\
|j_z = \frac{1}{2}\rangle_2 &= \left(\cos \frac{\theta}{2}, \sin \frac{\theta}{2}, 0, 0\right)^\top \\
|j_z = -\frac{1}{2}\rangle_1 &= \left(0, 0, \sin \frac{\theta}{2}, \cos \frac{\theta}{2}\right)^\top \\
|j_z = -\frac{1}{2}\rangle_2 &= \left(0, 0, -\cos \frac{\theta}{2}, \sin \frac{\theta}{2}\right)^\top.
\end{aligned} \tag{7}$$

Here we take the strong SOC limit such that the mixing between $J = 3/2$ and $J = 1/2$ is much smaller than their splitting in energy, or symbolically, $\theta \ll 1$. This is equivalent to assuming that the hole wave function at \mathbf{L}_i is almost isotropic. We schematically show the bands splitting in Fig.2. The Fermi level is taken up by $|j_z = \pm\frac{1}{2}\rangle_2$ with the lowest energy in the conduction bands. We finally project the states $\hat{\phi}_w^\dagger(\mathbf{k})|0\rangle$ in each

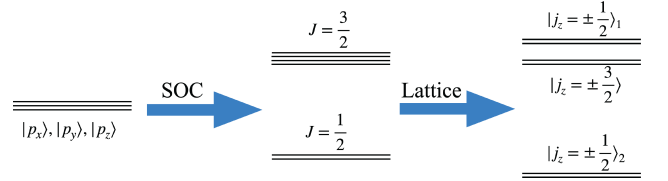


FIG. 2. The figure for the bands splitting. The original degenerated states in p_x , p_y and p_z orbitals are splitted into two levels, one as a doublet state $J = \frac{1}{2}$ and the other as a quartet state $J = \frac{3}{2}$. Then the bands are tuned by the potential of the lattice field. States of $|J = \frac{1}{2}, j_z = \pm\frac{1}{2}\rangle$ and $|J = \frac{3}{2}, j_z = \pm\frac{1}{2}\rangle$ are mixed with each other, resulting the energy of $|j_z = \pm\frac{1}{2}\rangle_2$ lifted up, while the energy of $|j_z = \pm\frac{1}{2}\rangle_1$ suppressed down.

local reference frame to $|j_z = \pm\frac{1}{2}\rangle_2$ states on the same Fermi surface using Table.II and Eq.7. The results are listed in Table.III.

C. Mean-field superconducting orders

So far, we have projected the orbital basis in the global reference frame to the band basis shown in Appendix.B. We use $\hat{c}_{\mathbf{k},\uparrow(\downarrow)}^{m\dagger}$ to denote the creation operator of $|j_z = \frac{1}{2}\rangle_2$ ($|j_z = -\frac{1}{2}\rangle_2$) in the m -th pocket and $\hat{c}_{\mathbf{k},\uparrow(\downarrow)}^m$ to denote the annihilation operator. For superconductivity, the pairing happens between the states on the same Fermi surface with opposite momentum. The interaction in Eq.4 is projected on the band basis and becomes as,

TABLE III. The projection from the orbital basis to the band basis on the Fermi level. We list the orbital basis in the left column and the obtained bands after projection in the right column.

original basis	after projection
$ p_x, \uparrow\rangle$	$(\frac{1}{\sqrt{3}} \cos(\frac{\theta}{2}) + \frac{1}{\sqrt{6}} \sin(\frac{\theta}{2})) j_z = -\frac{1}{2}\rangle_2$
$ p_y, \uparrow\rangle$	$-i(\frac{1}{\sqrt{3}} \cos(\frac{\theta}{2}) + \frac{1}{\sqrt{6}} \sin(\frac{\theta}{2})) j_z = -\frac{1}{2}\rangle_2$
$ p_z, \uparrow\rangle$	$(\sqrt{\frac{2}{3}} \sin(\frac{\theta}{2}) - \frac{1}{\sqrt{3}} \cos(\frac{\theta}{2})) j_z = \frac{1}{2}\rangle_2$
$ p_x, \downarrow\rangle$	$-(\frac{1}{\sqrt{3}} \cos(\frac{\theta}{2}) + \frac{1}{\sqrt{6}} \sin(\frac{\theta}{2})) j_z = \frac{1}{2}\rangle_2$
$ p_y, \downarrow\rangle$	$-i(\frac{1}{\sqrt{3}} \cos(\frac{\theta}{2}) + \frac{1}{\sqrt{6}} \sin(\frac{\theta}{2})) j_z = \frac{1}{2}\rangle_2$
$ p_z, \downarrow\rangle$	$(\sqrt{\frac{2}{3}} \sin(\frac{\theta}{2}) - \frac{1}{\sqrt{3}} \cos(\frac{\theta}{2})) j_z = -\frac{1}{2}\rangle_2$

$$H_{\text{int}} = \sum_{\mathbf{k}_1, \mathbf{k}_2} \sum_{m, n, s_1, s_2} f'_{s_1 s_2}(\mathbf{L}_{mn} + \mathbf{k}_1 - \mathbf{k}_2) \hat{c}_{\mathbf{k}_1, s_1}^{m\dagger} \hat{c}_{-\mathbf{k}_1, s_2}^{m\dagger} \hat{c}_{-\mathbf{k}_2, s_2}^n \hat{c}_{\mathbf{k}_2, s_1}^n + \text{non-SC}, \quad (8)$$

where $s_{1(2)} = 1, 2$ indicates pseudo-spin up and down \uparrow, \downarrow ; $f'_{s_1 s_2}$ is the interaction strength between the bands of

four pockets. In our approximation, $f'_{s_1, s_2}(\mathbf{L}_{mn} + \mathbf{k}_1 - \mathbf{k}_2)$ is expanded to the second order of $\mathbf{k}_1 - \mathbf{k}_2$, so the interaction can be rewritten as,

$$H_{\text{int}} = \sum_{\mathbf{k}_1, \mathbf{k}_2} \sum_{m, n, s_1, s_2} \left(g_{s_1 s_2}^{(0m)}(\mathbf{k}_1) g_{s_1 s_2}^{(0n)*}(\mathbf{k}_2) + g_{s_1 s_2}^{(0m)}(\mathbf{k}_1) g_{s_1 s_2}^{(2n)*}(\mathbf{k}_2) + g_{s_1 s_2}^{(2m)}(\mathbf{k}_1) g_{s_1 s_2}^{(0n)*}(\mathbf{k}_2) \right) \hat{c}_{\mathbf{k}_1, s_1}^{m\dagger} \hat{c}_{-\mathbf{k}_1, s_2}^{m\dagger} \hat{c}_{-\mathbf{k}_2, s_2}^n \hat{c}_{\mathbf{k}_2, s_1}^n \\ + \sum_{\mathbf{k}_1, \mathbf{k}_2} \sum_{m, n, s_1, s_2} g_{s_1 s_2}^{(1m)}(\mathbf{k}_1) g_{s_1 s_2}^{(1n)*}(\mathbf{k}_2) \hat{c}_{\mathbf{k}_1, s_1}^{m\dagger} \hat{c}_{-\mathbf{k}_1, s_2}^{m\dagger} \hat{c}_{-\mathbf{k}_2, s_2}^n \hat{c}_{\mathbf{k}_2, s_1}^n, \quad (9)$$

where $g_{s_1 s_2}^{(0(1,2)m)}(\mathbf{k})$ is the pairing function of the zeroth (first, second) order of \mathbf{k} in the m -th pocket and on each pocket the symmetries of the group D_{3d} are respected, so the pairing $g_{s_1 s_2}^{(0(1,2)m)}(\mathbf{k}_1) \hat{c}_{\mathbf{k}_1, s_1}^{m\dagger} \hat{c}_{-\mathbf{k}_1, s_2}^{m\dagger}$ can be represented by the irreps basis of the D_{3d} group in the m -th pocket. We list the irreps basis $\hat{\delta}_i(\mathbf{k})$ in the zeroth and first order of \mathbf{k} in Table IV. The irrep basis from different pockets take the same form if we use the local frame of reference at each pocket and we suppress the superscript m in $\hat{c}_{\mathbf{k}, \uparrow(\downarrow)}^m$ to indicate any of the four pockets. The pairings in the second order of \mathbf{k} are not taken into our consideration which is discussed in the later calculation and thus we do not show the corresponding irreps basis in Table IV. The inter-pocket interaction relates different pockets to each

other by C_4 rotation and induce the symmetry group from point group D_{3d} to point group O_h . The detailed procedure of the inducing is shown in Appendix C. The basis obtained from the direct summation of the D_{3d} irreps basis $\hat{\delta}_i(\mathbf{k})$ in four pockets are always reducible in the group O_h . We decompose the representation to the irreps of group O_h and obtain the irreps basis composed by $\hat{\delta}_i(\mathbf{k})$ in four pockets. We use $\hat{\delta}_i(m, \mathbf{k})$ to indicate $\hat{\delta}_i(\mathbf{k})$ in the m -th pocket and list the induced irreps basis of the group O_h in Table V. Combining with Table IV and Table V, we can represent $g_{s_1 s_2}^m(\mathbf{k}_1) \hat{c}_{\mathbf{k}_1, s_1}^{m\dagger} \hat{c}_{-\mathbf{k}_1, s_2}^{m\dagger}$ with the irreps basis of the group O_h and the interaction is decomposed as,

$$H_{\text{int}} = \sum_{\epsilon, \kappa, \zeta, \mathbf{k}, \mathbf{k}'} \frac{1}{N} \tilde{f}_{\kappa}^{\epsilon}(U_0, U_1, U_2, \theta) \hat{\Delta}_{\kappa, \zeta}^{\epsilon}(\mathbf{k})^{\dagger} \hat{\Delta}_{\kappa, \zeta}^{\epsilon}(\mathbf{k}') + \text{non-SC}, \quad (10)$$

where $\tilde{f}_{\kappa}^{\epsilon}(U_0, U_1, U_2, \theta)$ is the coefficient of the κ -

th channel with the symmetry denoted by ϵ , $\epsilon =$

TABLE IV. The irreps basis of group D_{3d} . We use $\hat{\delta}_i(\mathbf{k})$ as the notation for the irreps basis of group D_{3d} . To simplify the expression, \uparrow and \downarrow stands no longer for the real spin defined above, but for the pseudo-spin $|j_z = \frac{1}{2}\rangle_2$ and $|j_z = -\frac{1}{2}\rangle_2$ shown in Eq.7. The symmetry of each basis is listed in the right column. For $i = 1, 2, 3, 4$, the irreps are one dimensional and only have one component, while for $i = 5, 6, 7$, the e_u irrep is two dimensional and we use $\hat{\delta}_{i,1(2)}(\mathbf{k})$ to denote the first (second) component of the basis.

Irreps basis		Symmetry
$\hat{\delta}_1(\mathbf{k})$	$\frac{\sqrt{2}}{2}(\hat{c}_{\mathbf{k},\uparrow}\hat{c}_{-\mathbf{k},\downarrow} - \hat{c}_{\mathbf{k},\downarrow}\hat{c}_{-\mathbf{k},\uparrow})$	a_{1g}
$\hat{\delta}_2(\mathbf{k})$	$\frac{\sqrt{2}}{2}k_z(\hat{c}_{\mathbf{k},\uparrow}\hat{c}_{-\mathbf{k},\downarrow} + \hat{c}_{\mathbf{k},\downarrow}\hat{c}_{-\mathbf{k},\uparrow})$	a_{1u}
$\hat{\delta}_3(\mathbf{k})$	$\frac{1}{2}((ik_x + ky)\hat{c}_{\mathbf{k},\uparrow}\hat{c}_{-\mathbf{k},\uparrow} + (-ik_x + ky)\hat{c}_{\mathbf{k},\downarrow}\hat{c}_{-\mathbf{k},\downarrow})$	a_{1u}
$\hat{\delta}_4(\mathbf{k})$	$\frac{1}{2}((ik_x + ky)\hat{c}_{\mathbf{k},\uparrow}\hat{c}_{-\mathbf{k},\uparrow} - (-ik_x + ky)\hat{c}_{\mathbf{k},\downarrow}\hat{c}_{-\mathbf{k},\downarrow})$	a_{2u}
$\hat{\delta}_{5,1}(\mathbf{k})$	$\frac{\sqrt{2}}{2}(ik_x + ky)\hat{c}_{\mathbf{k},\downarrow}\hat{c}_{-\mathbf{k},\downarrow}$	e_u
$\hat{\delta}_{5,2}(\mathbf{k})$	$\frac{\sqrt{2}}{2}(-ik_x + ky)\hat{c}_{\mathbf{k},\uparrow}\hat{c}_{-\mathbf{k},\uparrow}$	
$\hat{\delta}_{6,1}(\mathbf{k})$	$k_z\hat{c}_{\mathbf{k},\downarrow}\hat{c}_{-\mathbf{k},\downarrow}$	e_u
$\hat{\delta}_{6,2}(\mathbf{k})$	$k_z\hat{c}_{\mathbf{k},\uparrow}\hat{c}_{-\mathbf{k},\uparrow}$	
$\hat{\delta}_{7,1}(\mathbf{k})$	$\frac{1}{2}(-ik_x + ky)(\hat{c}_{\mathbf{k},\uparrow}\hat{c}_{-\mathbf{k},\downarrow} + \hat{c}_{\mathbf{k},\downarrow}\hat{c}_{-\mathbf{k},\uparrow})$	e_u
$\hat{\delta}_{7,2}(\mathbf{k})$	$\frac{1}{2}(-ik_x + ky)(\hat{c}_{\mathbf{k},\uparrow}\hat{c}_{-\mathbf{k},\downarrow} - \hat{c}_{\mathbf{k},\downarrow}\hat{c}_{-\mathbf{k},\uparrow})$	

TABLE V. In the first column, the irreps of O_h group denoted as A_{1u} , A_{2u} , E_u , T_{1u} and T_{2u} are induced from the irreps of D_{3d} group listed in the second column. We show the corresponding basis constructed by the irreps basis of the second column, $\hat{\delta}_i(\mathbf{k})$, from four pockets in the third column. To distinguish the irreps basis from different pockets, we use $j = 1, 2, 3, 4$ to indicate the pocket and change the notation $\hat{\delta}_i(\mathbf{k})$ in Table.IV to $\hat{\delta}_i(j, \mathbf{k})$ and the irreps basis of different pockets take the same form in their own local reference frames.

Irreps of O_h	Induced from	Combination of irreps of D_{3d}	
A_{1u}	a_{1u}	$\frac{1}{2}(\hat{\delta}_i(1, \mathbf{k}) + \hat{\delta}_i(2, \mathbf{k}) + \hat{\delta}_i(3, \mathbf{k}) + \hat{\delta}_i(4, \mathbf{k}))$	$i = 2, 3$
T_{2u}		$\frac{1}{2}(\hat{\delta}_i(1, \mathbf{k}) - \hat{\delta}_i(2, \mathbf{k}) - \hat{\delta}_i(3, \mathbf{k}) + \hat{\delta}_i(4, \mathbf{k}))$	
		$\frac{1}{2}(\hat{\delta}_i(1, \mathbf{k}) + \hat{\delta}_i(2, \mathbf{k}) - \hat{\delta}_i(3, \mathbf{k}) - \hat{\delta}_i(4, \mathbf{k}))$	
		$\frac{1}{2}(\hat{\delta}_i(1, \mathbf{k}) - \hat{\delta}_i(2, \mathbf{k}) + \hat{\delta}_i(3, \mathbf{k}) - \hat{\delta}_i(4, \mathbf{k}))$	
A_{2u}	a_{2u}	$\frac{1}{2}(\hat{\delta}_i(1, \mathbf{k}) - \hat{\delta}_i(2, \mathbf{k}) + \hat{\delta}_i(3, \mathbf{k}) - \hat{\delta}_i(4, \mathbf{k}))$	$i = 4$
T_{1u}		$\frac{1}{2}(\hat{\delta}_i(1, \mathbf{k}) - \hat{\delta}_i(2, \mathbf{k}) - \hat{\delta}_i(3, \mathbf{k}) + \hat{\delta}_i(4, \mathbf{k}))$	
		$\frac{1}{2}(\hat{\delta}_i(1, \mathbf{k}) + \hat{\delta}_i(2, \mathbf{k}) - \hat{\delta}_i(3, \mathbf{k}) - \hat{\delta}_i(4, \mathbf{k}))$	
		$\frac{1}{2}(\hat{\delta}_i(1, \mathbf{k}) + \hat{\delta}_i(2, \mathbf{k}) + \hat{\delta}_i(3, \mathbf{k}) + \hat{\delta}_i(4, \mathbf{k}))$	
E_u	e_u	$\frac{1}{2}(\hat{\delta}_{i,1}(1, \mathbf{k}) + \hat{\delta}_{i,1}(2, \mathbf{k}) + \hat{\delta}_{i,1}(3, \mathbf{k}) + \hat{\delta}_{i,1}(4, \mathbf{k}))$	$i = 5, 6, 7$
		$\frac{1}{2}(\hat{\delta}_{i,2}(1, \mathbf{k}) - \hat{\delta}_{i,2}(2, \mathbf{k}) + \hat{\delta}_{i,2}(3, \mathbf{k}) - \hat{\delta}_{i,2}(4, \mathbf{k}))$	
T_{1u}		$\frac{\sqrt{3}}{4}(\hat{\delta}_{i,1}(1, \mathbf{k}) + \hat{\delta}_{i,1}(2, \mathbf{k}) - \hat{\delta}_{i,1}(3, \mathbf{k}) - \hat{\delta}_{i,1}(4, \mathbf{k})) + \frac{1}{4}(\hat{\delta}_{i,2}(1, \mathbf{k}) - \hat{\delta}_{i,2}(2, \mathbf{k}) - \hat{\delta}_{i,2}(3, \mathbf{k}) + \hat{\delta}_{i,2}(4, \mathbf{k}))$	
		$\frac{\sqrt{3}}{4}(-\hat{\delta}_{i,1}(1, \mathbf{k}) + \hat{\delta}_{i,1}(2, \mathbf{k}) + \hat{\delta}_{i,1}(3, \mathbf{k}) - \hat{\delta}_{i,1}(4, \mathbf{k})) + \frac{1}{4}(\hat{\delta}_{i,2}(1, \mathbf{k}) + \hat{\delta}_{i,2}(2, \mathbf{k}) - \hat{\delta}_{i,2}(3, \mathbf{k}) - \hat{\delta}_{i,2}(4, \mathbf{k}))$	
		$-\frac{1}{2}(\hat{\delta}_{i,2}(1, \mathbf{k}) + \hat{\delta}_{i,2}(2, \mathbf{k}) + \hat{\delta}_{i,2}(3, \mathbf{k}) + \hat{\delta}_{i,2}(4, \mathbf{k}))$	
T_{2u}		$\frac{1}{4}(\hat{\delta}_{i,1}(1, \mathbf{k}) - \hat{\delta}_{i,1}(2, \mathbf{k}) - \hat{\delta}_{i,1}(3, \mathbf{k}) + \hat{\delta}_{i,1}(4, \mathbf{k})) + \frac{\sqrt{3}}{4}(\hat{\delta}_{i,2}(1, \mathbf{k}) + \hat{\delta}_{i,2}(2, \mathbf{k}) - \hat{\delta}_{i,2}(3, \mathbf{k}) - \hat{\delta}_{i,2}(4, \mathbf{k}))$	
		$\frac{\sqrt{3}}{4}(\hat{\delta}_{i,1}(1, \mathbf{k}) + \hat{\delta}_{i,1}(2, \mathbf{k}) - \hat{\delta}_{i,1}(3, \mathbf{k}) - \hat{\delta}_{i,1}(4, \mathbf{k})) + \frac{1}{4}(-\hat{\delta}_{i,2}(1, \mathbf{k}) + \hat{\delta}_{i,2}(2, \mathbf{k}) + \hat{\delta}_{i,2}(3, \mathbf{k}) - \hat{\delta}_{i,2}(4, \mathbf{k}))$	
		$\frac{1}{2}(-\hat{\delta}_{i,2}(1, \mathbf{k}) + \hat{\delta}_{i,2}(2, \mathbf{k}) - \hat{\delta}_{i,2}(3, \mathbf{k}) + \hat{\delta}_{i,2}(4, \mathbf{k}))$	

$A_{1g(u)}, A_{2g(u)}, E_{g(u)}, T_{1g(u)}$ and $T_{2g(u)}$. We assume the strength of the on-site interaction is much bigger than the other two, $|U_0| \gg |U_1|, |U_2|$. When U_0 is negative, the ground state is the BCS type which is topologically trivial. When U_0 is positive, the irreps with even parity are excluded from the phase diagram, which

is shown in Appendix.D, so we set $U_0 > 0$ and only focus on the irreps with triplet pairings. We have in total 15 channels in five pairing symmetries: $2A_{1u}$, $1A_{2u}$, $3E_u$, $4T_{1u}$ and $5T_{2u}$. After taking the mean-field approximation, $\sum_{\mathbf{k}} \frac{1}{N} f_{\kappa}^e(U_0, U_1, U_2, \theta) \hat{\Delta}_{\kappa, \zeta}^e(\mathbf{k})^\dagger = \langle \tilde{f}_{\kappa}^e(U_0, U_1, U_2, \theta) \hat{\Delta}_{\kappa, \zeta}^e(\mathbf{k})^\dagger \rangle = \lambda_{\kappa, \zeta}^e$, we obtain the so called BdG Hamiltonian,

$$H_{\text{BdG}} = H_0 + \sum_{\epsilon, \kappa, \zeta, \mathbf{k}} (\lambda_{\kappa, \zeta}^{\epsilon} \hat{\Delta}_{\kappa, \zeta}^{\epsilon}(\mathbf{k}) + \lambda_{\kappa, \zeta}^{\epsilon*} \hat{\Delta}_{\kappa, \zeta}^{\epsilon}(\mathbf{k})^{\dagger} - \frac{N|\lambda_{\kappa, \zeta}^{\epsilon}|^2}{\tilde{f}_{\kappa}^{\epsilon}(U_0, U_1, U_2, \theta)}) + \text{non-SC}, \quad (11)$$

where H_0 is the normal state in Eq.1. We then calculate the free energy of each channel in Appendix.E to obtain the ground states and we also study the symmetries and topological properties of the ground states in the next section.

III. RESULTS

As shown above, for each pairing symmetry there can be multiple linearly independent channels for the Cooper pairs. For example, there are three E_u channels and five T_{2u} channels. For channels of higher than one dimensional irreps, there are multiple components in each channel. If a pairing symmetry ϵ has κ channels and each channel is a ζ -dimensional irrep, we need two complex vectors $(r_1^{\epsilon}, \dots, r_{\kappa}^{\epsilon}) \otimes (t_1^{\epsilon}, \dots, t_{\zeta}^{\epsilon})$ to describe the superconducting ground states. For instance, the E_u state can be described as $(r_1^{E_u}, r_2^{E_u}, r_3^{E_u}) \otimes (t_1^{E_u}, t_2^{E_u})$ in general. Obviously, the above vector satisfies $r_{\kappa}^{\epsilon} t_{\zeta}^{\epsilon} = \lambda_{\kappa, \zeta}^{\epsilon}$ with $\lambda_{\kappa, \zeta}^{\epsilon}$ being the coefficients in Eq.(11) for irrep ϵ . By calculating and minimizing the mean-field free energy, which is shown detailly in Appendix.E, we can get the irrep and the corresponding coefficients \mathbf{r} and \mathbf{t} for the superconducting ground states (details in appendix). The topological properties of the ground states can be analyzed accordingly.

A. Phase diagrams

We mainly focus on the ground states with respect to the Fermi surface anisotropy ξ introduced in Eq.(1) and the nearest and next-nearest neighbor interaction U_1, U_2 in Eq.(A1). Notice that if both U_1 and U_2 are repulsive, superconductivity will not be favored on the mean-field level. Therefore, we focus on the following three scenarios: (i) $U_1 > 0, U_2 < 0$, (ii) $U_1 < 0, U_2 > 0$, and (iii) $U_1 < 0, U_2 < 0$. In the calculation, we treat the ratio $|U_2/U_1|$ as a tunable parameter for fixed $U_1/m = 4$, and the other parameters are taken as $\mu/m = 1, \theta = 0.1$. We plot the superconducting phase diagrams in Fig.3.

1. $U_1 > 0, U_2 < 0$

For the first scenario with $U_1 > 0$ and $U_2 < 0$, as shown in Fig.3(a) only the states belonging to the A_{1u} and E_u irreps are favored. Both of the two states are fully gapped with the E_u state possessing a more anisotropic superconducting gap as indicated in

Figs.4(a1)(c1). The A_{1u} state can be described by the vector $(r_1^{A_{1u}}, r_2^{A_{1u}}) \otimes 1$ and the E_u state can be described by $(r_1^{E_u}, r_2^{E_u}, r_3^{E_u}) \otimes (1, 0)$. It is easy to check that, the A_{1u} state respects all the symmetries in the point group O_h ; while the E_u state breaks the 3-fold rotational symmetry along the Γ -L direction and preserves the D_{4h} point group. This information can be readout from Table.VI: on the E_u row, only operations that are diagonal can preserve $\mathbf{t} = (1, 0)$, thus remaining symmetries in the ordered phase.

In Fig.3(a) there is an obvious feature that, the phase diagram is dominated by the A_{1u} state and the E_u state only appears in the region with small U_2 and ξ . This actually results from the fact that U_1 is highly anisotropic (isotropic) for the inter-pocket (intro-pocket) interaction while U_2 is isotropic for both the inter-pocket and intro-pocket interactions, as shown in Table.I. More specifically, in the limit $\theta \rightarrow 0$ the main driving force for superconductivity is the negative U_2 which prefers an isotropic superconducting gap on the Fermi surfaces, *i.e.* the A_{1u} state; the inter-pocket interaction from U_1 shown in Table.I tends to introduce anisotropy to the superconducting gap, which is responsible for the gap structure in Figs.4(c1).

2. $U_1 < 0, U_2 > 0$

In the second scenario where $U_1 < 0$ and $U_2 > 0$, three different states, the A_{1u} , A_{2u} and T_{2u} states, can appear in the phase diagram as presented in Fig.3(b). The A_{1u} state is fully gapped. The T_{2u} state is also nodeless and it can be characterized by a vector $(r_1^{T_{2u}}, r_2^{T_{2u}}, r_3^{T_{2u}}, r_4^{T_{2u}}, r_5^{T_{2u}}) \otimes (0, 0, 1)$. Notice that the superconducting gap in the T_{2u} state is highly anisotropic as shown in Fig.4(d1). Similar to the E_u state in the first scenario, the T_{2u} state breaks the 3-fold rotational symmetry along the Γ -L direction and respects the D_{4h} point group, as indicated in Table.VI. The A_{2u} state can be characterized by the vector $1 \otimes 1$, which is gapless with robust nodal points located on the four Fermi surfaces along the Γ -L direction as shown in Fig.4(b1). There is no symmetry breaking in the A_{2u} state.

In the phase diagram, the A_{2u} state occupies the region with $\xi > 1$. This is closely related to that: (i) in the small θ limit the negative U_1 is vital for superconductivity and it can generate all the superconducting orders in Table.V (details in appendix); (ii) the condition $\xi > 1$ ($\xi < 1$) corresponds to a larger (smaller) Fermi velocity along the Γ -L direction; (iii) to lower the free energy it tends to open a larger superconducting gap on the part of the Fermi surface where there is larger density of states.

TABLE VI. Irreps of group O_h . C_{2a} , C_{2b} and C_{2c} are the three two fold rotation. The axis of C_{2a} goes along the x axis in the local reference frame. The axes of C_{2b} and C_{2c} can be obtained from the axis of C_{2a} by C_3 rotation.

	C_3	C_3^2	C_{2a}	C_{2b}	C_{2c}	C_4	C_4^2
$A_{1g}(A_{1u})$	1	1	1	1	1	1	1
$A_{2g}(A_{2u})$	1	1	-1	-1	-1	-1	1
$E_g(E_u)$	$\begin{pmatrix} -\frac{1}{2} & -\frac{\sqrt{3}}{2} \\ \frac{\sqrt{3}}{2} & -\frac{1}{2} \end{pmatrix}$	$\begin{pmatrix} -\frac{1}{2} & -\frac{\sqrt{3}}{2} \\ \frac{\sqrt{3}}{2} & -\frac{1}{2} \end{pmatrix}$	$\begin{pmatrix} 1 & 0 \\ 0 & -1 \end{pmatrix}$	$\begin{pmatrix} -\frac{1}{2} & \frac{\sqrt{3}}{2} \\ -\frac{\sqrt{3}}{2} & -\frac{1}{2} \end{pmatrix}$	$\begin{pmatrix} -\frac{1}{2} & \frac{\sqrt{3}}{2} \\ \frac{\sqrt{3}}{2} & -\frac{1}{2} \end{pmatrix}$	$\begin{pmatrix} 1 & 0 \\ 0 & -1 \end{pmatrix}$	$\begin{pmatrix} 1 & 0 \\ 0 & 1 \end{pmatrix}$
$T_{2g}(T_{2u})$	$\begin{pmatrix} 0 & 1 & 0 \\ 0 & 0 & 1 \\ 1 & 0 & 0 \end{pmatrix}$	$\begin{pmatrix} 0 & 0 & 1 \\ 1 & 0 & 0 \\ 0 & 1 & 0 \end{pmatrix}$	$\begin{pmatrix} 0 & 1 & 0 \\ 1 & 0 & 0 \\ 0 & 0 & 1 \end{pmatrix}$	$\begin{pmatrix} 0 & 0 & 1 \\ 0 & 1 & 0 \\ 1 & 0 & 0 \end{pmatrix}$	$\begin{pmatrix} 1 & 0 & 0 \\ 0 & 0 & 1 \\ 0 & 1 & 0 \end{pmatrix}$	$\begin{pmatrix} 0 & -1 & 0 \\ 1 & 0 & 0 \\ 0 & 0 & -1 \end{pmatrix}$	$\begin{pmatrix} -1 & 0 & 0 \\ 0 & -1 & 0 \\ 0 & 0 & 1 \end{pmatrix}$

The above facts make the A_{2u} state the ground state when $\xi > 1$. For $\xi < 1$, there is a competition between U_1 and the density of states on the Fermi surfaces. When U_1 is dominant, the full-gap A_{1u} state is preferred; as $|U_2/U_1|$ becomes larger, the positive isotropic U_2 interaction weakens the A_{1u} superconductivity and a full-gap but highly anisotropic T_{2u} state appears as the ground state.

3. $U_1 < 0, U_2 < 0$

At last, we consider the scenario with $U_1 < 0$ and $U_2 < 0$, where the A_{1u} , A_{2u} and E_u states appear in different regions of the parameter space shown in Fig.3(c). The gap structures in the three states are similar to that in the phase diagrams in Figs.3(a)(b).

In the current condition, both the negative U_1 and U_2 are responsible for the superconductivity. The phase diagram is consistent with the above analysis if the nature of the interaction and the density of states on the Fermi surfaces are taken into account. Specifically, in the region where U_1 dominates U_2 and there is smaller density of states along the Γ -L direction on the Fermi surfaces ($\xi > 1$), the A_{2u} state appears as the ground state because the large density of states on the Fermi surface can overlap with a large superconducting gap; in the region where U_2 is dominant or the Fermi velocity is smaller ($\xi < 1$) along the Γ -L direction, the A_{1u} states is preferred. In the intermediate region where U_2 is comparable to U_1 with $\xi > 1$, the competition between U_1 and U_2 results in the anisotropic full-gap E_u state.

B. Topological property of the ground state

In this part, we analyze the topological properties of the superconducting ground states in the phase diagrams in Fig.3. Since all the states in the phase diagrams are time reversal invariant, the SC belongs to class DIII according to the Altland-Zirnbauer classification^{89,90}. Considering that there are four Fermi surfaces related by the C_4 rotational symmetry in the system and all the states in Fig.4 (including the point-group symmetry breaking

states E_u and T_{2u}) preserve the C_4 rotational symmetry, we take the following strategy in the analysis. We first analyze the topological property of the superconductivity on the L_1 Fermi surface. Then, the topological superconductivity contributed by the other three Fermi surfaces can be inferred from the constraints of the C_4 rotational symmetry. Taking all the Fermi surfaces into account, we know the topological property of the whole system for each ground state in the phase diagrams in Fig.3.

To study the topological property of the ground states, it is convenient to take the basis $\hat{\gamma}_{\mathbf{k}}^\dagger = (\hat{c}_{\mathbf{k}}^\dagger, i\sigma_2 \hat{c}_{-\mathbf{k}})$, with $\hat{c}_{\mathbf{k}}^\dagger$ the basis for the normal-state Hamiltonian in Eq.(1). With the above choice, the BdG Hamiltonian can be written as

$$H_{\text{BdG}} = H_0 \eta_3 + \Delta(\mathbf{k}) \eta_1, \quad (12)$$

where the Pauli matrix η is defined in the Nambu space. The odd-parity superconductivity can be described by a vector $\mathbf{d}(\mathbf{k}) = (d_1(\mathbf{k}), d_2(\mathbf{k}), d_3(\mathbf{k}))$ and the superconducting order can be expressed as $\Delta(\mathbf{k}) = \mathbf{d}(\mathbf{k}) \cdot \boldsymbol{\sigma}$. Comparing Eq.(12) and Eq.(11), it is easy to obtain $\hat{\psi}_{\mathbf{k}}^\dagger(\mathbf{d}(\mathbf{k}) \cdot \boldsymbol{\sigma} \eta_1) \hat{\psi}_{\mathbf{k}} = \sum_{\kappa, \zeta} (\lambda_{\epsilon, \kappa, \zeta} \hat{\Delta}_{\epsilon, \kappa, \zeta}(\mathbf{k}) + \lambda_{\epsilon, \kappa, \zeta}^* \hat{\Delta}_{\epsilon, \kappa, \zeta}^\dagger(\mathbf{k}))$ for each irrep channel labeled by ϵ .

1. A_{1u}

We start with the A_{1u} state. The A_{1u} state is fully gapped and it respects the full symmetry of the O_h point group. The topological property of such SCs is featured by the 3D winding number⁸⁹⁻⁹¹. On the L_1 Fermi surface, this state can be described by a vector $\mathbf{d}(\mathbf{k}) = (\alpha k_x, \alpha k_y, \beta k_z)$ (α, β are coefficients determined by the parameters in the mean-field calculations). Obviously, the superconductivity on the L_1 Fermi surface is topologically equal to the famous $^3\text{He-B}$ phase⁹² which is featured by a 3D winding number $w_1 = \text{sgn}(\alpha\beta)$ with sgn the sign function, and this leads to a Majorana cone on the surface as shown in Fig.4(a2). Since the A_{1u} pairing is C_4 even, we can conclude that the winding numbers contributed by the superconductivity on the four Fermi surfaces are all the same, and the whole system is characterized by a winding number $w = 4w_1$. Accordingly, there will be totally four Majorana cones on the surfaces.

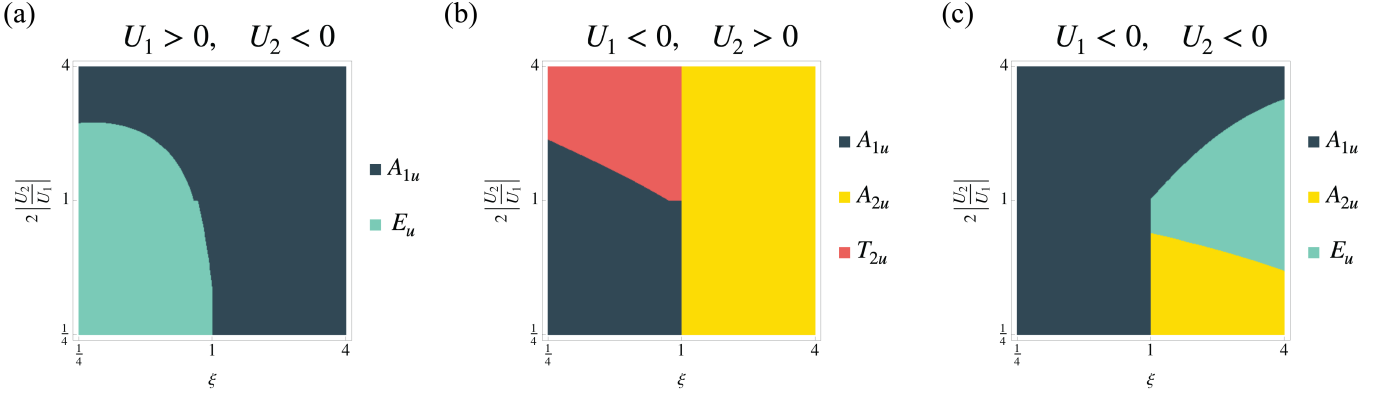


FIG. 3. The phase diagram of the ground state of the Hamiltonian in Eq. 11 with respect to the anisotropy parameter ξ and the interaction parameter $2|U_2/U_1|$ on logarithmic scale.

Specifically, on the (001) surface two Majorana cones are expected to be centered at \bar{X} , the projection of L_n on the surface BZ, as sketched in Fig. 4(a3).

2. A_{2u}

Similar to the A_{1u} state, the A_{2u} state also preserves the O_h point group. However, different from the A_{1u} state it possesses robust nodes on the Fermi surfaces along the Γ -L direction, making the A_{2u} SCs the so-called topological Dirac SCs⁹³. We still take the L_1 Fermi surface for example, where the superconductivity can be described by a vector $\mathbf{d}(\mathbf{k}) = (-\alpha k_y, \alpha k_x, 0)$ on the L_1 Fermi surface. Namely, in the local frame on the L_1 Fermi surface the pairing takes the form $\hat{\Delta}(\mathbf{k}) \sim (ik_x + k_y)\hat{c}_{\mathbf{k},\uparrow}\hat{c}_{-\mathbf{k},\uparrow} + (ik_x - k_y)\hat{c}_{\mathbf{k},\downarrow}\hat{c}_{-\mathbf{k},\downarrow}$. This is similar to the planar phase of the ^3He superfluid⁹², where the pairing occurs between electrons with the same spin and carries opposite angular momentum for Cooper pairs with opposite spin. Apparently, Dirac nodes will appear on the rotation axis, *i.e.* the Γ -L direction on the Fermi surface. Moreover, the Dirac nodes lead to zero-energy arcs on the surfaces, which are guaranteed by both the mirror symmetry and the chiral symmetry (more details in appendix). Specifically, on the (001) surface the superconductivity on each Fermi surface results in surface modes in Fig. 4(b2), and taking all the Fermi surfaces into consideration we can get the zero-energy arcs illustrated in Fig. 4(b3) (more details in appendix).

3. E_u

The E_u state is fully gapped with symmetry breaking from point group O_h to D_{4h} . Despite of the symmetry breaking, the E_u state shares similar topological property with the A_{1u} state. On the L_1 Fermi surface, it can be described by a vector $\mathbf{d}(\mathbf{k}) = (\alpha k_x, \alpha k_y + \beta k_z, \gamma k_y)$, which contributes a winding number $w_1 = -\text{sgn}(\alpha\beta\gamma)$.

Moreover, the C_4 rotational symmetry preserves in the E_u state and the superconducting order remains invariant under the C_4 rotational symmetry. Hence, the superconductivity on the four Fermi surfaces contribute the same winding number and the whole system has a total winding number $w = 4w_1$. The surface modes for the E_u state are expected to be similar to that in the A_{1u} state, as indicated in Fig. 4(c2)(c3).

4. T_{2u}

In the T_{2u} state, the SC has a nodeless and strongly anisotropic gap structure shown in Fig. 4(d1). Similar to the E_u state, there is symmetry breaking from point group O_h to D_{4h} in this state. But the topological property is completely different here. We still begin with the superconductivity on the L_1 Fermi surface, which can be described by a vector $\mathbf{d}(\mathbf{k}) = (\alpha k_x, \beta_1 k_y + \beta_2 k_z, \gamma_1 k_y + \gamma_2 k_z)$. Obviously, the L_1 Fermi surface contributes a winding number $w_1 = \text{sgn}(\alpha\beta_1\gamma_2 - \alpha\beta_2\gamma_1)$, as indicated in Fig. 4(d2). As mentioned, the T_{2u} state keeps the C_4 rotational symmetry. However, in this case the superconducting order is C_4 odd, namely there is a π phase difference between the pairing amplitude on the L_1, L_3 Fermi surfaces and the superconducting orders on the L_2, L_4 Fermi surfaces in Fig. 1(b). Therefore, the winding numbers contributed by the four Fermi surfaces have the following relation $w_1 = -w_2 = w_3 = -w_4$, and the whole system has a total winding number $w = 0$.

Though the T_{2u} state has a total winding number zero, it belongs to a second-order TSC state^{19,94–104}. Moreover, as we shall show below, the second-order topological superconductivity here thoroughly stems from the pairing on the Fermi surfaces and is protected by the mirror symmetry intrinsically. This is different from the previous studies where the second-order topological superconductivity is realized by introducing external mass domain into the edge modes of a topological insulator^{101–104}. Specifically, we consider the mirror

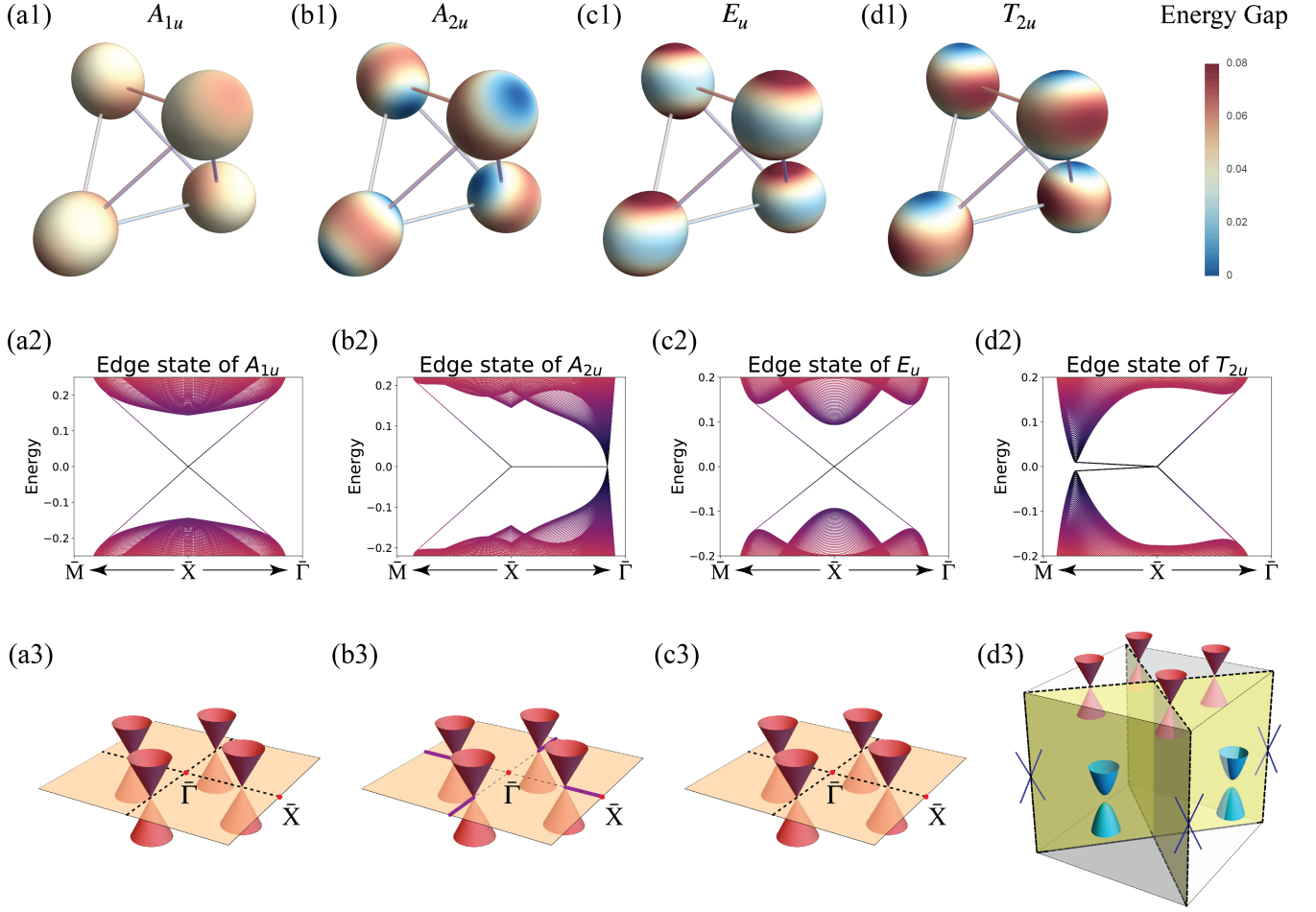


FIG. 4. (a1)~(d1) show the superconducting gap on the Fermi surfaces corresponding to the A_{1u} , A_{2u} , E_u and T_{2u} states in the under-doped AB-type IV-VI semiconductors. The figures share the same color bar shown on the right top of the figure. The A_{1u} , E_u and T_{2u} states are full-gap with the T_{2u} state being highly anisotropic; the A_{2u} state is gapless with nodes located on the Fermi surfaces along the Γ -L direction. From (a1)~(d1) it can be noticed that, the A_{1u} and A_{2u} states respect all the symmetries of point group O_h , while the E_u and T_{2u} states break the C_3 rotational symmetry along Γ L and respect the D_{4h} point group rather than the O_h point group. In (a2)~(d2), we plot the surface states on the (001) surface corresponding to the states in figures (a1)~(d1) in the condition where only the superconductivity on the L_1 Fermi surface is considered. The calculation of the edge states is shown in Appendix G. Obviously, the topological superconductivity on the L_1 Fermi surface leads to a single Majorana cone around \bar{X} in A_{1u} , E_u and T_{2u} states and a two-fold degenerate zero-energy flat band along $\bar{X}\bar{\Gamma}$ in the A_{2u} channel. By taking the superconductivity on the four Fermi surfaces into account, we schematically show the surface modes on the (001) surface corresponding to the A_{1u} , A_{2u} , E_u and T_{2u} states in (a3)~(d3). As shown in Fig. 1(b), both the L_1 and L_3 points from the bulk project onto the same \bar{X} point in the surface BZ. Therefore, on the (001) surface the two Majorana cones from the L_1 and L_3 Fermi surfaces will split along $\bar{\Gamma}\bar{X}$, the intersection line between the mirror plane and the (001)-surface. Notice that There is no essential difference between the A_{1u} state in (a3) and the E_u state in (c3), because the qualitative feature of the E_u state is the breaking of 3-fold rotational axis, which does not show on the (001) surface. In (b3), the purple lines denote the 4-fold degenerate zero-energy arcs of the A_{2u} state. (d3) shows the surface modes and hinge modes of the second-order TSC of the T_{2u} state. The yellow planes in (d3) stand for the mirror planes, and the helical Majorana hinge modes are represented by the blue crossing lines.

symmetry M_a which maps $(k_X, k_Y, k_Z) \mapsto (k_Y, k_X, k_Z)$ for the global frame and $(k_x, k_y, k_z) \mapsto (-k_x, k_y, k_z)$ for the local frame defined at the L_1 point in Fig. 1(b). Moreover, M_a constrains the superconducting order as $M_a \Delta(\mathbf{k}) M_a^T = \Delta(M_a \mathbf{k})$ on the L_1 Fermi surface. For such superconductivity, in each of the M_a invariant subspaces the particle-hole symmetry is preserved while the

the time reversal symmetry is no longer maintained. Therefore, we can consider the mirror Chern number in the $\Gamma L_1 L_3$ plane in Fig. 1(b). Since the two mirror invariant subspaces are related by the time reversal symmetry, the Chern numbers in the two subspaces are always opposite with each other, and the mirror Chern number satisfies $C_M = (C_{+i} - C_{-i})/2$ with $\pm i$ the eigenvalues

of M_a . It is easy to check the superconductivity on the L_1 Fermi surface contributes mirror Chern number 1 or -1 . Besides the L_1 Fermi surface, the L_3 Fermi surface also has contributions to the mirror Chern number as indicated in Fig.1(b). Considering that L_1 and L_3 are related by the C_2 rotational symmetry under which the superconducting order keeps invariant, it is obvious to conclude that the superconductivity on the L_3 Fermi surface contributes the same mirror Chern number with the L_1 Fermi surface. Therefore, the SC has $|C_M| = 2$ on the $\Gamma L_1 L_3$ plane. For a SC with an even mirror Chern number, it must be a second-order TSC protected by the mirror symmetry^{99,105}. Correspondingly, two Majorana cones are expected on the surfaces where M_a is preserved, such as the (001) plane, along $\bar{\Gamma}\bar{X}$ as shown in Fig.4(d3), and there will be one pair of helical Majorana modes localized on each hinge respecting the mirror symmetry M_a such as the intersection between the (100) and (010) surfaces. At last, it is worth mentioning that since the T_{2u} state respects the D_{4h} point group, the other mirror symmetries equivalent to M_a under C_4 will lead to similar topological states. Accordingly, we sketch the topological surface states and hinge states in Fig.4(d3). The detailed discuss of the symmetries and topological properties is listed in Appendix.F.

IV. DISCUSSION AND CONCLUSION

Our theory may account for the interesting results in the typical IV-VI semiconductor such as SnTe in recent experiments, including the zero-bias peak in In-doped SnTe in the soft point-contact spectroscopy measurements⁸⁷ and the gapless excitations on the surface of superconducting $Pb_{1-x}Sn_xTe$ revealed by the high-resolution STM measurements⁸⁸ where both of the measurements are done on the (001) surface. Besides, the penetration depth¹⁰⁶ and the STM⁸⁸ measurements indicate a nodeless superconducting gap in $Sn_{1-x}In_xTe$ and $Pb_{1-x}Sn_xTe$ respectively. Since the anisotropic Fermi surfaces in SnTe have smaller Fermi velocity along the Γ -L direction, namely $\xi < 1$, as indicated in the phase diagram in Fig.3 the A_{1u} , E_u and T_{2u} superconductivity can be candidates for the ground states. This is different from the previous study¹⁰⁷, where SnTe has been predicted to be in the A_{1u} state. According to our theory, all of the three states are fully gapped and support gapless excitations on the (001) surface, as illustrated in Fig.4. To distinguish the three states, the upper critical field measurements can provide important information. As the E_u and T_{2u} states break the 3-fold rotational symmetry along the [111] direction, the upper critical field is expected to break the 3-fold rotational symmetry accordingly, if the field is applied perpendicular to the [111] direction. The T_{2u} state can be distinguished from the E_u state by measuring the surface modes on different surfaces. Since the T_{2u} state is a second-order TSC, it only supports gapless surface modes on the (001) surface, as

illustrated in Fig.4(d3); the E_u state is a first-order TSC with winding number 4, which supports Majorana modes on every surface. For instance, if the soft point-contact spectroscopy measurements are done on the (111) surface, a zero-bias peak is expected in the E_u state while it is absent for the T_{2u} state; similarly, if we take the high-resolution quasiparticle interference measurements on the (111) surface, the gapless excitations can be observed only in the E_u state. Moreover, the helical Majorana modes at the intersection between the (100) and (010) surfaces can provide smoking-gun evidence for the T_{2u} state, which can be detected by the high-resolution STM measurements.

Though the A_{2u} state does not seem to be the ground state for SnTe, it may be favored in other doped superconducting IV-VI semiconductors or systems with similar crystal and electronic structures. Therefore, we also discuss its experimental characteristics here. Due to the Dirac points in its energy spectrum, the specific heat would scales with T^3 at low temperature; the zero-energy arcs on the surface, as shown in Fig.4(b3), can provide further evidences in the quasiparticle interference measurements.

In summary, the superconductivity in under-doped AB-type IV-VI semiconductors has been studied theoretically. We start from a spin-orbit-coupled p -orbital model with interaction restricted to the next-nearest neighbour. By projecting the p orbitals onto the Fermi surfaces, a single-band effective model is derived. We solve the model in the mean-field level and study the possible spin-triplet superconductivity systematically. We find that various superconducting states, including the A_{1u} , A_{2u} , E_u and T_{2u} states, appear in the phase diagram with respect to the anisotropy of the Fermi surface and the interaction strength. All the states are time reversal invariant. Symmetry breaking from group O_h to D_{4h} exists in the E_u and T_{2u} states, while no symmetry breaking appears in the other two states. The topological property of each ground state has been analyzed. Specifically, the A_{1u} and E_u states are both TSCs with winding number 4, the A_{2u} state is a topological Dirac superconductor with robust Dirac nodes, and the T_{2u} state is a second-order TSC protected by the mirror symmetry. To our knowledge, the T_{2u} superconductivity is the first symmetry-protected second-order topological superconductivity proposed in 3D superconductors. The corresponding edge states are presented. The experimental detections for the ground states are discussed.

ACKNOWLEDGMENTS

The work is supported by the Ministry of Science and Technology of China (Grant No. 2016YFA0302400) and Chinese Academy of Sciences (Grant No. XDB33000000).

- * qinshengshan@iphy.ac.cn
† cfang@iphy.ac.cn
- ¹ M. Z. Hasan and C. L. Kane, *Rev. Mod. Phys.* **82**, 3045 (2010).
 - ² X.-L. Qi and S.-C. Zhang, *Rev. Mod. Phys.* **83**, 1057 (2011).
 - ³ A. Bansil, H. Lin, and T. Das, *Rev. Mod. Phys.* **88**, 021004 (2016).
 - ⁴ C.-K. Chiu, J. C. Y. Teo, A. P. Schnyder, and S. Ryu, *Rev. Mod. Phys.* **88**, 035005 (2016).
 - ⁵ N. P. Armitage, E. J. Mele, and A. Vishwanath, *Rev. Mod. Phys.* **90**, 015001 (2018).
 - ⁶ Y. Ando and L. Fu, *Annual Review of Condensed Matter Physics* **6**, 361 (2015), <https://doi.org/10.1146/annurev-conmatphys-031214-014501>.
 - ⁷ B. J. Wieder, B. Bradlyn, J. Cano, Z. Wang, M. G. Vergniory, L. Elcoro, A. A. Soluyanov, C. Felser, T. Neupert, N. Regnault, *et al.*, arXiv preprint arXiv:2106.00709 (2021).
 - ⁸ Y. Ando, *Journal of the Physical Society of Japan* **82**, 102001 (2013), <https://doi.org/10.7566/JPSJ.82.102001>.
 - ⁹ M. König, S. Wiedmann, C. Brüne, A. Roth, H. Buhmann, L. W. Molenkamp, X.-L. Qi, and S.-C. Zhang, *Science* **318**, 766 (2007), <https://science.sciencemag.org/content/318/5851/766.full.pdf>.
 - ¹⁰ D. Hsieh, D. Qian, L. Wray, Y. Xia, Y. S. Hor, R. J. Cava, and M. Z. Hasan, *Nature* **452**, 970 (2008).
 - ¹¹ Y. Tanaka, Z. Ren, T. Sato, K. Nakayama, S. Souma, T. Takahashi, K. Segawa, and Y. Ando, *Nature Physics* **8**, 800 (2012).
 - ¹² Z. K. Liu, B. Zhou, Y. Zhang, Z. J. Wang, H. M. Weng, D. Prabhakaran, S.-K. Mo, Z. X. Shen, Z. Fang, X. Dai, Z. Hussain, and Y. L. Chen, *Science* **343**, 864 (2014), <https://science.sciencemag.org/content/343/6173/864.full.pdf>.
 - ¹³ Z. Liu, J. Jiang, B. Zhou, Z. Wang, Y. Zhang, H. Weng, D. Prabhakaran, S. K. Mo, H. Peng, P. Dudin, *et al.*, *Nature materials* **13**, 677 (2014).
 - ¹⁴ B. Q. Lv, H. M. Weng, B. B. Fu, X. P. Wang, H. Miao, J. Ma, P. Richard, X. C. Huang, L. X. Zhao, G. F. Chen, Z. Fang, X. Dai, T. Qian, and H. Ding, *Phys. Rev. X* **5**, 031013 (2015).
 - ¹⁵ S.-Y. Xu, I. Belopolski, N. Alidoust, M. Neupane, G. Bian, C. Zhang, R. Sankar, G. Chang, Z. Yuan, C.-C. Lee, S.-M. Huang, H. Zheng, J. Ma, D. S. Sanchez, B. Wang, A. Bansil, F. Chou, P. P. Shibayev, H. Lin, S. Jia, and M. Z. Hasan, *Science* **349**, 613 (2015), <https://science.sciencemag.org/content/349/6248/613.full.pdf>.
 - ¹⁶ L. Lu, Z. Wang, D. Ye, L. Ran, L. Fu, J. D. Joannopoulos, and M. Soljačić, *Science* **349**, 622 (2015), <https://science.sciencemag.org/content/349/6248/622.full.pdf>.
 - ¹⁷ J. Ma, C. Yi, B. Lv, Z. Wang, S. Nie, L. Wang, L. Kong, Y. Huang, P. Richard, P. Zhang, K. Yaji, K. Kuroda, S. Shin, H. Weng, B. A. Bernevig, Y. Shi, T. Qian, and H. Ding, *Science Advances* **3** (2017), 10.1126/sciadv.1602415, <https://advances.sciencemag.org/content/3/5/e1602415.full.pdf>.
 - ¹⁸ G. Bian, T.-R. Chang, R. Sankar, S.-Y. Xu, H. Zheng, T. Neupert, C.-K. Chiu, S.-M. Huang, G. Chang, I. Belopolski, *et al.*, *Nature communications* **7**, 1 (2016).
 - ¹⁹ F. Schindler, Z. Wang, M. G. Vergniory, A. M. Cook, A. Murani, S. Sengupta, A. Y. Kasumov, R. Deblock, S. Jeon, I. Drozdov, *et al.*, *Nature physics* **14**, 918 (2018).
 - ²⁰ Z. Rao, H. Li, T. Zhang, S. Tian, C. Li, B. Fu, C. Tang, L. Wang, Z. Li, W. Fan, *et al.*, *Nature* **567**, 496 (2019).
 - ²¹ P. Zhang, Z. Wang, X. Wu, K. Yaji, Y. Ishida, Y. Kohama, G. Dai, Y. Sun, C. Bareille, K. Kuroda, *et al.*, *Nature Physics* **15**, 41 (2019).
 - ²² J. Alicea, *Reports on Progress in Physics* **75**, 076501 (2012).
 - ²³ M. Sato and S. Fujimoto, *Journal of the Physical Society of Japan* **85**, 072001 (2016), <https://doi.org/10.7566/JPSJ.85.072001>.
 - ²⁴ M. Sato and Y. Ando, *Reports on Progress in Physics* **80**, 076501 (2017).
 - ²⁵ S. Sasaki, M. Kriener, K. Segawa, K. Yada, Y. Tanaka, M. Sato, and Y. Ando, *Phys. Rev. Lett.* **107**, 217001 (2011).
 - ²⁶ V. Mourik, K. Zuo, S. M. Frolov, S. R. Plissard, E. P. A. M. Bakkers, and L. P. Kouwenhoven, *Science* **336**, 1003 (2012), <https://science.sciencemag.org/content/336/6084/1003.full.pdf>.
 - ²⁷ A. Das, Y. Ronen, Y. Most, Y. Oreg, M. Heiblum, and H. Shtrikman, *Nature Physics* **8**, 887 (2012).
 - ²⁸ S. Nadj-Perge, I. K. Drozdov, J. Li, H. Chen, S. Jeon, J. Seo, A. H. MacDonald, B. A. Bernevig, and A. Yazdani, *Science* **346** (2014), 10.1126/science.1259327.
 - ²⁹ J.-P. Xu, M.-X. Wang, Z. L. Liu, J.-F. Ge, X. Yang, C. Liu, Z. A. Xu, D. Guan, C. L. Gao, D. Qian, Y. Liu, Q.-H. Wang, F.-C. Zhang, Q.-K. Xue, and J.-F. Jia, *Phys. Rev. Lett.* **114**, 017001 (2015).
 - ³⁰ J.-X. Yin, Z. Wu, J. Wang, Z. Ye, J. Gong, X. Hou, L. Shan, A. Li, X. Liang, X. Wu, *et al.*, *Nature Physics* **11**, 543 (2015).
 - ³¹ D. Wang, L. Kong, P. Fan, H. Chen, S. Zhu, W. Liu, L. Cao, Y. Sun, S. Du, J. Schneeloch, *et al.*, *Science* **362** (2018), 10.1126/science.aao1797.
 - ³² H. Ren, F. Pientka, S. Hart, A. T. Pierce, M. Kosowsky, L. Lunczer, R. Schlereth, B. Scharf, E. M. Hankiewicz, L. W. Molenkamp, *et al.*, *Nature* **569**, 93 (2019).
 - ³³ A. Fornieri, A. M. Whiticar, F. Setiawan, E. Portolés, A. C. Drachmann, A. Keselman, S. Gronin, C. Thomas, T. Wang, R. Kallaher, *et al.*, *Nature* **569**, 89 (2019).
 - ³⁴ A. Palacio-Morales, E. Mascot, S. Cocklin, H. Kim, S. Rachel, D. K. Morr, and R. Wiesendanger, *Science Advances* **5** (2019), 10.1126/sciadv.aav6600, <https://advances.sciencemag.org/content/5/7/eaav6600.full.pdf>.
 - ³⁵ S. Kezilebieke, M. N. Huda, V. Vaño, M. Aapro, S. C. Ganguli, O. J. Silveira, S. Glódzik, A. S. Foster, T. Ojanen, and P. Liljeroth, *Nature* **588**, 424 (2020).
 - ³⁶ C. Chen, K. Jiang, Y. Zhang, C. Liu, Y. Liu, Z. Wang, and J. Wang, *Nature Physics* **16**, 536 (2020).
 - ³⁷ S. Vaitiekėnas, G. W. Winkler, B. van Heck, T. Karzig, M.-T. Deng, K. Flensberg, L. I. Glazman, C. Nayak, P. Krogstrup, R. M. Lutchyn, and C. M. Marcus, *Science* **367** (2020), 10.1126/science.aav3392, <https://science.sciencemag.org/content/367/6485/eaav3392.full.pdf>.
 - ³⁸ C. Nayak, S. H. Simon, A. Stern, M. Freedman, and S. Das Sarma, *Rev. Mod. Phys.* **80**, 1083 (2008).
 - ³⁹ S. Vijay, T. H. Hsieh, and L. Fu, *Phys. Rev. X* **5**, 041038 (2015).
 - ⁴⁰ B. Lian, X.-Q. Sun, A. Vaezi, X.-L. Qi, and S.-C. Zhang, *Proceedings of the Na-*

- tional Academy of Sciences **115**, 10938 (2018), <https://www.pnas.org/content/115/43/10938.full.pdf>.
- ⁴¹ L. Fu and C. L. Kane, *Phys. Rev. Lett.* **100**, 096407 (2008).
 - ⁴² H.-H. Sun, K.-W. Zhang, L.-H. Hu, C. Li, G.-Y. Wang, H.-Y. Ma, Z.-A. Xu, C.-L. Gao, D.-D. Guan, Y.-Y. Li, C. Liu, D. Qian, Y. Zhou, L. Fu, S.-C. Li, F.-C. Zhang, and J.-F. Jia, *Phys. Rev. Lett.* **116**, 257003 (2016).
 - ⁴³ Y.-F. Lv, W.-L. Wang, Y.-M. Zhang, H. Ding, W. Li, L. Wang, K. He, C.-L. Song, X.-C. Ma, and Q.-K. Xue, *Science Bulletin* **62**, 852 (2017).
 - ⁴⁴ Y. Yuan, J. Pan, X. Wang, Y. Fang, C. Song, L. Wang, K. He, X. Ma, H. Zhang, F. Huang, *et al.*, *Nature Physics* **15**, 1046 (2019).
 - ⁴⁵ Y. Li, H. Zheng, Y. Fang, D. Zhang, Y. Chen, C. Chen, A. Liang, W. Shi, D. Pei, L. Xu, *et al.*, *Nature communications* **12**, 1 (2021).
 - ⁴⁶ P. Zhang, K. Yaji, T. Hashimoto, Y. Ota, T. Kondo, K. Okazaki, Z. Wang, J. Wen, G. D. Gu, H. Ding, and S. Shin, *Science* **360**, 182 (2018), <https://science.sciencemag.org/content/360/6385/182.full.pdf>.
 - ⁴⁷ Q. Liu, C. Chen, T. Zhang, R. Peng, Y.-J. Yan, C.-H.-P. Wen, X. Lou, Y.-L. Huang, J.-P. Tian, X.-L. Dong, G.-W. Wang, W.-C. Bao, Q.-H. Wang, Z.-P. Yin, Z.-X. Zhao, and D.-L. Feng, *Phys. Rev. X* **8**, 041056 (2018).
 - ⁴⁸ L. Kong, S. Zhu, M. Papaj, H. Chen, L. Cao, H. Isobe, Y. Xing, W. Liu, D. Wang, P. Fan, *et al.*, *Nature Physics* **15**, 1181 (2019).
 - ⁴⁹ S. Zhu, L. Kong, L. Cao, H. Chen, M. Papaj, S. Du, Y. Xing, W. Liu, D. Wang, C. Shen, F. Yang, J. Schneeloch, R. Zhong, G. Gu, L. Fu, Y.-Y. Zhang, H. Ding, and H.-J. Gao, *Science* **367**, 189 (2020), <https://science.sciencemag.org/content/367/6474/189.full.pdf>.
 - ⁵⁰ T. Machida, Y. Sun, S. Pyon, S. Takeda, Y. Kohsaka, T. Hanaguri, T. Sasagawa, and T. Tamegai, *Nature materials* **18**, 811 (2019).
 - ⁵¹ W. Liu, L. Cao, S. Zhu, L. Kong, G. Wang, M. Papaj, P. Zhang, Y.-B. Liu, H. Chen, G. Li, *et al.*, *Nature communications* **11**, 1 (2020).
 - ⁵² L. Kong, L. Cao, S. Zhu, M. Papaj, G. Dai, G. Li, P. Fan, W. Liu, F. Yang, X. Wang, *et al.*, *arXiv preprint arXiv:2010.04735* (2020).
 - ⁵³ G. Xu, B. Lian, P. Tang, X.-L. Qi, and S.-C. Zhang, *Phys. Rev. Lett.* **117**, 047001 (2016).
 - ⁵⁴ Z. Wang, P. Zhang, G. Xu, L. K. Zeng, H. Miao, X. Xu, T. Qian, H. Weng, P. Richard, A. V. Fedorov, H. Ding, X. Dai, and Z. Fang, *Phys. Rev. B* **92**, 115119 (2015).
 - ⁵⁵ A. Y. Kitaev, *Physics-Uspekhi* **44**, 131 (2001).
 - ⁵⁶ A. P. Mackenzie and Y. Maeno, *Rev. Mod. Phys.* **75**, 657 (2003).
 - ⁵⁷ Y. Maeno, S. Kittaka, T. Nomura, S. Yonezawa, and K. Ishida, *Journal of the Physical Society of Japan* **81**, 011009 (2011).
 - ⁵⁸ C. Kallin and J. Berlinsky, *Reports on Progress in Physics* **79**, 054502 (2016).
 - ⁵⁹ L. Jiao, S. Howard, S. Ran, Z. Wang, J. O. Rodriguez, M. Sigrist, Z. Wang, N. P. Butch, and V. Madhavan, *Nature* **579**, 523 (2020).
 - ⁶⁰ X.-L. Qi, T. L. Hughes, and S.-C. Zhang, *Phys. Rev. B* **82**, 184516 (2010).
 - ⁶¹ J. D. Sau, R. M. Lutchyn, S. Tewari, and S. Das Sarma, *Phys. Rev. Lett.* **104**, 040502 (2010).
 - ⁶² R. M. Lutchyn, J. D. Sau, and S. Das Sarma, *Phys. Rev. Lett.* **105**, 077001 (2010).
 - ⁶³ Y. Oreg, G. Refael, and F. von Oppen, *Phys. Rev. Lett.* **105**, 177002 (2010).
 - ⁶⁴ J. Alicea, *Phys. Rev. B* **81**, 125318 (2010).
 - ⁶⁵ Y. Ando and L. Fu, *Annual Review of Condensed Matter Physics* **6**, 361 (2015), <https://doi.org/10.1146/annurev-conmatphys-031214-014501>.
 - ⁶⁶ S. Sasaki and T. Mizushima, *Physica C: Superconductivity and its Applications* **514**, 206 (2015), superconducting Materials: Conventional, Unconventional and Undetermined.
 - ⁶⁷ H. Zhang, C.-X. Liu, X.-L. Qi, X. Dai, Z. Fang, and S.-C. Zhang, *Nature physics* **5**, 438 (2009).
 - ⁶⁸ Y. Xia, D. Qian, D. Hsieh, L. Wray, A. Pal, H. Lin, A. Bansil, D. Grauer, Y. S. Hor, R. J. Cava, *et al.*, *Nature physics* **5**, 398 (2009).
 - ⁶⁹ Y. L. Chen, J. G. Analytis, J.-H. Chu, Z. K. Liu, S.-K. Mo, X. L. Qi, H. J. Zhang, D. H. Lu, X. Dai, Z. Fang, S. C. Zhang, I. R. Fisher, Z. Hussain, and Z.-X. Shen, *Science* **325**, 178 (2009), <https://science.sciencemag.org/content/325/5937/178.full.pdf>.
 - ⁷⁰ D. Hsieh, Y. Xia, L. Wray, D. Qian, A. Pal, J. H. Dil, J. Osterwalder, F. Meier, G. Bihlmayer, C. L. Kane, Y. S. Hor, R. J. Cava, and M. Z. Hasan, *Science* **323**, 919 (2009), <https://science.sciencemag.org/content/323/5916/919.full.pdf>.
 - ⁷¹ Y. S. Hor, A. J. Williams, J. G. Checkelsky, P. Roushan, J. Seo, Q. Xu, H. W. Zandbergen, A. Yazdani, N. P. Ong, and R. J. Cava, *Phys. Rev. Lett.* **104**, 057001 (2010).
 - ⁷² Z. Liu, X. Yao, J. Shao, M. Zuo, L. Pi, S. Tan, C. Zhang, and Y. Zhang, *Journal of the American Chemical Society* **137**, 10512 (2015), PMID: 26262431, <https://doi.org/10.1021/jacs.5b06815>.
 - ⁷³ Shruti, V. K. Maurya, P. Neha, P. Srivastava, and S. Patnaik, *Phys. Rev. B* **92**, 020506 (2015).
 - ⁷⁴ Y. Qiu, K. N. Sanders, J. Dai, J. E. Medvedeva, W. Wu, P. Ghaemi, T. Vojta, and Y. S. Hor, *arXiv preprint arXiv:1512.03519* (2015).
 - ⁷⁵ Z. Wang, A. A. Taskin, T. Frölich, M. Braden, and Y. Ando, *Chemistry of Materials* **28**, 779 (2016), <https://doi.org/10.1021/acs.chemmater.5b03727>.
 - ⁷⁶ S. Yonezawa, K. Tajiri, S. Nakata, Y. Nagai, Z. Wang, K. Segawa, Y. Ando, and Y. Maeno, *Nature Physics* **13**, 123 (2017).
 - ⁷⁷ K. Matano, M. Kriener, K. Segawa, Y. Ando, and G.-q. Zheng, *Nature Physics* **12**, 852 (2016).
 - ⁷⁸ R. Tao, Y.-J. Yan, X. Liu, Z.-W. Wang, Y. Ando, Q.-H. Wang, T. Zhang, and D.-L. Feng, *Phys. Rev. X* **8**, 041024 (2018).
 - ⁷⁹ T. Asaba, B. J. Lawson, C. Tinsman, L. Chen, P. Corbae, G. Li, Y. Qiu, Y. S. Hor, L. Fu, and L. Li, *Phys. Rev. X* **7**, 011009 (2017).
 - ⁸⁰ G. Du, Y. Li, J. Schneeloch, R. Zhong, G. Gu, H. Yang, H. Lin, and H.-H. Wen, *Science China Physics, Mechanics & Astronomy* **60**, 037411 (2017).
 - ⁸¹ Y. Pan, A. Nikitin, G. Araizi, Y. Huang, Y. Matsushita, T. Naka, and A. De Visser, *Scientific reports* **6**, 1 (2016).
 - ⁸² L. Fu and E. Berg, *Phys. Rev. Lett.* **105**, 097001 (2010).
 - ⁸³ J. W. F. Venderbos, V. Kozii, and L. Fu, *Phys. Rev. B* **94**, 180504 (2016).
 - ⁸⁴ T. H. Hsieh, H. Lin, J. Liu, W. Duan, A. Bansil, and L. Fu, *Nature communications* **3**, 1 (2012).
 - ⁸⁵ A. S. Erickson, J.-H. Chu, M. F. Toney, T. H. Geballe, and I. R. Fisher, *Phys. Rev. B* **79**, 024520 (2009).
 - ⁸⁶ Y. Matsushita, H. Bluhm, T. H. Geballe, and I. R. Fisher,

- Phys. Rev. Lett. **94**, 157002 (2005).
- ⁸⁷ S. Sasaki, Z. Ren, A. A. Taskin, K. Segawa, L. Fu, and Y. Ando, Phys. Rev. Lett. **109**, 217004 (2012).
- ⁸⁸ H. Yang, Y.-Y. Li, T.-T. Liu, D.-D. Guan, S.-Y. Wang, H. Zheng, C. Liu, L. Fu, and J.-F. Jia, Phys. Rev. Lett. **125**, 136802 (2020).
- ⁸⁹ A. P. Schnyder, S. Ryu, A. Furusaki, and A. W. W. Ludwig, Phys. Rev. B **78**, 195125 (2008).
- ⁹⁰ S. Ryu, A. P. Schnyder, A. Furusaki, and A. W. W. Ludwig, New Journal of Physics **12**, 065010 (2010).
- ⁹¹ X.-L. Qi, T. L. Hughes, and S.-C. Zhang, Phys. Rev. B **81**, 134508 (2010).
- ⁹² G. E. Volovik, *The universe in a helium droplet*, Vol. 117 (Oxford University Press on Demand, 2003).
- ⁹³ S. A. Yang, H. Pan, and F. Zhang, Phys. Rev. Lett. **113**, 046401 (2014).
- ⁹⁴ W. A. Benalcazar, B. A. Bernevig, and T. L. Hughes, Science **357**, 61 (2017).
- ⁹⁵ W. A. Benalcazar, B. A. Bernevig, and T. L. Hughes, Phys. Rev. B **96**, 245115 (2017).
- ⁹⁶ Z. Song, Z. Fang, and C. Fang, Phys. Rev. Lett. **119**, 246402 (2017).
- ⁹⁷ E. Khalaf, Phys. Rev. B **97**, 205136 (2018).
- ⁹⁸ S. Ono, H. C. Po, and H. Watanabe, Science Advances **6** (2020), 10.1126/sciadv.aaz8367, <https://advances.sciencemag.org/content/6/18/eaaz8367.full.pdf>.
- ⁹⁹ F. Schindler, A. M. Cook, M. G. Vergniory, Z. Wang, S. S. P. Parkin, B. A. Bernevig, and T. Neupert, Science Advances **4** (2018), 10.1126/sciadv.aat0346, <https://advances.sciencemag.org/content/4/6/eaat0346.full.pdf>.
- ¹⁰⁰ J. Langbehn, Y. Peng, L. Trifunovic, F. von Oppen, and P. W. Brouwer, Phys. Rev. Lett. **119**, 246401 (2017).
- ¹⁰¹ F. Zhang, C. L. Kane, and E. J. Mele, Phys. Rev. Lett. **110**, 046404 (2013).
- ¹⁰² Z. Yan, F. Song, and Z. Wang, Phys. Rev. Lett. **121**, 096803 (2018).
- ¹⁰³ Q. Wang, C.-C. Liu, Y.-M. Lu, and F. Zhang, Phys. Rev. Lett. **121**, 186801 (2018).
- ¹⁰⁴ R.-X. Zhang, W. S. Cole, and S. Das Sarma, Phys. Rev. Lett. **122**, 187001 (2019).
- ¹⁰⁵ S. Qin, C. Fang, F.-C. Zhang, and J. Hu, arXiv preprint arXiv:2106.04200 (2021).
- ¹⁰⁶ V. K. Maurya, Shruti, P. Srivastava, and S. Patnaik, EPL (Europhysics Letters) **108**, 37010 (2014).
- ¹⁰⁷ T. Hashimoto, K. Yada, M. Sato, and Y. Tanaka, Phys. Rev. B **92**, 174527 (2015).

Appendix A: Momentum dependence of intra- and inter-pocket interaction

The lattice structure and Brillouin zone are shown as Fig.1. We introduce the density density interaction in the paper written as below,

$$H_{\text{int}} = U_0 \sum_i \hat{n}_i \hat{n}_i + \frac{U_1}{2} \sum_{\langle ij \rangle} \hat{n}_i \hat{n}_j + \frac{U_2}{2} \sum_{\langle\langle ij \rangle\rangle} \hat{n}_i \hat{n}_j. \quad (\text{A1})$$

We take the Fourier transformation to Eq.A1 and obtain,

$$H_{\text{int}} = \frac{1}{N} \sum_{\mathbf{K}_1, \mathbf{K}_2, \mathbf{q}, l_1, l_2} \hat{\psi}_{\mathbf{K}_1+\mathbf{q}, l_1}^\dagger \hat{\psi}_{\mathbf{K}_1, l_1} \hat{\psi}_{\mathbf{K}_2-\mathbf{q}, l_2}^\dagger \hat{\psi}_{\mathbf{K}_2, l_2} \left(U_0 + \frac{U_1}{2} \sum_{\langle ij \rangle} e^{-i\mathbf{r}_{ij} \cdot \mathbf{q}} + \frac{U_2}{2} \sum_{\langle\langle ij \rangle\rangle} e^{-i\mathbf{r}_{ij} \cdot \mathbf{q}} \right), \quad (\text{A2})$$

where N is the number of the sites. We restrict the electronic states involved in the interaction within an area near the Fermi surfaces and set $\mathbf{K} = \mathbf{L}_n + \mathbf{k}$, $\mathbf{K} + \mathbf{q} = \mathbf{L}_m + \mathbf{k}'$, $|E_{\mathbf{k}} - \mu| < \delta\mu$, $|E_{\mathbf{k}'} - \mu| < \delta\mu$, where \mathbf{L}_m is the vector from the Γ point to \mathbf{L}_m point; $E_{\mathbf{k}}$ is the kinetic energy of the states with momentum $\mathbf{L}_{1,2,3,4} + \mathbf{k}$; μ is the chemical potential and $\delta\mu$ is the cutoff energy in the summation, $\delta\mu \ll \mu$. We can derive $|\mathbf{k}|, |\mathbf{k}'| \sim k_F \ll |\mathbf{L}_{1,2,3,4}|$, $\mathbf{q} = \mathbf{L}_m - \mathbf{L}_n + \mathbf{k}' - \mathbf{k} = \mathbf{L}_{mn} + \tilde{\mathbf{q}}$ with $\mathbf{L}_{mn} = \mathbf{L}_m - \mathbf{L}_n$ and $\tilde{\mathbf{q}} \equiv \mathbf{k}' - \mathbf{k}$, $|\tilde{\mathbf{q}}| \ll |\mathbf{L}_{mn}|$. We define a new density operator $\hat{\rho}_{\tilde{\mathbf{q}}, mn} = \widetilde{\sum_{\mathbf{k}, l}} \hat{\psi}_l^\dagger(\mathbf{k} + \tilde{\mathbf{q}} + \mathbf{L}_m) \hat{\psi}_l(\mathbf{k} + \mathbf{L}_n)$, where we use $\widetilde{\sum_{\mathbf{k}}}$ to denote a cutoff on both the kinetic energy $E_{\mathbf{k}}$ and $E_{\mathbf{k}+\tilde{\mathbf{q}}}$ in the summation. The superconductivity is contributed by the pairs of electronic states with opposite momentum on the same Fermi surface. The interaction can be decomposed into two parts, one as the superconductivity pairing with $\mathbf{K}_1 = \mathbf{L}_m + \mathbf{k}$ and $\mathbf{K}_2 = \mathbf{L}_m - \mathbf{k}$ and the other as the non-superconductivity part,

$$\begin{aligned} H_{\text{int}} = & \frac{1}{N} \widetilde{\sum_{\tilde{\mathbf{q}}, m=n}} \hat{\rho}_{\tilde{\mathbf{q}}, mm} \hat{\rho}_{-\tilde{\mathbf{q}}, mm} \left(U_0 + \frac{U_1}{2} \sum_{\langle ij \rangle} e^{-i\mathbf{r}_{ij} \cdot \tilde{\mathbf{q}}} + \frac{U_2}{2} \sum_{\langle\langle ij \rangle\rangle} e^{-i\mathbf{r}_{ij} \cdot \tilde{\mathbf{q}}} \right) \\ & + \frac{1}{N} \widetilde{\sum_{\tilde{\mathbf{q}}, m, n}} \hat{\rho}_{\tilde{\mathbf{q}}, mn} \hat{\rho}_{-\tilde{\mathbf{q}}, mn} \left(U_0 + \frac{U_1}{2} \sum_{\langle ij \rangle} e^{-i\mathbf{r}_{ij} \cdot (\tilde{\mathbf{q}} + \mathbf{L}_{mn})} + \frac{U_2}{2} \sum_{\langle\langle ij \rangle\rangle} e^{-i\mathbf{r}_{ij} \cdot (\tilde{\mathbf{q}} + \mathbf{L}_{mn})} \right) \\ & + \text{Non-SC}. \end{aligned} \quad (\text{A3})$$

From Fig.1(a) we can obtain $\mathbf{r}_{\langle ij \rangle} = \frac{a_0}{2}(\pm 1, \pm 1, 0)^\top$, $\frac{a_0}{2}(\pm 1, 0, \pm 1)^\top$, $\frac{a_0}{2}(0, \pm 1, \pm 1)^\top$ and $\mathbf{r}_{\langle\langle ij \rangle\rangle} = a_0(\pm 1, 0, 0)^\top$, $a_0(0, \pm 1, 0)^\top$, $a_0(0, 0, \pm 1)^\top$. From Fig.1(b) we can obtain $\mathbf{L}_{mn} = \frac{2\pi}{a_0}(\pm 1, 0, 0)^\top$, $\frac{2\pi}{a_0}(0, \pm 1, 0)^\top$, $\frac{2\pi}{a_0}(0, 0, \pm 1)^\top$. We substitute $\mathbf{r}_{\langle ij \rangle}$, $\mathbf{r}_{\langle\langle ij \rangle\rangle}$ and \mathbf{L}_{mn} into Eq.A3 and obtain the coefficient functions of the terms contributing to the superconductivity as follows,

a. *Intra-pocket the nearest neighbors,*

$$\begin{aligned} H_{\text{int-intra-n}} = & \frac{1}{N} \frac{U_1}{2} \sum_{\tilde{\mathbf{q}}, m} \sum_{\omega, \omega' = x, y, z}^{\omega \neq \omega'} \hat{\rho}_{\tilde{\mathbf{q}}, mm} \hat{\rho}_{-\tilde{\mathbf{q}}, mm} \left(e^{-i\frac{a_0}{2}(\tilde{q}_\omega + \tilde{q}_{\omega'})} + e^{-i\frac{a_0}{2}(\tilde{q}_\omega - \tilde{q}_{\omega'})} + e^{-i\frac{a_0}{2}(-\tilde{q}_\omega + \tilde{q}_{\omega'})} + e^{-i\frac{a_0}{2}(-\tilde{q}_\omega - \tilde{q}_{\omega'})} \right) \\ = & \frac{1}{N} U_1 \sum_{\tilde{\mathbf{q}}, m} \sum_{\omega, \omega' = x, y, z}^{\omega \neq \omega'} \hat{\rho}_{\tilde{\mathbf{q}}, mm} \hat{\rho}_{-\tilde{\mathbf{q}}, mm} \left(\cos\left(\frac{a_0}{2}(\tilde{q}_\omega + \tilde{q}_{\omega'})\right) + \cos\left(\frac{a_0}{2}(\tilde{q}_\omega - \tilde{q}_{\omega'})\right) \right) \\ = & \frac{1}{N} U_1 \sum_{\tilde{\mathbf{q}}, m} \hat{\rho}_{\tilde{\mathbf{q}}, mm} \hat{\rho}_{-\tilde{\mathbf{q}}, mm} \left(6 - \frac{a_0^2}{2}(\tilde{q}_x^2 + \tilde{q}_y^2 + \tilde{q}_z^2) \right), \end{aligned} \quad (\text{A4})$$

b. *Intra-pocket the next nearest neighbors,*

$$\begin{aligned} H_{\text{int-intra-nn}} = & \frac{1}{N} \frac{U_2}{2} \sum_{\tilde{\mathbf{q}}, m} \hat{\rho}_{\tilde{\mathbf{q}}, mm} \hat{\rho}_{-\tilde{\mathbf{q}}, mm} \left(e^{ia_0\tilde{q}_x} + e^{-ia_0\tilde{q}_x} + e^{ia_0\tilde{q}_y} + e^{-ia_0\tilde{q}_y} + e^{i\frac{a_0}{2}\tilde{q}_z} + e^{-i\frac{a_0}{2}\tilde{q}_z} \right) \\ = & \frac{1}{N} U_2 \sum_{\tilde{\mathbf{q}}, m} \hat{\rho}_{\tilde{\mathbf{q}}, mm} \hat{\rho}_{-\tilde{\mathbf{q}}, mm} \left(\cos(a_0\tilde{q}_x) + \cos(a_0\tilde{q}_y) + \cos(a_0\tilde{q}_z) \right) \\ = & \frac{1}{N} U_1 \sum_{\tilde{\mathbf{q}}, m} \hat{\rho}_{\tilde{\mathbf{q}}, mm} \hat{\rho}_{-\tilde{\mathbf{q}}, mm} \left(3 - \frac{a_0^2}{2}(\tilde{q}_x^2 + \tilde{q}_y^2 + \tilde{q}_z^2) \right), \end{aligned} \quad (\text{A5})$$

c. *Inter-pocket the nearest neighbors,*

$$\begin{aligned}
H_{\text{int-inter-n}} &= \frac{1}{N} \frac{U_1}{2} \sum_{\tilde{\mathbf{q}}mn} \sum_{\langle ij \rangle} \hat{\rho}_{\tilde{\mathbf{q}},mn} \hat{\rho}_{-\tilde{\mathbf{q}},mn} e^{-i(\mathbf{L}_{mn} \cdot \mathbf{r}_{ij} + \tilde{\mathbf{q}} \cdot \mathbf{r}_{ij})} \\
&= \frac{1}{N} U_1 \sum_{\tilde{\mathbf{q}}mn} \hat{\rho}_{\tilde{\mathbf{q}},mn} \hat{\rho}_{-\tilde{\mathbf{q}},mn} \left(\cos(\pi + \frac{a_0}{2}(\tilde{q}_{\perp 1} + \tilde{q}_{\parallel})) + \cos(\pi + \frac{a_0}{2}(\tilde{q}_{\perp 1} - \tilde{q}_{\parallel})) \right. \\
&\quad \left. + \cos(\pi + \frac{a_0}{2}(\tilde{q}_{\perp 2} + \tilde{q}_{\parallel})) + \cos(\pi + \frac{a_0}{2}(\tilde{q}_{\perp 2} - \tilde{q}_{\parallel})) + \cos(\frac{a_0}{2}(\tilde{q}_{\perp 1} + \tilde{q}_{\perp 2})) + \cos(\frac{a_0}{2}(\tilde{q}_{\perp 1} - \tilde{q}_{\perp 2})) \right) \\
&= \frac{1}{N} U_1 \sum_{\tilde{\mathbf{q}}mn} \hat{\rho}_{\tilde{\mathbf{q}},mn} \hat{\rho}_{-\tilde{\mathbf{q}},mn} (-2 + \frac{1}{2} \tilde{q}_{\parallel}^2),
\end{aligned} \tag{A6}$$

where we use \tilde{q}_{\parallel} to denote the component of $\tilde{\mathbf{q}}$ parallel to \mathbf{L}_{mn} and $\tilde{q}_{\perp 1,2}$ to denote the other two components perpendicular to \mathbf{L}_{mn} . For example, we take $m = 1$, $n = 2$, $\mathbf{L}_{12} = \frac{2\pi}{a_0}(-1, 0, 0)$. \tilde{q}_{\parallel} is taken as \tilde{q}_x and $\tilde{q}_{\perp 1,2}$ are taken as \tilde{q}_y and \tilde{q}_z .

d. *Inter-pocket the next nearest neighbors,*

$$\begin{aligned}
H_{\text{int-intra-nn}} &= \frac{1}{N} \frac{U_2}{2} \sum_{\tilde{\mathbf{q}}mn} \hat{\rho}_{\tilde{\mathbf{q}},mn} \hat{\rho}_{-\tilde{\mathbf{q}},mn} \left(e^{i(2\pi + a_0 \tilde{q}_{\parallel})} + e^{i(2\pi - a_0 \tilde{q}_{\parallel})} + e^{ia_0 \tilde{q}_{\perp 1}} + e^{-ia_0 \tilde{q}_{\perp 1}} + e^{i\frac{a_0}{2} \tilde{q}_{\perp 2}} + e^{-i\frac{a_0}{2} \tilde{q}_{\perp 2}} \right) \\
&= \frac{1}{N} U_2 \sum_{\tilde{\mathbf{q}}} \hat{\rho}_{\tilde{\mathbf{q}},mn} \hat{\rho}_{-\tilde{\mathbf{q}},mn} \left(\cos(a_0 \tilde{q}_{\parallel}) + \cos(a_0 \tilde{q}_{\perp 1}) + \cos(a_0 \tilde{q}_{\perp 2}) \right) \\
&= \frac{1}{N} U_1 \sum_{\tilde{\mathbf{q}}} \hat{\rho}_{\tilde{\mathbf{q}},mn} \hat{\rho}_{-\tilde{\mathbf{q}},mn} \left(3 - \frac{a_0^2}{2} (\tilde{q}_{\parallel}^2 + \tilde{q}_{\perp 1}^2 + \tilde{q}_{\perp 2}^2) \right).
\end{aligned} \tag{A7}$$

Here we simplify $\tilde{q}_x^2 + \tilde{q}_y^2 + \tilde{q}_z^2$ and $\tilde{q}_{\parallel}^2 + \tilde{q}_{\perp 1}^2 + \tilde{q}_{\perp 2}^2$ as \tilde{q}^2 and write the interaction as $H_{\text{int}} = \sum_{i,\tilde{\mathbf{q}}} \frac{1}{N} U_i f_i(\tilde{\mathbf{q}} + \mathbf{L}_{mn}) \hat{\rho}_{\tilde{\mathbf{q}},mn} \hat{\rho}_{-\tilde{\mathbf{q}},mn}$ with $f_i(\tilde{\mathbf{q}} + \mathbf{L}_{mn})$ listed in Table I.

Appendix B: Projection from orbital basis to the band basis

In the weak pairing limit, only the interaction between the states on the Fermi level is essential. In the above, we have constrained the momentum \mathbf{K} and $\mathbf{K} + \mathbf{q}$ near the Fermi surfaces and take an energy cutoff in the summation. To obtain the interaction generating the superconductivities, we need to project the states near the Fermi surfaces involved in the interaction to the states occupying the Fermi level, which are labelled by the angular momentum along $\Gamma\mathbf{L}_m$. We first establish four local reference frames with \mathbf{L}_m as the coordinate origin and $\Gamma\mathbf{L}_m$ as the z axis shown in Fig. 5. The axes of the local reference frame on \mathbf{L}_1 written in the global reference frame are defined as,

$$\begin{aligned}
\mathbf{x} &= \left(\frac{\sqrt{2}}{2}, -\frac{\sqrt{2}}{2}, 0 \right)^{\text{T}} \\
\mathbf{y} &= \left(\frac{\sqrt{6}}{6}, \frac{\sqrt{6}}{6}, -\sqrt{\frac{2}{3}} \right)^{\text{T}} \\
\mathbf{z} &= \left(\sqrt{\frac{1}{3}}, \sqrt{\frac{1}{3}}, \sqrt{\frac{1}{3}} \right)^{\text{T}},
\end{aligned}$$

and the other three coordinates of the local reference frames can be obtained by taking C_4 rotation on the first one along k_Z axis. We transform the states created by the operator $\hat{\psi}^{\dagger}(\mathbf{k} + \mathbf{L}_m)$ in the global reference frame to the states created by the operator $\hat{\phi}^{\dagger}(\mathbf{k})$ in the local reference frames by the operator \hat{U}_m , $\hat{\psi}_l^{\dagger}(\mathbf{k} + \mathbf{L}_m) = \hat{U}_m \hat{\phi}_{m,l}^{\dagger}(\mathbf{k}) \hat{U}_m^{\dagger} = \sum_w \mathcal{U}_{wl}^m \hat{\phi}_{m,w}^{\dagger}(\mathbf{k})$ and $\hat{\psi}_l(\mathbf{k} + \mathbf{L}_m) = \hat{U}_m \hat{\phi}_{m,l}(\mathbf{k}) \hat{U}_m^{\dagger} = \sum_w \mathcal{U}_{wl}^{m*} \hat{\phi}_{m,w}(\mathbf{k})$. For the intra-pocket interaction, $m = n$, the

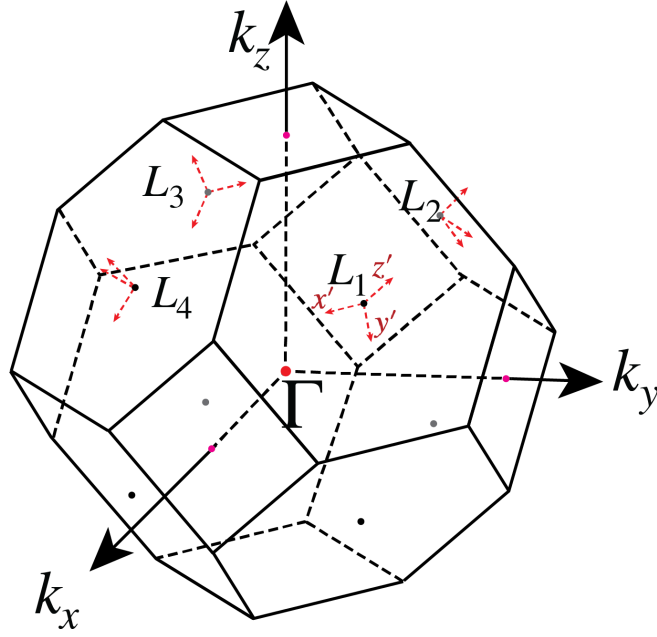


FIG. 5. The local reference coordinates on four L points.

density operator is transformed as,

$$\begin{aligned}
 \hat{\rho}_{\tilde{\mathbf{q}},mm} &= \widetilde{\sum_{\mathbf{k},l}} \hat{\psi}_l^\dagger(\mathbf{k} + \tilde{\mathbf{q}} + \mathbf{L}_m) \hat{\psi}_l(\mathbf{k} + \mathbf{L}_m) \\
 &= \widetilde{\sum_{\mathbf{k},l}} \hat{U}_m \hat{\phi}_{m,l}^\dagger(\mathbf{k} + \tilde{\mathbf{q}}) \hat{U}_m^\dagger \hat{U}_m \hat{\phi}_{n,l}(\mathbf{k}) \hat{U}_m^\dagger \\
 &= \widetilde{\sum_{\mathbf{k},l,w,v}} \mathcal{U}_{wl}^m \mathcal{U}_{vl}^{m*} \hat{\phi}_{m,w}^\dagger(\mathbf{k} + \tilde{\mathbf{q}}) \hat{\phi}_{n,v}(\mathbf{k}) \\
 &= \widetilde{\sum_{\mathbf{k},w}} \hat{\phi}_{m,w}^\dagger(\mathbf{k} + \tilde{\mathbf{q}}) \hat{\phi}_{m,w}(\mathbf{k}).
 \end{aligned} \tag{B1}$$

We use the fact that the similarity transformation matrix \mathcal{U}^m is unitary and $\sum_l \mathcal{U}_{wl}^m \mathcal{U}_{vl}^{m*} = \delta_{wv}$. For the inter-pocket interaction, $m \neq n$, we have,

$$\begin{aligned}
 \hat{\rho}_{\tilde{\mathbf{q}},mn} &= \widetilde{\sum_{\mathbf{k},l}} \hat{\psi}_l^\dagger(\mathbf{k} + \tilde{\mathbf{q}} + \mathbf{L}_m) \hat{\psi}_l(\mathbf{k} + \mathbf{L}_n) \\
 &= \widetilde{\sum_{\mathbf{k},l}} \hat{U}_m \hat{\phi}_{m,l}^\dagger(\mathbf{k} + \tilde{\mathbf{q}}) \hat{U}_m^\dagger \hat{U}_n \hat{\phi}_{n,l}(\mathbf{k}) \hat{U}_n^\dagger \\
 &= \widetilde{\sum_{\mathbf{k},l,w,v}} \mathcal{U}_{wl}^m \mathcal{U}_{vl}^{n*} \hat{\phi}_{m,w}^\dagger(\mathbf{k} + \tilde{\mathbf{q}}) \hat{\phi}_{n,v}(\mathbf{k}) \\
 &= \widetilde{\sum_{\mathbf{k},w,v}} \mathcal{D}_{wv}^{mn} \hat{\phi}_{m,w}^\dagger(\mathbf{k} + \tilde{\mathbf{q}}) \hat{\phi}_{n,v}(\mathbf{k}),
 \end{aligned} \tag{B2}$$

where the matrix \mathcal{D}^{mn} can be obtained by the following two steps. (i) The representation of the density operator $\hat{\rho}_{\tilde{\mathbf{q}},mn}$ is an identity matrix in the global reference frame and is invariant under the similarity transformation. We take a rotation on the global reference frame and make the directions of the axes coinciding with the local reference frame on L_1 . (ii) We take C_4 rotation to transform the orbitals defined in the reference coordinates of the local reference frame on L_1 to the orbitals in the local reference frames m and n , so the matrix \mathcal{U}^m can be obtained as $\mathcal{U}^m = e^{-\frac{i}{2}(m-1)\frac{\pi}{2}\boldsymbol{\sigma}\cdot\hat{\mathbf{z}}} \otimes e^{-i(m-1)\frac{\pi}{2}\mathbf{s}\cdot\hat{\mathbf{z}}}$. $\boldsymbol{\sigma} = (\sigma_x, \sigma_y, \sigma_z)$, $\mathbf{s} = (s_x, s_y, s_z)$. $\sigma_{x,y,z}$ and $s_{x,y,z}$ are the generators of $SU(2)$

and $SO(3)$ group. \hat{z} is the unit vector in the direction of the k_Z axis in the local reference frame, $\hat{z} = (0, -\sqrt{\frac{2}{3}}, \sqrt{\frac{1}{3}})^T$. The matrix \mathcal{D}^{mn} is obtained as $\mathcal{D}^{mn} = \mathcal{U}^m \mathcal{U}^{n\dagger}$. The interaction under the basis of the four local reference frames is obtained as,

$$\begin{aligned} H_{\text{int}} = & \sum_{m\tilde{\mathbf{q}}\mathbf{k}l_1l_2} \hat{\phi}_{m,\mathbf{k}+\tilde{\mathbf{q}},l_1}^\dagger \hat{\phi}_{m,-\mathbf{k}-\tilde{\mathbf{q}},l_2}^\dagger \hat{\phi}_{m,-\mathbf{k},l_2} \hat{\phi}_{m,\mathbf{k},l_1} (U_0 + U_1 f_1(\tilde{\mathbf{q}}) + U_2 f_2(\tilde{\mathbf{q}})) \\ & + \sum_{\tilde{\mathbf{q}}\mathbf{k}mn} \sum_{w_1w_2v_1v_2} \mathcal{D}_{w_1v_1}^{mn} \mathcal{D}_{w_2v_2}^{mn} \hat{\phi}_{m,\mathbf{k}+\tilde{\mathbf{q}},w_1}^\dagger \hat{\phi}_{m,-\mathbf{k}-\tilde{\mathbf{q}},w_2}^\dagger \hat{\phi}_{n,-\mathbf{k},v_2} \hat{\phi}_{n,\mathbf{k},v_1} (U_0 + U_1 f_1(\tilde{\mathbf{q}} + \mathbf{L}_{mn}) + U_2 f_2(\tilde{\mathbf{q}} + \mathbf{L}_{mn})) \quad (\text{B3}) \\ & + \text{Non-SC.} \end{aligned}$$

For the next step, we transform the orbital w_1, w_2, v_1 and v_2 in the local reference frames to the eigenstates of the C_3 rotation along ΓL_m with eigenvalues $j_z = \pm\frac{1}{2}, |J = \frac{3}{2}, j_z = \pm\frac{1}{2}\rangle, |J = \frac{1}{2}, j_z = \pm\frac{1}{2}\rangle$ in each pocket. The relations between the orbital basis and angular momentum basis can be obtained by Clebsch-Gordan coefficients,

$$\begin{aligned} |J = \frac{1}{2}, j_z = \frac{1}{2}\rangle &= -\frac{1}{\sqrt{3}}|p_z, \uparrow\rangle - \frac{1}{\sqrt{3}}|p_x, \downarrow\rangle - \frac{i}{\sqrt{3}}|p_y, \downarrow\rangle \\ |J = \frac{3}{2}, j_z = \frac{1}{2}\rangle &= \sqrt{\frac{2}{3}}|p_z, \uparrow\rangle - \frac{1}{\sqrt{6}}|p_x, \downarrow\rangle - \frac{i}{\sqrt{6}}|p_y, \downarrow\rangle \\ |J = \frac{1}{2}, j_z = -\frac{1}{2}\rangle &= \frac{1}{\sqrt{3}}|p_z, \downarrow\rangle - \frac{1}{\sqrt{3}}|p_x, \uparrow\rangle + \frac{i}{\sqrt{3}}|p_y, \uparrow\rangle \\ |J = \frac{3}{2}, j_z = -\frac{1}{2}\rangle &= \sqrt{\frac{2}{3}}|p_z, \downarrow\rangle + \frac{1}{\sqrt{6}}|p_x, \uparrow\rangle - \frac{i}{\sqrt{6}}|p_y, \uparrow\rangle. \end{aligned} \quad (\text{B4})$$

We obtain the interaction under the angular momentum basis as,

$$\begin{aligned} H_{\text{int}} = & \sum_{m\tilde{\mathbf{q}}\mathbf{k}t_1t_2} \hat{\phi}_{m,\mathbf{k}+\tilde{\mathbf{q}},t_1}^\dagger \hat{\phi}_{m,-\mathbf{k}-\tilde{\mathbf{q}},t_2}^\dagger \hat{\phi}_{m,-\mathbf{k},t_2} \hat{\phi}_{m,\mathbf{k},t_1} (U_0 + U_1 f_1(\tilde{\mathbf{q}}) + U_2 f_2(\tilde{\mathbf{q}})) \\ & + \sum_{\tilde{\mathbf{q}}\mathbf{k}mn} \sum_{w_1w_2v_1v_2} \sum_{t_1t_2r_1r_2} \mathcal{G}_{w_1t_1}^* \mathcal{D}_{w_1v_1}^{mn} \mathcal{G}_{v_1r_1} \mathcal{G}_{w_2t_2}^* \mathcal{D}_{w_2v_2}^{mn} \mathcal{G}_{v_2r_2} \hat{\phi}_{m,\mathbf{k}+\tilde{\mathbf{q}},t_1}^\dagger \hat{\phi}_{m,-\mathbf{k}-\tilde{\mathbf{q}},t_2}^\dagger \hat{\phi}_{n,-\mathbf{k},r_2} \hat{\phi}_{n,\mathbf{k},r_1} (U_0 + U_1 f_1(\mathbf{q}) + U_2 f_2(\mathbf{q})) \\ & + \text{Non-SC,} \end{aligned} \quad (\text{B5})$$

where we have the indices $t_{1,2}, r_{1,2} = 1, 2, 3, 4$ denoting the basis $|J = \frac{1}{2}, j_z = \frac{1}{2}\rangle, |J = \frac{3}{2}, j_z = \frac{1}{2}\rangle, |J = -\frac{1}{2}, j_z = \frac{1}{2}\rangle$ and $|J = \frac{3}{2}, j_z = -\frac{1}{2}\rangle$, respectively. $\mathcal{G}_{w'_1t_1}$ is the transformation coefficient with $w'_1 = 1, 2, 3, 4, 5, 6$ indicate the orbitals in the local reference frame $(\uparrow, \downarrow) \otimes (p_x, p_y, p_z)$,

$$\mathcal{G} = \begin{pmatrix} 0 & 0 & -\frac{1}{\sqrt{3}} & \frac{1}{\sqrt{6}} \\ 0 & 0 & \frac{i}{\sqrt{3}} & -\frac{i}{\sqrt{6}} \\ -\frac{1}{\sqrt{3}} & \sqrt{\frac{2}{3}} & 0 & 0 \\ -\frac{1}{\sqrt{3}} & -\frac{1}{\sqrt{6}} & 0 & 0 \\ -\frac{i}{\sqrt{3}} & -\frac{i}{\sqrt{6}} & 0 & 0 \\ 0 & 0 & \frac{1}{\sqrt{3}} & \sqrt{\frac{2}{3}} \end{pmatrix} \quad (\text{B6})$$

We can simplify the interaction as,

$$\begin{aligned} H_{\text{int}} = & \sum_{m\tilde{\mathbf{q}}\mathbf{k}t_1t_2} \hat{\phi}_{m,\mathbf{k}+\tilde{\mathbf{q}},t_1}^\dagger \hat{\phi}_{m,-\mathbf{k}-\tilde{\mathbf{q}},t_2}^\dagger \hat{\phi}_{m,-\mathbf{k},t_2} \hat{\phi}_{m,\mathbf{k},t_1} (U_0 + U_1 f_1(\tilde{\mathbf{q}}) + U_2 f_2(\tilde{\mathbf{q}})) \\ & + \sum_{\tilde{\mathbf{q}}\mathbf{k}mn} \sum_{t_1t_2r_1r_2} (\mathcal{G}^\dagger \mathcal{D}^{mn} \mathcal{G})_{t_1r_1} (\mathcal{G}^\dagger \mathcal{D}^{mn} \mathcal{G})_{t_2r_2} \hat{\phi}_{m,\mathbf{k}+\tilde{\mathbf{q}},t_1}^\dagger \hat{\phi}_{m,-\mathbf{k}-\tilde{\mathbf{q}},t_2}^\dagger \hat{\phi}_{n,-\mathbf{k},r_2} \hat{\phi}_{n,\mathbf{k},r_1} (U_0 + U_1 f_1(\mathbf{q}) + U_2 f_2(\mathbf{q})) \end{aligned} \quad (\text{B7})$$

and according to the effective Hamiltonian H_{mix} on the Fermi surface introduced in the paper, we take the two eigenstates $|j_z = \pm\frac{1}{2}\rangle_2$ as the states occupying the Fermi level. Finally, we project the interaction in the global

reference frame to the band basis on four Fermi surfaces and obtain as below,

$$\begin{aligned}
H_{\text{int}} = & \sum_{m\tilde{\mathbf{q}}\mathbf{k}d_1d_2} \hat{c}_{m,\mathbf{k}+\tilde{m},\mathbf{q},d_1}^\dagger \hat{c}_{m,-\mathbf{k}-\tilde{\mathbf{q}},d_2}^\dagger \hat{c}_{m,-\mathbf{k},d_2} \hat{c}_{m,\mathbf{k},d_1} (U_0 + U_1 f_1(\tilde{\mathbf{q}}) + U_2 f_2(\tilde{\mathbf{q}})) \\
& + \sum_{\tilde{\mathbf{q}}\mathbf{k}mn} \sum_{d_1d_2g_1g_2} (\mathcal{M}^\dagger \mathcal{G}^\dagger \mathcal{D}^{mn} \mathcal{G} \mathcal{M})_{d_1g_1} (\mathcal{M}^\dagger \mathcal{G}^\dagger \mathcal{D}^{mn} \mathcal{G} \mathcal{M})_{d_2g_2} \hat{c}_{m,\mathbf{k}+\tilde{\mathbf{q}},d_1}^\dagger \hat{c}_{m,-\mathbf{k}-\tilde{\mathbf{q}},d_2}^\dagger \hat{c}_{n,-\mathbf{k},g_2} \hat{c}_{n,\mathbf{k},g_1} (U_0 + U_1 f_1(\mathbf{q}) + U_2 f_2(\mathbf{q})) \\
& + \text{Non-SC.}
\end{aligned} \tag{B8}$$

Here we use $\hat{c}_{m,\mathbf{k},d}$ to denote the states on the Fermi level of the m -th pocket with pseudo-spin d taken as \uparrow or \downarrow . \mathcal{M} is composed by the eigenstates $|j_z = \pm \frac{1}{2}\rangle_2$,

$$\mathcal{M} = \begin{pmatrix} \cos \frac{\theta}{2} & 0 \\ \sin \frac{\theta}{2} & 0 \\ 0 & -\cos \frac{\theta}{2} \\ 0 & \sin \frac{\theta}{2} \end{pmatrix} \tag{B9}$$

Appendix C: Inducing irreps of point group O_h from point group D_{3d}

The point group O_h is the semidirect product of point group D_{3d} and the four fold cyclic group $\{C_4, C_4^2, C_4^3, C_4^4\}$, which means $O_h = \{D_{3d}, C_4 D_{3d}, C_4^2 D_{3d}, C_4^3 D_{3d}\} = \{D_{3d}, D_{3d} C_4, D_{3d} C_4^2, D_{3d} C_4^3\}$. So we can obtain that for any element R_1 in the point group D_{3d} , we can always find another element R_2 also in D_{3d} which satisfies $R_1 C_4^\alpha = C_4^\beta R_2$. α can be taken as 1, 2, 3, 4 and with a certain α , we can find a β satisfying the relation,

$$\forall \alpha \in \{1, 2, 3, 4\}, R_1 \in D_{3d}, \exists \beta \in \{1, 2, 3, 4\}, R_2 \in D_{3d}, R_1 C_4^\alpha = C_4^\beta R_2. \tag{C1}$$

In the point group D_{3d} , there are three C_2 rotation symmetry denoted as C_{2a} , C_{2b} and C_{2c} . The axis of C_{2a} coincides with the x axis in the local reference frame. The axes of C_{2b} and C_{2c} are obtained by the C_3 rotation of the axis of C_{2a} along ΓL . We take one element from each class of D_{3d} , C_3 and C_{2a} , to solve the relations in Eq. C1. S_6 and σ_d are trivial for they are the products of C_3 , C_2 and the inversion symmetry which irrep is an identity matrix for even parity and an identity matrix with a minus sign for odd parity,

$$\begin{aligned}
C_3 C_4 &= C_4^3 C_3^2 \\
C_3 C_4^2 &= C_4 C_{2b} \\
C_3 C_4^3 &= C_4^2 C_{2c},
\end{aligned} \tag{C2}$$

$$\begin{aligned}
C_{2a} C_4 &= C_4^3 C_{2a}^2 \\
C_{2a} C_4^2 &= C_4^2 C_{2a} \\
C_3 C_4^3 &= C_4 C_{2a}.
\end{aligned} \tag{C3}$$

In the paper we have already shown the irreps basis of D_{3d} denoted as $\hat{\delta}_{\iota,\eta}$. The index ι indicates the irreps and η indicates the component of the irreps. For the one dimensional irreps like $a_{1g(u)}$ and $a_{2g(u)}$, $\eta = 1$, while for $e_{u(g)}$, $\eta = 1, 2$. For the element R in the group D_{3d} , we have,

$$R \hat{\delta}_{\iota,\eta_1} = \sum_{\eta_2} \hat{\delta}_{\eta_2} \mathcal{R}_\iota(R)_{\eta_2 \eta_1}, \tag{C4}$$

where $\mathcal{R}_\eta(R)$ is the irreps matrix of the element R . Now we add a superscript m on the irreps basis to denote $\hat{\delta}_{\iota,\eta}^m$ on the m -th pocket. In the last section, we act C_4 rotation on the first local reference frame directly to obtain the

other three, so we have $C_4^i \hat{\delta}_{\iota, \eta}^m = \hat{\delta}_{\iota, \eta}^{(m+i) \bmod 4}$. We can obtain the representations of C_4 and C_4^2 in the equation below,

$$\begin{aligned} \mathbb{R}_\iota(C_4) &= \begin{pmatrix} 0 & 0 & 0 & \mathcal{I}_\iota \\ \mathcal{I}_\iota & 0 & 0 & 0 \\ 0 & \mathcal{I}_\iota & 0 & 0 \\ 0 & 0 & \mathcal{I}_\iota & 0 \end{pmatrix} \\ \mathbb{D}(C_4^2) &= \begin{pmatrix} 0 & 0 & \mathcal{I}_\iota & 0 \\ 0 & 0 & 0 & \mathcal{I}_\iota \\ \mathcal{I}_\iota & 0 & 0 & 0 \\ 0 & \mathcal{I}_\iota & 0 & 0 \end{pmatrix}, \end{aligned} \tag{C5}$$

where we use \mathcal{I}_ι to denote the identity matrix with the same dimension as the irreps of D_{3d} indicated by ι . With Eq.C2, Eq.C3 and Eq.C4 we can induce the representations of group O_h based on the irreps basis of group D_{3d} , $\{\hat{\delta}_\iota^1, \hat{\delta}_\iota^2, \hat{\delta}_\iota^3, \hat{\delta}_\iota^4\}$. We suppress the index η to denote $\hat{\delta}_\iota^m$ as a vector written as $\{\hat{\delta}_{\iota,1}^m, \dots, \hat{\delta}_{\iota,\eta}^m\}$,

$$\begin{aligned} C_3 \hat{\delta}_\iota^1 &= \hat{\delta}_\iota^1 \mathcal{R}_\iota(C_3) \\ C_3 \hat{\delta}_\iota^2 &= C_3 C_4 \hat{\delta}_\iota^1 \\ &= C_4^3 C_3^2 \hat{\delta}_\iota^1 \\ &= C_4^3 \hat{\delta}_\iota^1 \mathcal{R}_\iota(C_3^2) \\ &= \hat{\delta}_\iota^4 \mathcal{R}_\iota(C_3^2) \\ C_3 \hat{\delta}_\iota^3 &= C_3 C_4^2 \hat{\delta}_\iota^1 \\ &= C_4 C_{2b} \hat{\delta}_\iota^1 \\ &= C_4 \hat{\delta}_\iota^1 \mathcal{R}_\iota(C_{2b}) \\ &= \hat{\delta}_\iota^2 \mathcal{R}_\iota(C_{2b}) \\ C_3 \hat{\delta}_\iota^4 &= C_3 C_4^3 \hat{\delta}_\iota^1 \\ &= C_4^2 C_{2c} \hat{\delta}_\iota^1 \\ &= C_4^2 \hat{\delta}_\iota^1 \mathcal{R}_\iota(C_{2c}) \\ &= \hat{\delta}_\iota^3 \mathcal{R}_\iota(C_{2c}), \end{aligned} \tag{C6}$$

and similarly, for C_{2a} we have,

$$\begin{aligned}
C_{2a}\hat{\delta}_l^1 &= \hat{\delta}_l^1 \mathcal{R}_l(C_{2a}) \\
C_{2a}\hat{\delta}_l^2 &= C_{2a}C_4\hat{\delta}_l^1 \\
&= C_4^3 C_{2a}\hat{\delta}_l^1 \\
&= C_4^3 \hat{\delta}_l^1 \mathcal{R}_l(C_{2a}) \\
&= \hat{\delta}_l^4 \mathcal{R}_l(C_{2a}) \\
C_{2a}\hat{\delta}_l^3 &= C_{2a}C_4^2\hat{\delta}_l^1 \\
&= C_4^2 C_{2a}\hat{\delta}_l^1 \\
&= C_4^2 \hat{\delta}_l^1 \mathcal{R}_l(C_{2a}) \\
&= \hat{\delta}_l^3 \mathcal{R}_l(C_{2b}) \\
C_{2a}\hat{\delta}_l^4 &= C_{2a}C_4^3\hat{\delta}_l^1 \\
&= C_4 C_{2a}\hat{\delta}_l^1 \\
&= C_4 \hat{\delta}_l^1 \mathcal{R}_l(C_{2a}) \\
&= \hat{\delta}_l^2 \mathcal{R}_l(C_{2a}).
\end{aligned} \tag{C7}$$

With the two equations above, we can obtain the induced representation of C_3 and C_{2a} of group O_h as,

$$\mathbb{R}_l(C_3) = \begin{pmatrix} \mathcal{R}_l(C_3) & 0 & 0 & 0 \\ 0 & 0 & \mathcal{R}_l(C_{2b}) & 0 \\ 0 & 0 & 0 & \mathcal{R}_l(C_{2c}) \\ 0 & \mathcal{R}_l(C_3^2) & 0 & 0 \end{pmatrix} \tag{C8}$$

$$\mathbb{R}_l(C_{2a}) = \begin{pmatrix} \mathcal{R}_l(C_{2a}) & 0 & 0 & 0 \\ 0 & 0 & 0 & \mathcal{R}_l(C_{2a}) \\ 0 & 0 & \mathcal{R}_l(C_{2a}) & 0 \\ 0 & \mathcal{R}_l(C_{2a}) & 0 & 0 \end{pmatrix} \tag{C9}$$

We use $\mathbb{R}_l(R)$ to denote the representations of O_h and all of the irreps of D_{3d} , $\mathcal{R}_l(R)$, are listed in Table.VIII. So far,

TABLE VII. The irreps matrices of point group D_{3d}

	C_3	C_3^2	C_{2a}	C_{2b}	C_{2c}
$a_{1g}(u)$	1	1	1	1	1
$a_{2g}(u)$	1	1	-1	-1	-1
$e_{g(u)}$	$\begin{pmatrix} -\frac{1}{2} & -\frac{\sqrt{3}}{2} \\ \frac{\sqrt{3}}{2} & -\frac{1}{2} \end{pmatrix}$	$\begin{pmatrix} -\frac{1}{2} & \frac{\sqrt{3}}{2} \\ -\frac{\sqrt{3}}{2} & -\frac{1}{2} \end{pmatrix}$	$\begin{pmatrix} 1 & 0 \\ 0 & -1 \end{pmatrix}$	$\begin{pmatrix} -\frac{1}{2} & -\frac{\sqrt{3}}{2} \\ -\frac{\sqrt{3}}{2} & \frac{1}{2} \end{pmatrix}$	$\begin{pmatrix} -\frac{1}{2} & \frac{\sqrt{3}}{2} \\ \frac{\sqrt{3}}{2} & \frac{1}{2} \end{pmatrix}$

we have obtained the induced representations of C_3 , C_{2a} , C_4 and C_4^2 which belong to different classes in group O_h . The induced representations are not irreps apparently and we decompose the induced representations into the irreps as the equation below,

$$X\mathbb{R}_l(R)X^\dagger = \bigoplus_{\epsilon} \left(\bigoplus_{c_\epsilon} \mathcal{R}_\epsilon(R) \right), \tag{C10}$$

where X is a similarity transformation matrix and c_ϵ denotes how many times the irrep $\mathcal{R}_\epsilon(R)$ appear in the decomposition with ϵ indicating the irreps of O_h . c_ϵ can be obtained as $c_\epsilon = \sum_{R \in O_h} \frac{1}{g} \chi_\epsilon(R)^* \chi(R)$. g is the order of the

group which equals to 48 for O_h . $\chi_\epsilon(R)$ is the character of the irreps of the element R and $\chi(R)$ is the character of \mathbb{R}_ϵ . At last, we decompose the induced representations as below,

$$\begin{aligned} X_1 \mathbb{R}_{a_{1u(g)}}(R) X_1^\dagger &= \mathcal{R}_{A_{1u(g)}}(R) \oplus \mathcal{R}_{T_{2u(g)}}(R) \\ X_2 \mathbb{R}_{a_{2u(g)}}(R) X_2^\dagger &= \mathcal{R}_{A_{2u(g)}}(R) \oplus \mathcal{R}_{T_{1u(g)}}(R) \\ X_3 \mathbb{R}_{e_{u(g)}}(R) X_3^\dagger &= \mathcal{R}_{E_{u(g)}}(R) \oplus \mathcal{R}_{T_{1u(g)}}(R) \oplus \mathcal{R}_{T_{2u(g)}}(R). \end{aligned} \quad (C11)$$

We use $a_{1u(g)}$, $a_{2u(g)}$ and $e_{u(g)}$ to denote irreps of D_{3d} distinguishing with the irreps of O_h written as $A_{1u(g)}$, $A_{2u(g)}$, $E_{u(g)}$, $T_{1u(g)}$ and $T_{2u(g)}$. The similarity matrices $X_{1,2,3}$ can be solved out to obtain the induced irreps basis of group O_h which are shown explicitly in the paper.

Appendix D: Singlet states excluded from our consideration

We expand the interaction to the second order of \mathbf{q} . The pairing function of the zeroth order is a constant and the interaction in the zeroth order is decomposed into $\hat{\delta}_{a_{1g}}^\dagger \hat{\delta}_{a_{1g}}$. The pairing function of the second order takes the form as $\tilde{\mathbf{q}}^2 = \mathbf{k}^2 + \mathbf{k}'^2 - 2\mathbf{k}\mathbf{k}'$. Among them, \mathbf{k}^2 and \mathbf{k}'^2 are the singlet pairing functions. So the interaction is decomposed as $\hat{\delta}_\epsilon^\dagger \hat{\delta}_{a_{1g}} + \text{h.c.}$. The irrep a_{1g} can only be induced as A_{1g} and T_{2g} of group O_h , so the singlet pairing channels can be only the A_{1g} channel and T_{2g} channel. For A_{1g} channel, the representation is trivial for every group element which is topologically trivial. For T_{2g} channel, the topologically nontrivial structure is protected by the mirror symmetry σ_d , however, the mirror plane of σ_d doesn't go through the Fermi surfaces and the T_{2g} channel is topologically trivial too.

We assume the on-site interaction strength $|U_0|$ much bigger than the other two, $|U_0| \gg |U_1|, |U_2|$. When the on-site interaction is attractive, $U_0 < 0$, the interaction in Eq.B8 is dominated by the term in the zeroth order of \mathbf{k} . The intra-pocket interaction can be decomposed as,

$$X_1 \bigoplus_m \left(\hat{\delta}_{a_{1g}}^{m\dagger} \hat{\delta}_{a_{1g}}^m \right) X_1^\dagger = \hat{\Delta}_{A_{1g}}^\dagger \hat{\Delta}_{A_{1g}} \oplus \hat{\Delta}_{T_{2g}}^\dagger \hat{\Delta}_{T_{2g}}. \quad (D1)$$

We use $\hat{\Delta}_\epsilon$ to denote the irreps basis of O_h group. For the inter-pocket interaction, the interaction in the zeroth order of \mathbf{k} can be written in the matrix form as,

$$H_{\text{int, inter, 0th}} = U_0 \left(\hat{\delta}_{a_{1g}}^{1\dagger}, \hat{\delta}_{a_{1g}}^{2\dagger}, \hat{\delta}_{a_{1g}}^{3\dagger}, \hat{\delta}_{a_{1g}}^{4\dagger} \right) \bigoplus_{m,n \in \{1,2,3,4\}} ((\mathcal{M}^\dagger \mathcal{G}^\dagger \mathcal{D}^{mn} \mathcal{G} \mathcal{M})(\mathcal{M}^\dagger \mathcal{G}^\dagger \mathcal{D}^{mn} \mathcal{G} \mathcal{M})) \begin{pmatrix} \hat{\delta}_{a_{1g}}^1 \\ \hat{\delta}_{a_{1g}}^2 \\ \hat{\delta}_{a_{1g}}^3 \\ \hat{\delta}_{a_{1g}}^4 \end{pmatrix} \quad (D2)$$

The singlet pairing only has one state, so we suppress the index t_1, t_2, r_1, r_2 in Eq.B8 and by calculation, we have,

$$\bigoplus_{m,n \in \{1,2,3,4\}} ((\mathcal{M}^\dagger \mathcal{G}^\dagger \mathcal{D}^{mn} \mathcal{G} \mathcal{M})(\mathcal{M}^\dagger \mathcal{G}^\dagger \mathcal{D}^{mn} \mathcal{G} \mathcal{M})) = \frac{1}{12} (4 \cos(\theta) + 3 \cos(2\theta) + 5) \begin{pmatrix} 0 & 1 & 1 & 1 \\ 1 & 0 & 1 & 1 \\ 1 & 1 & 0 & 1 \\ 1 & 1 & 1 & 0 \end{pmatrix}, \quad (D3)$$

and the inter-pocket interaction in the zeroth order of \mathbf{k} can be decomposed as,

$$X_1 H_{\text{int, inter, 0th}} X_1^\dagger = \frac{1}{12} (4 \cos(\theta) + 3 \cos(2\theta) + 5) U_0 \left(3 \hat{\Delta}_{A_{1g}}^\dagger \hat{\Delta}_{A_{1g}} \oplus (-1) \hat{\Delta}_{T_{2g}}^\dagger \hat{\Delta}_{T_{2g}} \right). \quad (D4)$$

θ depicts the mixing extent between the states of $|J = \frac{3}{2}, j_z = \pm \frac{1}{2}\rangle$ and $|J = \frac{1}{2}, j_z = \pm \frac{1}{2}\rangle$ which is small but not zero. So we have $\frac{1}{12} (4 \cos(\theta) + 3 \cos(2\theta) + 5) < 1$ and $3 + \frac{1}{12} (4 \cos(\theta) + 3 \cos(2\theta) + 5) \gg 1 - \left(\frac{1}{12} (4 \cos(\theta) + 3 \cos(2\theta) + 5) \right)$. The interaction is dominated by the topologically trivial A_{1g} channel.

To seek for the topologically nontrivial structure, we set the on-site interaction repulsive, $U_0 > 0$. The coefficients of the channels decomposed from the interaction expanded to the zeroth order are positive. We then expand the interaction to the second order of \mathbf{k} . Here we use $\hat{\Delta}_{A_{1g}}^0$ and $\hat{\Delta}_{T_{2g}}^0$ to denote the basis composed by the pairs in the zeroth order of \mathbf{k} and $\hat{\Delta}_{A_{1g}}^2$ and $\hat{\Delta}_{T_{2g}}^2$ to denote the basis composed by the pairs in the second order of \mathbf{k} . The interaction decomposed into A_{1g} channel can be written as,

$$H_{\text{int}} = \left(\hat{\Delta}_{A_{1g}}^{0\dagger}, \hat{\Delta}_{A_{1g}}^{2\dagger} \right) \begin{pmatrix} h_0(\theta, U_0) & h(\theta, U_1, U_2) \\ h(\theta, U_1, U_2)^* & 0 \end{pmatrix} \begin{pmatrix} \hat{\Delta}_{A_{1g}}^0 \\ \hat{\Delta}_{A_{1g}}^2 \end{pmatrix}, \quad (D5)$$

where $h_0(\theta, U_0) = 3 + \frac{1}{12}(4\cos(\theta) + 3\cos(2\theta) + 5)$ obtained in the above and $|h(\theta, U_1, U_2)| \ll |h_0(\theta, U_0)|$. We diagonalize the H_{int} matrix and obtain the coefficient of each A_{1g} channel as $\frac{h_0(\theta, U_0)}{2} \pm \sqrt{\frac{h_0(\theta, U_0)^2}{4} + |h(\theta, U_1, U_2)|^2}$. And one of the two eigenvalues is negative but close to zero, $\lim_{|h(\theta, U_1, U_2)| \ll |h_0(\theta, U_0)|} \frac{h_0(\theta, U_0)}{2} - \sqrt{\frac{h_0(\theta, U_0)^2}{4} + |h(\theta, U_1, U_2)|^2} = -|\frac{h(\theta, U_1, U_2)}{h_0(\theta, U_0)}| |h(\theta, U_1, U_2)| \sim 0$. And the analysis for the T_{2g} channel is similar to A_{1g} . So in the condition of a repulsive on-site interaction, singlet pairing channels will not appear in the phase diagram and we only focus on the triplet pairing channels.

Appendix E: Mean-field approximation calculation

We use Δ to denote the superconducting gap, μ to denote the chemical potential. The interaction is restricted in the region near the Fermi surfaces so we integrate the dispersion of the BdG Hamiltonian with negative values within a shell in the Brillouin zone which contains the Fermi surfaces in it and we take the thickness of the shell as $2\delta\mu$, $\mu - \delta\mu < \frac{k_x^2 + k_y^2}{2m} + \frac{\xi k_z^2}{2m} < \mu + \delta\mu$. In the weak pairing limit, we have,

$$\Delta \ll \delta\mu \ll \mu. \quad (\text{E1})$$

The pairing part of the BdG Hamiltonian is written as,

$$H_{\text{pairing}} = (\hat{c}_{\mathbf{k},\uparrow}, \hat{c}_{\mathbf{k},\downarrow}) (id_1(\mathbf{k})\sigma_1\sigma_2 + id_2(\mathbf{k})\sigma_2\sigma_2 + id_3(\mathbf{k})\sigma_3\sigma_2) \begin{pmatrix} \hat{c}_{-\mathbf{k},\uparrow} \\ \hat{c}_{-\mathbf{k},\downarrow} \end{pmatrix} + \text{h.c.}, \quad (\text{E2})$$

where σ is the Pauli matrices. For the triplet states in the interaction expanded to the second order of \mathbf{k} , $d_{1,2,3}(\mathbf{k})$ are the linear functions of \mathbf{k} . In the spherical coordinates, $\mathbf{k} = k(\sin\theta\cos\phi, \sin\theta\sin\phi, \cos\theta)$, the linear function $d_{1,2,3}(\mathbf{k})$ can be written as $kd_{1,2,3}(\theta, \phi)$, where k is the magnitude of \mathbf{k} . We also write $d_i(\theta, \phi)$ into the vector form, $\mathbf{d} = (d_1(\theta, \phi), d_2(\theta, \phi), d_3(\theta, \phi))$. The dispersion of the BdG Hamiltonian can be obtained as,

$$E(k, \theta, \phi) = \pm \sqrt{\left(\frac{g(\theta, \phi)}{2m}k^2 - \mu\right)^2 + k^2\mathbf{d}^2 \pm 2k^2\sqrt{(\text{Re}(\mathbf{d}) \times \text{Im}(\mathbf{d})) \cdot (\text{Re}(\mathbf{d}) \times \text{Im}(\mathbf{d}))}}. \quad (\text{E3})$$

In the equation above, $g(\theta, \phi) = \sin^2\theta + \xi\cos^2\theta$. ξ is used to depict the anisotropy of the Fermi surfaces. For the simplicity, we suppress the variables θ, ϕ and write $g(\theta, \phi)$ and $d_i(\theta, \phi)$ as g and d_i in the following calculation. When the d_i function have the same phase, $\arg(d_1) = \arg(d_2) = \arg(d_3)$, we have $\text{Re}(\mathbf{d}) \times \text{Im}(\mathbf{d}) = 0$. In this condition, the system has lower free energy and the time reversal symmetry is respected. We take a gauge where $\arg(d_1) = \arg(d_2) = \arg(d_3) = 0$, d_1, d_2 and d_3 are all real and the dispersion takes the form as,

$$E(k, \theta, \phi) = \pm \sqrt{\left(\frac{g(\theta, \phi)}{2m}k^2 - \mu\right)^2 + k^2\mathbf{d}^2}. \quad (\text{E4})$$

We integrate the eigenvalues with minus sign over an area of a shell containing the Fermi surface on four pockets with a thickness of $\delta\mu$ to obtain the free energy. The free energy saved by the superconductivities is shown in the equation below,

$$\Delta E = \int d\Omega \int_{\frac{g}{2m}k^2 = \mu - \delta\mu}^{\frac{g}{2m}k^2 = \mu + \delta\mu} \rho_{\mathbf{k}} k^2 dk \left(\sqrt{\left(\frac{g}{2m}k^2 - \mu\right)^2 + \mathbf{d}^2 k^2} - \left|\frac{g}{2m}k^2 - \mu\right| \right) + \frac{N\lambda^2}{\tilde{f}(U_1, U_2)}, \quad (\text{E5})$$

where Ω stands for the solid angle, $d\Omega = \sin\theta d\theta d\phi$, $\rho_{\mathbf{k}}$ is the density of the states with respect of \mathbf{k} which is treated as a constant in the integral area. In the equation above, λ and $\tilde{f}(U_1, U_2)$ are short for λ_{ϵ} and $\tilde{f}_{\epsilon}(U_1, U_2)$. ϵ labels the channels with different symmetries and suppressed to not indicate any specific channel. λ_{ϵ} is the modulus of the vector $\Lambda_{\epsilon} = (\lambda_{\epsilon,1,1}, \dots, \lambda_{\epsilon,\kappa,\zeta})^T$ obtained from the meanfield approximation, $\lambda_{\epsilon,\kappa,\zeta} = \frac{1}{N} \sum_{\mathbf{k}} \tilde{f}_{\epsilon,\kappa}(U_1, U_2) \hat{\Delta}_{\epsilon,\kappa,\zeta} = \langle \tilde{f}_{\epsilon,\kappa}(U_1, U_2) \hat{\Delta}_{\epsilon,\kappa,\zeta} \rangle$ and $\hat{\Delta}_{\epsilon,\kappa,\zeta}$ is the ζ -th basis of the κ -th irrep in the channel ϵ . For example, we totally have 5 T_{2u} and T_{2u} is a three dimensional irrep. We take $\epsilon = T_{2u}$, $\kappa = 1, 2, 3, 4, 5$, $\zeta = 1, 2, 3$. In general, $\lambda_{\epsilon,\kappa,\zeta}$ is a complex number, however, constrained by the time reversal symmetry, we can take a gauge where $\lambda_{\epsilon,\kappa,\zeta}$ is real. $\tilde{f}_{\epsilon}(U_1, U_2)$ is the effective coefficient of the channel, $\tilde{f}_{\epsilon}(U_1, U_2) = \lambda_{\epsilon}^2 / \sum_{\kappa,\zeta} \frac{\lambda_{\epsilon,\kappa,\zeta}^2}{\tilde{f}_{\epsilon,\kappa}(U_1, U_2)}$. We write ΔE as $\Delta E' + \frac{\lambda^2}{\tilde{f}(U_1, U_2)}$. $\Delta E'$ is the

integral part of the equation above and we change the variable k in the integral to $x = k^2$ obtaining,

$$\Delta E' = \int d\Omega \int_{\frac{2m}{g}(\mu-\delta\mu)}^{\frac{2m}{g}(\mu+\delta\mu)} \rho_{\mathbf{k}} dx \frac{\sqrt{x}}{2} \left(\sqrt{\left(\frac{g}{2m}x - \mu\right)^2 + \mathbf{d}^2 x} - \left|\frac{g}{2m}x - \mu\right| \right), \quad (\text{E6})$$

and then we substitute x with $\frac{2m\mu}{g}t$ into the equation above and obtain,

$$\begin{aligned} \Delta E' &= \int d\Omega \int_{1-\frac{\delta\mu}{\mu}}^{1+\frac{\delta\mu}{\mu}} \rho_{\mathbf{k}} dt \frac{(2m)^{\frac{3}{2}} \mu^{\frac{5}{2}}}{2g^{\frac{3}{2}}} \sqrt{t} \left(\sqrt{(t-1)^2 + \frac{2m\mathbf{d}^2}{g\mu}t} - |t-1| \right) \\ &= \int d\Omega \int_{-\frac{\delta\mu}{\mu}}^{\frac{\delta\mu}{\mu}} \rho_{\mathbf{k}} dt \frac{(2m)^{\frac{3}{2}} \mu^{\frac{5}{2}}}{2g^{\frac{3}{2}}} \sqrt{t+1} \left(\sqrt{t^2 + \frac{2m\mathbf{d}^2}{g\mu}(t+1)} - |t| \right) \end{aligned} \quad (\text{E7})$$

According to the relation in Eq.E1, $\frac{\delta\mu}{\mu} \ll 1$, we have

$$\lim_{t \rightarrow 0} \sqrt{t+1} \left(\sqrt{t^2 + \frac{2m\mathbf{d}^2}{g\mu}(t+1)} - |t| \right) = \sqrt{t^2 + \frac{2m\mathbf{d}^2}{g\mu}} - |t| \quad (\text{E8})$$

We substitute Eq.E8 into Eq.E7 and simplify and calculate the integral as below,

$$\begin{aligned} \Delta E' &= \rho_{\mathbf{k}} \int d\Omega \frac{(2m)^{\frac{3}{2}} \mu^{\frac{5}{2}}}{g^{\frac{3}{2}}} \int_0^{\frac{\delta\mu}{\mu}} \left(\sqrt{t^2 + \frac{2m\mathbf{d}^2}{g\mu}} - t \right) \\ &= \rho_{\mathbf{k}} \int d\Omega \frac{(2m)^{\frac{3}{2}} \mu^{\frac{5}{2}}}{g^{\frac{3}{2}}} \left(\frac{1}{2} \frac{\delta\mu}{\mu} \sqrt{\frac{2m\mathbf{d}^2}{g\mu} + \frac{\delta\mu^2}{\mu^2}} + \frac{1}{2} \frac{2m\mathbf{d}^2}{g\mu} \ln \left(\frac{\delta\mu}{\mu} + \sqrt{\frac{2m\mathbf{d}^2}{g\mu} + \frac{\delta\mu^2}{\mu^2}} \right) - \frac{1}{4} \frac{2m\mathbf{d}^2}{g\mu} \ln \frac{2m\mathbf{d}^2}{g\mu} - \frac{1}{2} \frac{\delta\mu^2}{\mu^2} \right) \end{aligned} \quad (\text{E9})$$

And we also have $\frac{2m\mathbf{d}^2}{g\mu} / \frac{\delta\mu^2}{\mu^2} \ll 1$ derived from,

$$\frac{2m\mathbf{d}^2}{g\mu} / \frac{\delta\mu^2}{\mu^2} = \frac{2m\mathbf{d}^2\mu}{\delta\mu^2 g} = \frac{\mathbf{d}^2 k_F^2 \mu}{\delta\mu^2 \frac{g}{2m} k_F^2} = \frac{\Delta^2 \mu}{\delta\mu^2 \mu} = \frac{\Delta^2}{\delta\mu^2} \ll 1. \quad (\text{E10})$$

We approximate $\sqrt{\frac{2m\mathbf{d}^2}{g\mu} + \frac{\delta\mu^2}{\mu^2}} - \frac{\delta\mu}{\mu}$ as $\frac{1}{2} \frac{2m\mathbf{d}^2}{g\delta\mu}$ and $\sqrt{\frac{2m\mathbf{d}^2}{g\mu} + \frac{\delta\mu^2}{\mu^2}} + \frac{\delta\mu}{\mu}$ as $2 \frac{\delta\mu}{\mu}$ and substitute into Eq.E9 obtaining,

$$\begin{aligned} \Delta E' &= \int \rho_{\mathbf{k}} d\Omega \frac{(2m)^{\frac{3}{2}} \mu^{\frac{5}{2}}}{g^{\frac{3}{2}}} \left(\frac{1}{4} \frac{2m\mathbf{d}^2}{g\mu} + \frac{1}{4} \frac{2m\mathbf{d}^2}{g\mu} \ln \left(\frac{4g\delta\mu^2}{2m\mu\mathbf{d}^2} \right) + 0(d^2) \right) \\ &\sim \int \rho_{\mathbf{k}} d\Omega \frac{(2m)^{\frac{3}{2}} \mu^{\frac{5}{2}}}{g^{\frac{3}{2}}} \frac{1}{4} \frac{2m\mathbf{d}^2}{g\mu} \ln \left(\frac{4g\delta\mu^2}{2m\mu\mathbf{d}^2} \right). \end{aligned} \quad (\text{E11})$$

In the second line of the equation above, we adopt the approximation $\ln \left(\frac{4g\delta\mu^2}{2m\mu\mathbf{d}^2} \right) \gg 1$. g and \mathbf{d}^2 are the functions of θ and ϕ , meanwhile \mathbf{d} is the linear function of $\lambda_{\kappa, \zeta}$ of the channel, $d_i(\theta, \phi) = \sum_{\kappa, \zeta} \mathcal{A}(\theta, \phi)_{i, \kappa, \zeta} \lambda_{\kappa, \zeta}$. Now, we use one index j to indicate both κ and ζ and simplify the equation in a vector form $d_i(\theta, \phi) = \sum_j \mathcal{A}(\theta, \phi)_{i, j} \lambda_j$, so we have $\mathbf{d}(\theta, \phi) = \mathcal{A}(\theta, \phi) \Lambda = \lambda \mathcal{A}(\theta, \phi) \hat{\Lambda}$, where $\hat{\Lambda}$ is a unit vector, $\hat{\Lambda}^\dagger \hat{\Lambda} = 1$. The gap function is obtained as,

$$\mathbf{d}(\theta, \phi)^2 = \lambda^2 \hat{\Lambda}^\dagger \mathcal{A}(\theta, \phi)^\dagger \mathcal{A}(\theta, \phi) \hat{\Lambda} \quad (\text{E12})$$

We define $\mathbb{A}(\theta, \phi) = \mathcal{A}(\theta, \phi)^\dagger \mathcal{A}(\theta, \phi)$ and substitute Eq.E12 into Eq.E11 and have,

$$\Delta E = -\frac{(2m)^{\frac{5}{2}} \mu^{\frac{3}{2}} \lambda^2 \rho_{\mathbf{k}}}{4} \ln \frac{m\mu\lambda^2}{2\delta\mu^2} \int d\Omega \frac{1}{g^{\frac{5}{2}}} \hat{\Lambda}^\dagger \mathbb{A} \hat{\Lambda} - \frac{(2m)^{\frac{5}{2}} \mu^{\frac{3}{2}} \lambda^2 \rho_{\mathbf{k}}}{4} \int d\Omega \frac{1}{g^{\frac{5}{2}}} \hat{\Lambda}^\dagger \mathbb{A} \hat{\Lambda} \ln \frac{\hat{\Lambda}^\dagger \mathbb{A} \hat{\Lambda}}{g} + \frac{N\lambda^2}{\tilde{f}(U_1, U_2)}. \quad (\text{E13})$$

We set $\frac{(2m)^{\frac{5}{2}} \mu^{\frac{3}{2}}}{4} \rho_{\mathbf{k}} = \alpha$, $\int d\Omega \frac{1}{g^{\frac{5}{2}}} \hat{\Lambda}^\dagger \mathbb{A} \hat{\Lambda} = A$, $\frac{m\mu}{2\delta\mu^2} = \beta^2$, $\int d\Omega \frac{1}{g^{\frac{5}{2}}} \hat{\Lambda}^\dagger \mathbb{A} \hat{\Lambda} \ln \frac{\hat{\Lambda}^\dagger \mathbb{A} \hat{\Lambda}}{g} = B$ and the equation above can be simplified as,

$$\Delta E = -2\alpha A \lambda^2 \ln \beta \lambda - \alpha B \lambda^2 + \frac{N\lambda^2}{\tilde{f}(U_1, U_2)} \quad (\text{E14})$$

For a system, ξ , U_1 and U_2 are all determined. ΔE depends on λ and we choose the λ making the free energy lowest and ΔE biggest. With a certain $\hat{\lambda}$ we can solve A and B for each channel and the maximum of ΔE has λ satisfying $\frac{\partial \Delta E}{\partial \lambda} = 0$.

$$2\alpha A \ln \beta \lambda = \frac{N}{\tilde{f}(U_1, U_2)} - \alpha A - \alpha B. \quad (\text{E15})$$

We substitute the relation into ΔE and obtain,

$$\Delta E = \frac{A\alpha}{\beta^2} \exp\left(\frac{N}{A\tilde{f}(U_1, U_2)\alpha} - \frac{B}{A} - 1\right) \quad (\text{E16})$$

In the equation above, we have $\tilde{f}(U_1, U_2)\alpha \sim 0$ derivated as follows,

$$\tilde{f}(U_1, U_2)\alpha = \tilde{f}(U_1, U_2) \frac{(2m)^{\frac{5}{2}} \mu^{\frac{3}{2}} \rho_{\mathbf{k}}}{4} = \frac{\tilde{f}(U_1, U_2) k_F^2 \rho_{\mathbf{k}} m k_F (2m)^{\frac{3}{2}} \mu^{\frac{3}{2}}}{2k_F^3} \quad (\text{E17})$$

where $\tilde{f}(U_1, U_2) k_F^2$ is the interaction strength expanded to the second order of $\tilde{\mathbf{q}}$. We have $\rho_{\mathbf{k}} 4\pi k^2 dk \sim \rho_E dE$ with ρ_E as the density of states about the energy and $dE \sim \frac{k}{m} dk$ so we can derivate $\rho_{\mathbf{k}} k m \sim \rho_E$. We substitute the relation into the equation above,

$$\tilde{f}(U_1, U_2)\alpha \sim \frac{\tilde{f}(U_1, U_2) k_F^2 \rho_{E=\mu} (2m)^{\frac{3}{2}} \mu^{\frac{3}{2}}}{2k_F^3} \sim \frac{\tilde{f}(U_1, U_2) k_F^2 \rho_{E=\mu} \mu^{\frac{3}{2}}}{2\mu^{\frac{3}{2}}} \sim \tilde{f}(U_1, U_2) k_F^2 \rho_{FS} \sim 0, \quad (\text{E18})$$

where $\rho_{E=\mu}$ is the density of states at the Fermi surfaces. Constrained by the weak pairing limit, the production of interaction strength and the density of states is near to zero $\tilde{f}(U_1, U_2) k_F^2 \rho_{FS} \sim 0$. For the absolute vaule of the exponent is much bigger than 1, we take logarithm on both sides of the equation to compare the saved free energy of each channel,

$$\ln \Delta E = \frac{N}{A\tilde{f}(U_1, U_2)\alpha} - \frac{B}{A} - 1 + \ln \frac{A\alpha}{\beta^2}. \quad (\text{E19})$$

α , β are the same for every channel, so we drop the invariant terms and only compare the residual $\frac{N}{A\tilde{f}(U_1, U_2)\alpha} - \frac{B}{A} + \ln A$. The first term $\frac{N}{A\tilde{f}(U_1, U_2)\alpha}$ domains the saved free energy. A can be written as $(\mathcal{A}\hat{\lambda})^\dagger (\mathcal{A}\hat{\lambda})$ which is positive while $\tilde{f}(U_1, U_2)$ is negative. The bigger $|\mathcal{A}\tilde{f}(U_1, U_2)|$ is, the more free energy the system saves. The vaules of $\mathcal{A}\tilde{f}(U_1, U_2)$ are degenerated in the space spanned by the order parameter in the freedom of the index ζ . We decompose the vector of order parameter $\lambda_\epsilon \hat{\Lambda}_\epsilon$ into the direct product of two parts $\lambda_\epsilon \hat{\Lambda}_{\epsilon,\kappa} \otimes \hat{\Lambda}_{\epsilon,\zeta}$ and we obtain $\hat{\Lambda}_{\epsilon,\kappa}$ by maximizing $|\mathcal{A}\tilde{f}(U_1, U_2)|$ and obtain $\hat{\Lambda}_{\epsilon,\zeta}$ by minimizing B .

In the limit of zero mixture between states $|J = \frac{1}{2}, j_z = \pm \frac{1}{2}\rangle$ and $|J = \frac{3}{2}, j_z = \pm \frac{1}{2}\rangle$ on the Fermi surfaces, the Fermi level is contributed by $|J = \frac{1}{2}, j_z = \pm \frac{1}{2}\rangle$ and we obtain the interaction coefficients of each channels listed in Table.VIII. We can see that the sign of the coefficients of each channel are determined by the sign of U_1 and U_2 . The results from the first principle calculation require a small mixture angle θ so we treat the mixture as a pertubation and discuss the following three situations,

TABLE VIII. The interaction coefficients of each irrep in the limit of no mixture between $|J = \frac{1}{2}, j_z = \pm \frac{1}{2}\rangle$ and $|J = \frac{3}{2}, j_z = \pm \frac{1}{2}\rangle$ on the Fermi surfaces.

Irreps of the channels	Coefficients $\tilde{f}_{\epsilon,\kappa}(U_1, U_2)$
A_{1u}	$4U_2, 2U_1$
A_{2u}	$2U_1$
E_u	$4U_2, 2U_1, 2U_1$
T_{1u}	$4U_2, 2U_1, 2U_1, 0$
T_{2u}	$4U_2, 2U_1, 2U_1, 0, 0$

a. $U_2 < 0$, $U_1 > 0$. According to Table.VIII, four channels can contribute superconductivities and they are composed by one A_{1u} , one E_u , one T_{1u} and one T_{2u} , respectively. The difference between the interaction coefficients $\tilde{f}_\epsilon(U_1, U_2)$ of the four channels is treated as pertubation for they have the same coefficient equalling to $4U_2$ in the limit of zero mixture. All of the channels have only one component for $\hat{\Lambda}_{A_{1u},\kappa}$. For the one dimensional irrep A_{1u} , $\hat{\Lambda}_\zeta$ has only one component, too. So $\hat{\Lambda}_{A_{1u}} = 1$. While for E_u , $\hat{\Lambda}_\kappa$ has two components. We write $\hat{\Lambda}_\kappa = (\sin \theta, \cos \theta)^\top$. For T_{1u} and T_{2u} , $\hat{\Lambda}_\kappa$ has three components. We write $\hat{\Lambda}_\kappa = (\sin \theta \cos \phi, \sin \theta \sin \phi, \cos \theta)^\top$. We sample on θ , ϕ to obtain the minimum of B and obatin $\hat{\Lambda}_{E_u,\zeta} = (1, 0)^\top$ and $\hat{\Lambda}_{T_{1u},\zeta}, \hat{\Lambda}_{T_{2u},\zeta} = (1, 0, 0)^\top, (0, 1, 0)^\top, (0, 0, 1)^\top$.

b. $U_2 > 0, U_1 < 0$. According to Table.VIII, five channels can contribute the superconductivities and they are composed by one A_{1u} , one A_{2u} , two E_u , two T_{1u} and two T_{2u} , respectively. Similar to the last condition, they have the same coefficients in the limit of zero mixture and we treat the difference between $\tilde{f}_\epsilon(U_1, U_2)$ as perturbation. For A_{1u} and A_{2u} , $\hat{\Lambda}_\epsilon$ only has one component. However, for other channels, they are composed by two irreps and the vector $\hat{\Lambda}_\kappa$ have two components. We diagonalize the matrix \mathbb{A} selecting the eigenvector with bigger eigenvalue and obtain $\hat{\Lambda}_{\epsilon, \kappa} = (v_{\epsilon, 1}, v_{\epsilon, 2})^\top$. And then we write $\hat{\Lambda}_{E_u, \zeta} = (\sin \theta, \cos \theta)^\top$ and $\hat{\Lambda}_{T_{1u}(T_{2u}), \zeta} = (\sin \theta \cos \phi, \sin \theta \sin \phi, \cos \theta)^\top$. We sample on θ, ϕ to minimizing B and obtain $\hat{\Lambda}_{E_u, \zeta} = (1, 0)^\top$ and $\hat{\Lambda}_{T_{1u}(T_{2u}), \zeta} = (1, 0, 0)^\top, (0, 1, 0)^\top, (0, 0, 1)^\top$.

c. $U_2 < 0, U_1 < 0$. According to Table.VIII, five channels can contribute the superconductivities and they are composed by two A_{1u} , one A_{2u} , three E_u , three T_{1u} and three T_{2u} , respectively. Different from the two conditions above, the interaction coefficients of different irreps within one channel are not the same and the difference between $\tilde{f}_\epsilon(U_1, U_2)$ can not be treated as perturbation anymore. There is only one A_{2u} irrep. $\hat{\Lambda}_{A_{2u}}$ is a one component vector. While for other channels, we consider $\frac{1}{A\tilde{f}_\epsilon(U_1, U_2)}$ as a whole and solve the $\hat{\Lambda}_{\epsilon, \kappa}$ maximizing $\frac{1}{A\tilde{f}_\epsilon(U_1, U_2)}$. For A_{1u} , there are two components in the vector $\hat{\Lambda}_{A_{1u}, \kappa}$ and we set $\hat{\Lambda}_{A_{1u}, \kappa} = (\varphi_1, \varphi_2)^\top$. The effective interaction coefficient of the channel with the symmetry of A_{1u} $\tilde{f}_{A_{1u}}(U_1, U_2)$ can be obtained as,

$$\tilde{f}_{A_{1u}} = \frac{1}{\frac{\varphi_1^2}{4U_2} + \frac{\varphi_2^2}{2U_1}}. \quad (\text{E20})$$

Under the basis of $\hat{\Lambda}_{A_{1u}, \kappa} = (1, 0)^\top, (0, 1)^\top$, \mathbb{A} is a two by two matrix and we can obtain,

$$\mathbb{A} = \begin{pmatrix} a_{11} & a_{12} \\ a_{21} & a_{22} \end{pmatrix}, \quad A = \hat{\Lambda}_{A_{1u}, \kappa}^\dagger \mathbb{A} \hat{\Lambda}_{A_{1u}, \kappa} = \varphi_1^2 a_{11} + \varphi_2^2 a_{22} + (a_{12} + a_{21}) \varphi_1 \varphi_2. \quad (\text{E21})$$

We substitute Eq.E20 and Eq.E21 into $A\tilde{f}_{A_{1u}}(U_1, U_2)$ and obtain,

$$A\tilde{f}_{A_{1u}}(U_1, U_2) = \frac{\varphi_1^2 a_{11} + \varphi_2^2 a_{22} + (a_{12} + a_{21}) \varphi_1 \varphi_2}{\frac{\varphi_1^2}{4U_2} + \frac{\varphi_2^2}{2U_1}} = \frac{a_{11} \frac{\varphi_1^2}{\varphi_2^2} + a_{22} + (a_{12} + a_{21}) \frac{\varphi_1}{\varphi_2}}{\frac{1}{4U_2} \frac{\varphi_1^2}{\varphi_2^2} + \frac{1}{2U_1}}. \quad (\text{E22})$$

We write $x = \frac{\varphi_1}{\varphi_2}$ and calculate the derivation of $A\tilde{f}_{A_{1u}}(U_1, U_2)$ about the variable x ,

$$\frac{dA\tilde{f}_\epsilon(U_1, U_2)}{dx} = \frac{(a_{12} + a_{21}) \left(\frac{1}{2U_1} - \frac{1}{4U_2} x^2 \right) + \left(-\frac{a_{22}}{2U_2} + \frac{a_{11}}{U_1} \right) x}{\left(\frac{1}{4U_2} x^2 + \frac{1}{2U_1} \right)^2} \quad (\text{E23})$$

The matrix \mathbb{A} is Hermitian, $\mathbb{A} = \mathcal{A}^\dagger \mathcal{A}$. So $a_{12} = a_{21}^*$, $a_{12} + a_{21}$ is a real number. In the limitation of $x \rightarrow \pm\infty$, the denominator is in the fourth order of x while the numerator is in the order up to 2 of x depending on whether a_{12} and $\frac{a_{11}}{U_1} - \frac{a_{22}}{2U_2}$ are zero or not, thus we have $\lim_{x \rightarrow \pm\infty} \lim_{x \rightarrow \pm\infty} d(A\tilde{f}_\epsilon(U_1, U_2))/dx = 0$. And in the situation of $x \rightarrow \infty$ and $x \rightarrow -\infty$, the vector of $\hat{\Lambda}_{A_{1u}, \kappa}$ is taken as $(1, 0)^\top$ and $(-1, 0)^\top$ respectively, which are equal to a global phase -1 . So we have $\lim_{x \rightarrow \infty} A\tilde{f}_{A_{1u}}(U_1, U_2) = \lim_{x \rightarrow -\infty} A\tilde{f}_{A_{1u}}(U_1, U_2)$. We show the dispersion of $A\tilde{f}_{A_{1u}}(U_1, U_2)$ with respect to x in Fig.6 In Fig.6(a), $a_{12} < 0$, the derivation of $A\tilde{f}_{A_{1u}}(U_1, U_2)$ in Eq.E23 is positive with x taken as infinity, $\lim_{x \rightarrow \pm\infty} d(A\tilde{f}_\epsilon(U_1, U_2))/dx > 0$. In Fig.6(b), $a_{12} < 0$, we have $\lim_{x \rightarrow \pm\infty} d(A\tilde{f}_\epsilon(U_1, U_2))/dx < 0$. In Fig.6(c) and Fig.6(d), $a_{12} = 0$ and the \mathbb{A} matrix is diagonal. The vector $\hat{\Lambda}_{A_{1u}, \kappa}$ is taken as $(0, 1)^\top$ for $a_{11}/U_1 - a_{22}/2U_2 > 0$ and $(1, 0)^\top$ for $a_{11}/U_1 - a_{22}/2U_2 < 0$.

For E_u , T_{1u} and T_{2u} , $\hat{\Lambda}_{\epsilon, \kappa}$ has three components and we write $A\tilde{f}_{\epsilon, \kappa}(U_1, U_2)$ as,

$$A\tilde{f}_\epsilon(U_1, U_2) = \frac{\hat{\Lambda}_{\epsilon, \kappa}^\dagger \mathbb{A} \hat{\Lambda}_{\epsilon, \kappa}}{\hat{\Lambda}_{\epsilon, \kappa}^\dagger \mathbb{F} \hat{\Lambda}_{\epsilon, \kappa}}, \quad (\text{E24})$$

where \mathbb{F} is a three dimensional matrix, $1/\hat{\Lambda}_{\epsilon, \kappa}^\dagger \mathbb{F} \hat{\Lambda}_{\epsilon, \kappa} = \tilde{f}_\epsilon(U_1, U_2)$. Under the basis of $\hat{\Lambda}_{\epsilon, \kappa} = (1, 0, 0)^\top, (0, 1, 0)^\top, (0, 0, 1)^\top$, we can write matrices \mathbb{A} and \mathbb{F} as,

$$\mathbb{A} = \begin{pmatrix} a_{11} & a_{12} & a_{31} \\ a_{21} & a_{22} & a_{23} \\ a_{31} & a_{32} & a_{33} \end{pmatrix}, \quad \mathbb{F} = \begin{pmatrix} \frac{1}{\tilde{f}_{\epsilon, 1}(U_1, U_2)} & 0 & 0 \\ 0 & \frac{1}{\tilde{f}_{\epsilon, 2}(U_1, U_2)} & 0 \\ 0 & 0 & \frac{1}{\tilde{f}_{\epsilon, 3}(U_1, U_2)} \end{pmatrix}. \quad (\text{E25})$$

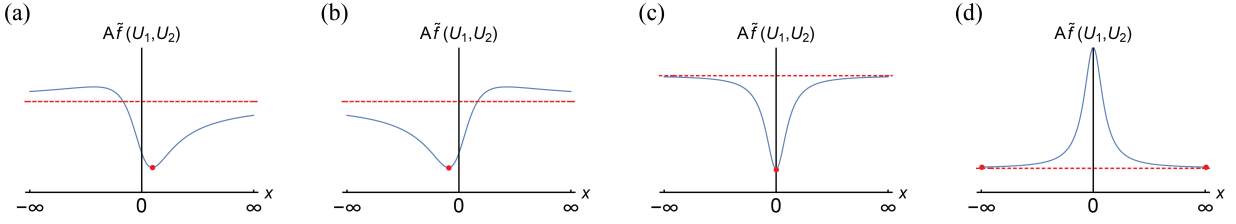


FIG. 6. Schematic plot for the dispersion of $A\tilde{f}_{A_{1u}(U_1, U_2)}$ with respect to x . In Fig.(a), we have $a_{12} < 0$. In Fig.(b) we have $a_{12} > 0$. In Fig.(c) we have $a_{12} = 0$, $-\frac{a_{22}}{2U_2} + \frac{a_{11}}{U_1} > 0$. In Fig.(d) we have $a_{12} = 0$, $-\frac{a_{22}}{2U_2} + \frac{a_{11}}{U_1} < 0$. The red points denote the minimum of $A\tilde{f}_\epsilon(U_1, U_2)$.

We diagonalize matrix \mathbb{A} and obtain three eigenvalues. Among them, there are two double degenerated eigenvalues denoted as a_1 and the third eigenvalue denoted as a_2 . Under the basis of the eigenvectors of matrix \mathbb{A} , we have,

$$\mathbb{A}' = \begin{pmatrix} a_1 & 0 & 0 \\ 0 & a_1 & 0 \\ 0 & 0 & a_2 \end{pmatrix}, \quad \mathbb{F}' = \begin{pmatrix} u_1 & 0 & u_{13} \\ 0 & u_2 & u_{23} \\ u_{13} & u_{23} & u_3 \end{pmatrix}, \quad (\text{E26})$$

where the 2 by 2 block on the left top of matrix \mathbb{F} can be diagonalized for the first two eigenvalues of matrix \mathbb{A} are degenerated. According to Table.VIII, in the limit of no mixture between states $|J = \frac{1}{2}, j_z = \pm \frac{1}{2}\rangle$ and $|J = \frac{3}{2}, j_z = \pm \frac{1}{2}\rangle$ on the Fermi surfaces, we have $\tilde{f}_{\epsilon,1}(U_1, U_2) = \tilde{f}_{\epsilon,2}(U_1, U_2) = 2U_1$, $\tilde{f}_{\epsilon,3}(U_1, U_2) = 4U_2$. The similarity transformation matrix transforming \mathbb{F} to \mathbb{F}' is composed by the eigenvectors of \mathbb{A} denoted as $\hat{\Lambda}_{\epsilon, \kappa} = (v_{\epsilon, \kappa, 1}, v_{\epsilon, \kappa, 2}, v_{\epsilon, \kappa, 3})^\top$. So we have:

$$\mathbb{F}_{12} = \frac{1}{2U_1} (v_{\epsilon, 1, 1}v_{\epsilon, 2, 1} + v_{\epsilon, 1, 2}v_{\epsilon, 2, 2}) + \frac{1}{4U_2} v_{\epsilon, 1, 3}v_{\epsilon, 2, 3} = 0 \quad (\text{E27})$$

And the orthogonality relation gives $\hat{\Lambda}_{\epsilon, \kappa_1}^\dagger \hat{\Lambda}_{\epsilon, \kappa_2} = \delta_{\kappa_1, \kappa_2}$,

$$v_{\epsilon, 1, 1}v_{\epsilon, 2, 1} + v_{\epsilon, 1, 2}v_{\epsilon, 2, 2} + v_{\epsilon, 1, 3}v_{\epsilon, 2, 3} = 0. \quad (\text{E28})$$

From Eq.E27 and Eq.E28 we can derive $v_{\epsilon, 1, 3}v_{\epsilon, 2, 3} = 0$ and we set $v_{\epsilon, 1, 3} = 0$. Constrained by $\hat{\Lambda}_{\epsilon, 1}^\dagger \hat{\Lambda}_{\epsilon, 3} = 0$, we can obtain,

$$\mathbb{F}_{13} = u_{13} = \frac{1}{2U_1} (v_{\epsilon, 1, 1}v_{\epsilon, 3, 1} + v_{\epsilon, 1, 2}v_{\epsilon, 3, 2}) = 0, \quad (\text{E29})$$

In the limitation of no mixture, we have $u_{13} = 0$ and we treat the mixture as perturbation and have $u_{13} \rightarrow 0$. We set $\hat{\Lambda}_{\epsilon, \kappa} = (\varphi_1, \varphi_2, \varphi_3)^\top$ and obtain,

$$A\tilde{f}_\epsilon(U_1, U_2) = \lim_{u_{13} \rightarrow 0} \frac{a_1\varphi_1^2 + a_1\varphi_2^2 + a_2\varphi_3^2}{u_1\varphi_1^2 + 2u_{13}\varphi_1\varphi_3 + u_2\varphi_2^2 + u_3\varphi_3^2 + 2u_{23}\varphi_2\varphi_3} \quad (\text{E30})$$

For a fraction takes the form as $\frac{a_1 + x^2 a_2}{b_1 + x^2 b_2 + x b_3}$ with x as a variable, $a_{1,2}$ and $b_{1,2,3}$ all positive. We have the extreme values taking at $x = \frac{2a_1 b_2 - 2a_2 b_1 \pm \sqrt{(2a_2 b_1 - 2a_1 b_2)^2 + 4a_1 a_2 b_3^2}}{2a_2 b_3}$. In the case of $b_3 \rightarrow 0$, the extreme values locate at $x = 0, \infty$ corresponding to $\frac{a_1 + x^2 a_2}{b_1 + x^2 b_2 + x b_3} = \frac{a_1}{b_1}$ and $\frac{a_1 + x^2 a_2}{b_1 + x^2 b_2 + x b_3} = \frac{a_2}{b_2}$, respectively. So the maximum of $|A\tilde{f}_\epsilon(U_1, U_2)|$ is near to $|\frac{a_1}{b_1}|$ or $|\frac{a_1\varphi_1^2 + a_2\varphi_3^2}{u_2\varphi_2^2 + u_3\varphi_3^2 + 2u_{23}\varphi_2\varphi_3}|$. We first seek for the maximum of $|\frac{a_1\varphi_1^2 + a_2\varphi_3^2}{u_2\varphi_2^2 + u_3\varphi_3^2 + 2u_{23}\varphi_2\varphi_3}|$ and obtain $\frac{\varphi_2}{\varphi_3}$ by solving the equation below and pick the x corresponding to the maximum,

$$\frac{d}{dx} \frac{a_1 x^2 + a_2}{u_2 x^2 + u_3 + 2u_{23}x} = 0 \quad (\text{E31})$$

where $x = \frac{\varphi_2}{\varphi_3}$. And then, we solve $\frac{\varphi_1}{\varphi_3}$ in the same way. Finally we obtain $\varphi_1 : \varphi_2 : \varphi_3$ and $\hat{\Lambda}_{\epsilon, \kappa}$ is determined.

We also set $\hat{\Lambda}_{\epsilon, \zeta} = (\sin \theta, \cos \theta)^\top$ for E_u and $\hat{\Lambda}_{\epsilon, \zeta} = (\sin \theta \cos \phi, \sin \theta \sin \phi, \cos \theta)^\top$ for T_{1u} and T_{2u} and sample on θ, ϕ to find the minimum of B . We obtain $\hat{\Lambda}_{E_u, \zeta} = (1, 0)^\top$ and $\hat{\Lambda}_{T_{1u}(T_{2u}), \zeta} = (1, 0, 0)^\top, (0, 1, 0)^\top, (0, 0, 1)^\top$.

Appendix F: Symmetries and topological properties of each channel

In the Nambu space, $\hat{\psi}_{\mathbf{k}}^\dagger = (\hat{c}_{\mathbf{k},\uparrow}^\dagger, \hat{c}_{\mathbf{k},\downarrow}^\dagger, \hat{c}_{-\mathbf{k},\uparrow}, \hat{c}_{-\mathbf{k},\downarrow})$, the particle-hole symmetry operator takes the form as $\mathcal{C} = \eta_1 \sigma_0 K$, where η and σ are Pauli matrices with η indicating the particle \hat{c}^\dagger or hole \hat{c} and σ indicating the pseudo-spin \uparrow or \downarrow . K is the conjugation operator. The time reversal symmetry operator takes the form as $\mathcal{T} = i\eta_0 \sigma_2 K$. With the particle-hole symmetry operator and time reversal operator we can define the chiral operator which is the product of these two, $\mathcal{S} = \mathcal{C}\mathcal{T} = i\eta_1 \sigma_2$. For the spacial symmetry operator R belonging to the D_{3d} group on the m -th pocket, we have,

$$\begin{aligned} R\hat{c}_{\mathbf{k},d}^{\dagger}R^\dagger &= \sum_{d'} \hat{c}_{R\mathbf{k},d'}^{\dagger} \mathcal{R}_{d'd} \\ R\hat{c}_{\mathbf{k},d}R^\dagger &= \sum_{d'} \hat{c}_{R\mathbf{k},d'}^{\dagger} \mathcal{R}_{d'd}^* \end{aligned} \quad (\text{F1})$$

where \mathcal{R} is the transformation matrix with d' as the row index and d as the column index. After the mean-field approximation, pairing part of the BdG Hamiltonian is obtained as $\sum_{m,d_1,d_2} \mathcal{H}_{d_1d_2}^m(\mathbf{k}) \hat{c}_{\mathbf{k},d_1}^{\dagger} \hat{c}_{-\mathbf{k},d_2}^{\dagger} + \text{h.c.}$ and transformed by the operator R as,

$$\begin{aligned} R \sum_{d_1,d_2} \mathcal{H}_{d_1d_2}^m(\mathbf{k}) \hat{c}_{\mathbf{k},d_1}^{\dagger} \hat{c}_{-\mathbf{k},d_2}^{\dagger} R^\dagger &= \sum_{d_1,d_2,d',d''} \mathcal{H}_{d_1d_2}^m(\mathbf{k}) \hat{c}_{R\mathbf{k},d'}^{\dagger} \mathcal{R}_{d'd_1} \hat{c}_{-R\mathbf{k},d''}^{\dagger} \mathcal{R}_{d''d_2} \\ &= \sum_{d',d''} (\mathcal{R} \mathcal{H}^m(\mathbf{k}) \mathcal{R}^\dagger)_{d'd''} \hat{c}_{R\mathbf{k},d'}^{\dagger} \hat{c}_{-R\mathbf{k},d''}^{\dagger}. \end{aligned} \quad (\text{F2})$$

In Eq.E2, we write the pairing as $\mathcal{H}^m(k) = i\boldsymbol{\sigma} \cdot \mathbf{d}(\mathbf{k})\sigma_2 = i\sigma_1\sigma_2d_1(\mathbf{k}) + i\sigma_2\sigma_2d_2(\mathbf{k}) + i\sigma_3\sigma_2d_3(\mathbf{k})$ and \mathcal{R} is the matrix representation of R . In the local reference frame, we take M_a as the mirror symmetry with the mirror plane perpendicular to the x axis and we obtain the matrix form of M_a under the basis $(\hat{c}_{\mathbf{k},\uparrow}^\dagger, \hat{c}_{\mathbf{k},\downarrow}^\dagger)$ which is denoted as \mathbb{M}_a , $\mathbb{M}_a = e^{-\frac{i}{2}\sigma_x\pi} = -i\sigma_1$. We act \mathbb{M}_a on the matrices $\boldsymbol{\sigma}\sigma_2$ and have,

$$\begin{aligned} \mathbb{M}_a\sigma_1\sigma_2\mathbb{M}_a^\dagger &= \sigma_1\sigma_2 \\ \mathbb{M}_a\sigma_2\sigma_2\mathbb{M}_a^\dagger &= -\sigma_2\sigma_2 \\ \mathbb{M}_a\sigma_3\sigma_2\mathbb{M}_a^\dagger &= -\sigma_3\sigma_2. \end{aligned} \quad (\text{F3})$$

Under M_a , the pairing is transformed as $\mathbb{M}_a\mathcal{H}(\mathbf{k})\mathbb{M}_a^\dagger = \tilde{\mathcal{H}}(\mathbf{k}) = i\sigma_1\sigma_2d_1(\mathbf{k}) - i\sigma_2\sigma_2d_2(\mathbf{k}) - i\sigma_3\sigma_2d_3(\mathbf{k}) = \ell\mathcal{H}(M_a\mathbf{k})$, where $\ell = \pm 1$ according to the form of $\mathbf{d}(\mathbf{k})$. In the Nambu space, we the matrix form of M_a as,

$$\mathcal{M}_a = \begin{pmatrix} \mathbb{M}_a & 0 \\ 0 & \ell\mathbb{M}_a^* \end{pmatrix}. \quad (\text{F4})$$

a. A_{1u} We start from the first pocket of the A_{1u} channel. The d -vector is obtained as $\mathbf{d}(\mathbf{k}) = (\alpha k_x, \alpha k_y, \beta k_z)$, where α and β are obtained from the mean field calculation. We write the pairing function $\mathcal{H}(\mathbf{k}) = \sum_{m,n=1,2,3} ik_m \mathcal{A}_{mn} \sigma_n \sigma_2$ and we use $k_{1,2,3}$ to denote $k_{x,y,z}$, respectively. The determinant of matrix \mathcal{A} is nonzero, $\det \mathcal{A} \neq 0$. So the A_{1u} channel is gapped. With the time reversal symmetry respected, the winding number of the single band Hamiltonian equals to $\text{sgn}(\det \mathcal{A})$. For the C_4 symmetry is trivial in the A_{1u} channel, the winding number of each pocket is the same and the system is characterized by the winding number $w = 4\text{sgn}(\alpha^2\beta)$.

b. A_{2u} The d -vector of the first pocket is taken as $\mathbf{d}(\mathbf{k}) = (-\alpha k_y, \alpha k_x, 0)$ and the determinant of matrix \mathcal{A} equals to 0, $\det \mathcal{A} = 0$. The A_{2u} state is gapless and protected by the mirror and chiral symmetry. The gapless point is shown in Fig.7(a). The pairing function is transformed by the mirror symmetry M_a as,

$$\mathbb{M}_a\mathcal{H}(\mathbf{k})\mathbb{M}_a^\dagger = \tilde{\mathcal{H}}(\mathbf{k}) = -i\sigma_1\sigma_2\alpha k_y - i\sigma_2\sigma_2\alpha k_x = \mathcal{H}(M_a\mathbf{k}). \quad (\text{F5})$$

The mirror symmetry M_a of the A_{2u} channel in the Nambu space is even, $\ell = 1$ and the chiral symmetry commutes with M_a . We first decompose the BdG Hamiltonian in the mirror plane of M_a ($k_x = 0$) into different mirror subspaces with the eigenvalues of M_a equalling to i and $-i$ separately,

$$H_{\text{BdG}}(\mathbf{k}, k_x = 0) = \begin{pmatrix} \frac{k_y^2}{2m} + \frac{\xi k_z^2}{2m} - \mu & -\alpha k_y & 0 & 0 \\ -\alpha k_y & -\frac{k_y^2}{2m} - \frac{\xi k_z^2}{2m} + \mu & 0 & 0 \\ 0 & 0 & \frac{k_y^2}{2m} + \frac{\xi k_z^2}{2m} - \mu & -\alpha k_y \\ 0 & 0 & -\alpha k_y & -\frac{k_y^2}{2m} - \frac{\xi k_z^2}{2m} + \mu \end{pmatrix}. \quad (\text{F6})$$

Within each subspace, the chiral symmetry is respected. We transform the basis of the mirror subspace to the eigenstates of chiral symmetry and the Hamiltonian in each subspace is off diagonalized,

$$H_{\text{sub-mirror}} = \begin{pmatrix} 0 & i\alpha k_y + \frac{k_y^2}{2m} + \frac{\xi k_z^2}{2m} - \mu \\ -i\alpha k_y + \frac{k_y^2}{2m} + \frac{\xi k_z^2}{2m} - \mu & 0 \end{pmatrix}. \quad (\text{F7})$$

To study the edge states on the (001) surface, we change Hamiltonian from the local to the global reference frame and have $k_y = \sqrt{\frac{1}{6}}(k_X + k_Y) - \sqrt{\frac{2}{3}}k_Z$, $k_z = \sqrt{\frac{1}{3}}(k_X + k_Y + k_Z)$, $k_X = k_Y$ (constrained by the mirror plane),

$$H_{\text{sub-mirror}} = \begin{pmatrix} 0 & i\alpha\sqrt{\frac{2}{3}}(k_X - k_Z) + \frac{(k_X - k_Z)^2}{3m} + \xi\frac{(2k_X + k_Z)^2}{6m} - \mu \\ -i\alpha\sqrt{\frac{2}{3}}(k_X - k_Z) + \frac{(k_X - k_Z)^2}{3m} + \xi\frac{(2k_X + k_Z)^2}{6m} - \mu & 0 \end{pmatrix}. \quad (\text{F8})$$

We take k_X satisfying $-\sqrt{\frac{2m\mu}{3\xi}} < k_X < \sqrt{\frac{2m\mu}{3\xi}}$ and set $k_X - k_Z = x$. The off diagonal entry of the matrix turns to $\pm i\alpha x + \frac{1}{3m}x^2 + \frac{\xi}{6m}(3k_X - x)^2 - \mu$. When we take x from $-\infty$ to ∞ , equivalent for k_Z from ∞ to $-\infty$, the complex phase of the off diagonal entry changes from 0 to -2π shown in Fig.7(b).

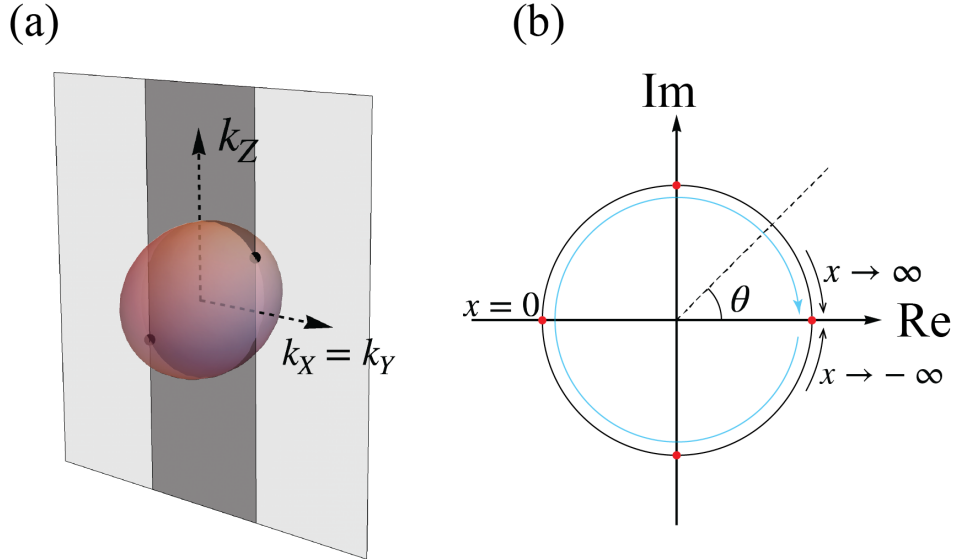


FIG. 7. (a) The Fermi surface of the first pocket of the A_{2u} channel. We use the transparent gray plane to denote the mirror plane. Two black points stand for the gapless points. There exists the arc at the intersection between the darker part of the plane and the (001) surface Brillouin zone. (b) Re and Im stand for the real and imaginary axis. θ is the complex phase of the off diagonal entry in Eq.F8. When we take x from $-\infty$ to ∞ , θ will travel on the circle along the direction of the blue trace. We approach to the right red point on the real axis from up and down side when we take $x \rightarrow \infty$ and $x \rightarrow -\infty$, respectively. When we take $x = 0$, the off diagonal entry is a negative real number and plotted as the left red point on the real axis. The up and down red points on the imaginary axis correspond to the two roots of the equation $\frac{1}{3m}x^2 + \frac{\xi}{6m}(3k_X - x)^2 - \mu = 0$ with opposite sign.

c. E_u For the E_u channel, the unit vector (t_1, t_2) in the order parameter is taken as $(1, 0)$. From the representation table in the paper we know that C_{2a} and C_4 symmetry is respected with the character of C_{2a} and C_4 symmetry equalling to 1. The symmetry of the system breaks from the group O_h to the A_{2u} irrep of the group D_{4h} . Similar with A_{1u} , the d -vector of the first pocket is taken as $(\alpha k_x, \alpha k_y + \beta k_z, \gamma k_y)$. We have $\det \mathcal{A} \neq 0$ and the system is characterized by the winding number $w = -4\text{sgn}(\alpha\beta\gamma)$.

d. T_{2u} For the T_{2u} channel, we take the unit vector (t_1, t_2, t_3) as $(0, 0, 1)$. C_{2a} and C_4 symmetry are respected according to the irreps table. The character of C_{2q} and C_4 equal to 1 and -1 , respectively. The symmetry of the system breaks from the O_h group to the B_{2u} irrep of the D_{4h} group. In the first pocket we have the d -vector as $\mathbf{d}(\mathbf{k}) = (\alpha k_x, \beta_1 k_y + \beta_2 k_z, \gamma_1 k_y + \gamma_2 k_z)$. The winding number of the first pocket is obtained as $w_1 = \text{sgn}(\det \mathcal{A}) = \text{sgn}(\alpha\beta_1\gamma_2 - \alpha\beta_2\gamma_1)$. However, different with A_{1u} and E_u , the C_4 symmetry in T_{2u} changes the sign of winding number

between different pockets and the winding numbers of the four pockets are taken as $w_1, -w_1, w_1, -w_1$, separately. We can see that the total winding number gives 0, however, the T_{2u} state is topologically nontrivial. The mirror symmetry M_a is odd, $M_a \mathcal{H}(\mathbf{k}) M_a^\dagger = \mathcal{H}(\mathbf{k}) = -\mathcal{H}(M_a \mathbf{k})$, $\ell = -1$. In the mirror plane we decompose the BdG Hamiltonian into the mirror subspace,

$$H_{\text{BdG}}(\mathbf{k}, k_x = 0) = \begin{pmatrix} -\frac{k_y^2}{2m} - \frac{\xi k_z^2}{2m} + \mu & -i\beta_1 k_y - i\beta_2 k_z - \gamma_1 k_y - \gamma_2 k_z & 0 & 0 \\ i\beta_1 k_y + i\beta_2 k_z - \gamma_1 k_y - \gamma_2 k_z & \frac{k_y^2}{2m} + \frac{\xi k_z^2}{2m} - \mu & 0 & 0 \\ 0 & 0 & -\frac{k_y^2}{2m} - \frac{\xi k_z^2}{2m} + \mu & \gamma_1 k_y + \gamma_2 k_z - i\beta_1 k_y - i\beta_2 k_z \\ 0 & 0 & \gamma_1 k_y + \gamma_2 k_z + i\beta_1 k_y + i\beta_2 k_z & \frac{k_y^2}{2m} + \frac{\xi k_z^2}{2m} - \mu \end{pmatrix}. \quad (\text{F9})$$

In each mirror subspace, there exists a gapless point at $k_x = k_y = k_z = 0$ when we take the chemical potential to zero, $\mu = 0$ and when $\mu < 0 (> 0)$, the system is topologically trivial (nontrivial), so $\mu = 0$ is a topological phase transition point in the mirror plane. We calculate the topological charge of the gapless point and we can obtain the mirror Chern number. In each mirror subspace we similarly define $\mathcal{H}_{\text{mirror sub}}(\mathbf{k}) = \sum_{m,n=1,2} k_m \mathcal{A}'_{mn} \sigma_n i \sigma_2$ with k_1, k_2 denoting k_y and k_z . The mirror Chern number for the first pocket is obtained as $\text{sgn}(\det \mathcal{A}') = \text{sgn}(\beta_1 \gamma_2 - \beta_2 \gamma_1)$ and the mirror plane is shared by two pockets related by C_4^2 symmetry, for example, pocket 1 and 3. And $C_4^2 = 1$, the mirror Chern number of these two pockets are the same, so the mirror Chern number of the mirror plane is even, $2\text{sgn}(\beta_1 \gamma_2 - \beta_2 \gamma_1)$, which suggests a second order topological superconductivity.

Appendix G: Calculation of edge states

We open the boundary along Z axis and write k_Z as $-i \frac{\partial}{\partial Z}$. And we write,

$$-i \frac{\partial}{\partial Z} |Z, k_x, k_y, w\rangle = -i \frac{|Z + dZ, k_x, k_y, w\rangle - |Z - dZ, k_x, k_y, w\rangle}{2dZ}, \quad (\text{G1})$$

where we use w to denote the pseudo-spin. We first write the BdG Hamiltonian in the basis of $(|Z_1, k_x, k_y, w\rangle, |Z_2, k_x, k_y, w\rangle, \dots, |Z_N, k_x, k_y, w\rangle)^\dagger$ and we totally have N sites along Z axis, $Z_{i+1} - Z_i = dZ \rightarrow 0$. In the periodic boundary condition, we stick the N -th site with the first site and take the first site the same as the $N + 1$ -th site. The operator \hat{k}_Z can be written as,

$$\hat{k}_Z = \frac{1}{2dZ} \begin{pmatrix} 0 & i & 0 & \cdots & 0 & -i \\ -i & 0 & i & \cdots & 0 & 0 \\ 0 & -i & 0 & \cdots & 0 & 0 \\ \vdots & \vdots & \vdots & \ddots & \vdots & \vdots \\ 0 & 0 & 0 & \cdots & 0 & i \\ i & 0 & 0 & \cdots & -i & 0 \end{pmatrix}. \quad (\text{G2})$$

While, for the open boundary condition, we cut off the loop and remove the N -th row and column in the matrix. So for the open boundary condition, we have the operator of \hat{k}_Z taken as,

$$\hat{k}_Z = \frac{1}{2dZ} \begin{pmatrix} 0 & i & 0 & \cdots & 0 & 0 \\ -i & 0 & i & \cdots & 0 & 0 \\ 0 & -i & 0 & \cdots & 0 & 0 \\ \vdots & \vdots & \vdots & \ddots & \vdots & \vdots \\ 0 & 0 & 0 & \cdots & 0 & i \\ 0 & 0 & 0 & \cdots & -i & 0 \end{pmatrix}. \quad (\text{G3})$$

For the second order derivation of Z , we have,

$$\hat{k}_Z^2 = -\frac{\partial^2}{\partial Z^2} |Z, k_x, k_y, w\rangle = -\frac{|Z + dZ, k_x, k_y, w\rangle + |Z - dZ, k_x, k_y, w\rangle - 2|Z, k_x, k_y, w\rangle}{dZ^2}. \quad (\text{G4})$$

And in the periodic condition we have,

$$\hat{k}_Z^2 = -\frac{1}{dZ^2} \begin{pmatrix} -2 & 1 & 0 & \cdots & 0 & 1 \\ 1 & -2 & 1 & \cdots & 0 & 0 \\ 0 & 1 & -2 & \cdots & 0 & 0 \\ \vdots & \vdots & \vdots & \ddots & \vdots & \vdots \\ 0 & 0 & 0 & \cdots & -2 & 1 \\ 1 & 0 & 0 & \cdots & 1 & -2 \end{pmatrix}. \quad (\text{G5})$$

For the open boundary condition we have,

$$\hat{k}_Z^2 = -\frac{1}{dZ^2} \begin{pmatrix} -2 & 1 & 0 & \cdots & 0 & 0 \\ 1 & -2 & 1 & \cdots & 0 & 0 \\ 0 & 1 & -2 & \cdots & 0 & 0 \\ \vdots & \vdots & \vdots & \ddots & \vdots & \vdots \\ 0 & 0 & 0 & \cdots & -2 & 1 \\ 0 & 0 & 0 & \cdots & 1 & -2 \end{pmatrix}. \quad (\text{G6})$$

We substitute \hat{k}_Z and \hat{k}_Z^2 under the open boundary condition in Eq.[G3](#) and Eq.[G6](#) into the BdG Hamiltonian and diagonalize the matrix to obtain the dispersion.